

# Fluorescent Proteins and Their Applications in Imaging Living Cells and Tissues

DMITRIY M. CHUDAKOV, MIKHAIL V. MATZ, SERGEY LUKYANOV, AND KONSTANTIN A. LUKYANOV

*Shemiakin-Ovchinnikov Institute of Bioorganic Chemistry, Moscow, Russia; and University of Texas at Austin, Austin, Texas*

---

|  |      |
|--|------|
| I. Introduction  | 1104 |
| II. Spatial Structure and Diversity of Chromophores  | 1105 |
| A. Structure   | 1105 |
| B. Natural diversity of chromophores   | 1107 |
| C. Artificial chromophores and colors  | 1112 |
| III. Evolution of Green Fluorescent Protein-like Proteins                                  | 1112 |
| A. Where do GFPs come from?  | 1113 |
| B. FP is an ancient metazoan gene  | 1115 |
| C. Overview of natural FP diversity  | 1117 |
| D. FPs form multigene families in host genomes   | 1118 |
| E. Color evolution   | 1118 |
| F. Biological functions of FPs   | 1119 |
| IV. Key Characteristics for Practical Use  | 1121 |
| A. Brightness: QY and EC   | 1121 |
| B. Maturation rate   | 1121 |
| C. Photostability and undesirable photoconversions   | 1122 |
| D. Oligomeric nature and aggregation   | 1123 |
| E. pH stability  | 1125 |
| V. Modern Palette of Fluorescent Proteins  | 1125 |
| A. Monomeric FPs   | 1125 |
| B. Tandems   | 1128 |
| C. Dimeric and tetrameric FPs  | 1128 |
| VI. Basic Applications of Fluorescent Proteins   | 1129 |
| A. Protein labeling  | 1129 |
| B. Photobleaching techniques   | 1130 |
| C. Subcellular localizations   | 1130 |
| D. Promoters tracking  | 1130 |
| E. Timers  | 1131 |
| F. Cell and tissue labeling  | 1132 |
| G. DNA and RNA labeling  | 1134 |
| VII. Studying Protein-Protein Interactions Using Fluorescent Proteins                      | 1134 |
| A. FRET  | 1134 |
| B. FCCS  | 1137 |
| C. Fluorescence complementation (split fluorescent proteins)                               | 1137 |
| VIII. Photoactivatable Fluorescent Proteins  | 1138 |
| A. Structural basis for the photoactivation  | 1138 |
| B. Key properties of PAFPs   | 1139 |
| C. Reversible PAFPs  | 1139 |
| D. Irreversible PAFPs  | 1141 |
| E. Super-resolution microscopy   | 1143 |
| IX. Genetically Encoded Sensors  | 1143 |
| A. Power of genetically encoded sensors  | 1143 |
| B. Sensors based on a single FP with no additional protein domains                         | 1144 |
| C. Sensors built on a single FP fused to the conformationally sensitive detector domain(s) | 1145 |
| D. FRET-based sensors  | 1146 |
| E. Translocation sensors/assays  | 1147 |
| X. Fluorescent Proteins as Photosensitizers  | 1148 |
| XI. Conclusions and Perspectives   | 1150 |

---

**Chudakov DM, Matz MV, Lukyanov S, Lukyanov KA.** Fluorescent Proteins and Their Applications in Imaging Living Cells and Tissues. *Physiol Rev* 90: 1103–1163, 2010; doi:10.1152/physrev.00038.2009.—Green fluorescent protein (GFP) from the jellyfish *Aequorea victoria* and its homologs from diverse marine animals are widely used as universal genetically encoded fluorescent labels. Many laboratories have focused their efforts on identification and development of fluorescent proteins with novel characteristics and enhanced properties, resulting in a powerful toolkit for visualization of structural organization and dynamic processes in living cells and organisms. The diversity of currently available fluorescent proteins covers nearly the entire visible spectrum, providing numerous alternative possibilities for multicolor labeling and studies of protein interactions. Photoactivatable fluorescent proteins enable tracking of photolabeled molecules and cells in space and time and can also be used for super-resolution imaging. Genetically encoded sensors make it possible to monitor the activity of enzymes and the concentrations of various analytes. Fast-maturing fluorescent proteins, cell clocks, and timers further expand the options for real time studies in living tissues. Here we focus on the structure, evolution, and function of GFP-like proteins and their numerous applications for *in vivo* imaging, with particular attention to recent techniques.

## I. INTRODUCTION

Currently, the term *green fluorescent protein* is well known beyond the realm of life science. The development of green pigs and cats has been well covered by the media, and transgenic fluorescent fish are common in home aquaria. However, for the long 30 years since the beginning of this story more than 45 years ago (392), green fluorescent protein (GFP) was of interest only to a handful of scientists studying luminescence of marine creatures. *Aequorea victoria* GFP began to garner much attention after its cloning in 1992 (348) and the first demonstration of its utility as a fluorescent tag for *in vivo* labeling in 1994 (63). GFP, a fully genetically encoded label, became a unique tool that enabled direct visualization of structures and processes in living cells and organisms. Afterward, a keen interest in the structure, biochemistry, and biophysics of GFP-like fluorescent proteins (FPs; here we will use this term only for GFP-like fluorescent proteins and not for other proteins possessing fluorescence such as iLOV, Ref. 64) arose, which resulted in an avalanche of scientific publications on FPs and their applications to solve basic problems in molecular and cell biology (Fig. 1).

A number of GFP-like proteins have been discovered in bioluminescent (a naturally occurring form of chemiluminescence) Hydrozoa and Anthozoa species, where FPs can re-emit light during bioluminescence resonance energy transfer (BRET). Nonbioluminescent Anthozoa also carry FPs (275) and GFP-like nonfluorescent chromoproteins (256). Moreover, recent studies revealed FPs in evolutionarily distant species, including crustaceans (383), comb jellies (143a), and even chordates (lancelets) (86) (see sect. III). In addition to the “original” GFP-like chromophore, which was described as early as 1979 (391) and refined in 1993 (75), its modified variants were described in natural FPs, including DsRed-like (132) and Kaede-like (294) red chromophores and a few other variations (see sect. II). The discovery and development of multiple spectral FP variants (see sect. V) has revolutionized studies of living systems. These achievements were recognized by the 2008 Nobel Prize in Chemistry

awarded “for the discovery and development of the green fluorescent protein, GFP” (Fig. 1).

Nowadays, GFP and its variants and homologs of different colors are used in a variety of applications to study the organization and function of living systems (Fig. 2) (see sect. VI). FPs encoded in frame with proteins of interest make it possible to observe their localization, movement, turnover, and even “aging” (i.e., time passed from protein synthesis). Nucleic acids also can be labeled via RNA- or DNA-binding protein domains. FPs targeted to cell organelles by specific protein localization signals enable visualization of their morphology, fusion and fission, segregation during cell division, etc. FPs are essential tools for individual cell labeling and tissue labeling to visualize morphology, location, and movement (e.g., during embryonic development and tumorigenesis), mitotic stages, and many other important cell characteristics. Finally, whole organisms can be labeled with FPs to discriminate between transgenic and wild-type individuals, as well as for entertainment, i.e., creation of unusually colored aquarium fish and other pets.

Moreover, complex functional studies can be performed using FPs. One can visualize protein-protein interactions in living cells (see sect. VII) and directly observe target promoters switching on and off, coactivation of two promoters, and a history of a promoter activation at the whole organism level (see sect. VI). The broad field of FP-based tools comprises a variety of fluorescent sensors that demonstrate environment-dependent changes in spectral characteristics. These genetically encoded sensors enable visualization of activities of target enzymes (e.g., protein kinases and proteases); measurements of the concentration of intracellular ions, metabolites, and messengers ( $H^+$ ,  $Ca^{2+}$ ,  $Cl^-$ ,  $H_2O_2$ , cAMP, etc.); and other cellular parameters (see sect. IX). An emerging area is FP-mediated light-induced production of reactive oxygen species (ROS) that can be used to locally inactivate target proteins, selectively kill cells, and study intracellular ROS signaling (see sect. X). This arsenal of FP-based methods can be used not only in basic studies but also for high-throughput screening of drug candidates and preclinical studies.

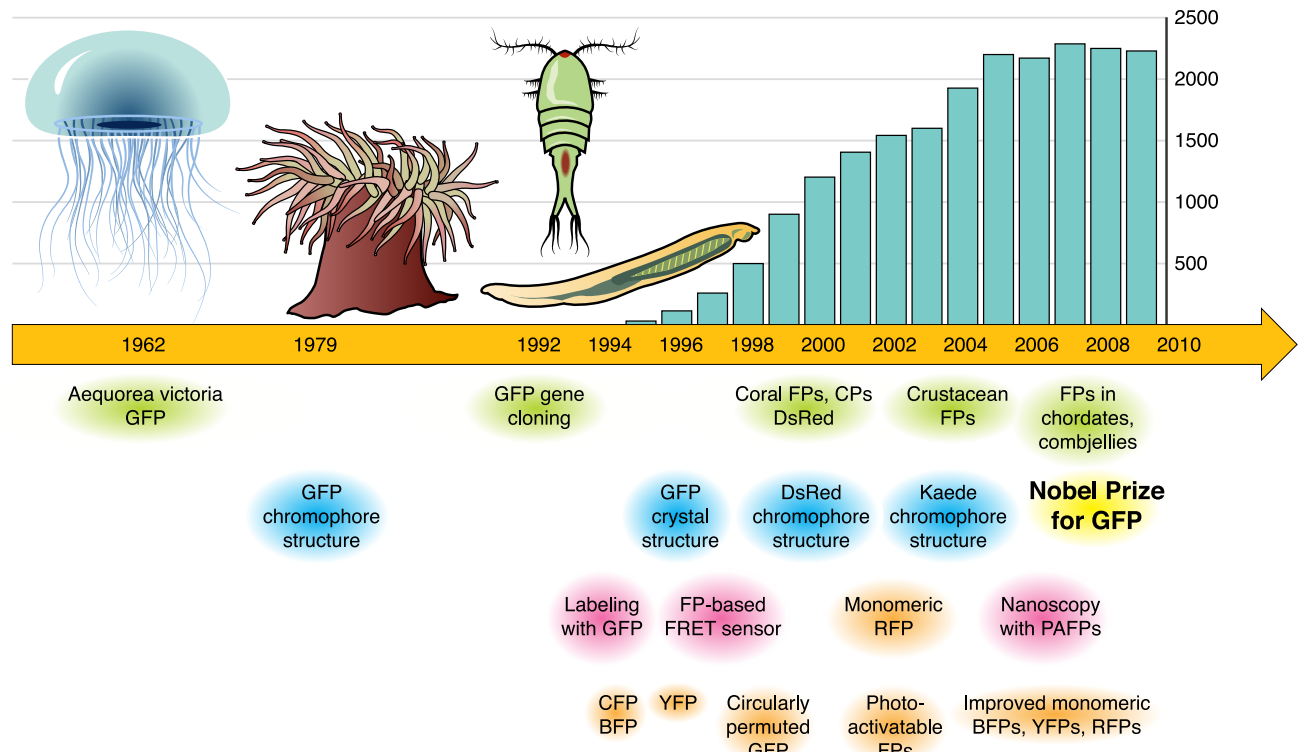


FIG. 1. A timeline of major achievements in the field. Green color below the text highlights basic studies of natural diversity of green fluorescent protein (GFP)-like proteins; blue, structural insights; orange, development of novel fluorescent protein (FP) variants; magenta, appearance of FP-based technologies. Drawings of representative animals having FPs are shown above the timeline (from left to right: jellyfish, sea anemone, copepod, and lancelet). Columns above the timeline show the number of scientific articles per corresponding year that can be found searching PubMed with the term *green fluorescent protein* (this search is not comprehensive but reflects the general dynamics of publications on fluorescent proteins).

A wide variety of FPs have become available thanks to extensive efforts to study their natural diversity and biochemistry. Along with pure academic interest, the practical applicability of FPs has prompted researchers to study the phylogeny and biological functions of this protein family, spatial protein structure, chemical structure and mechanisms of formation of chromophores, photophysical properties and their structural determinants, etc. New insights into FP biochemistry have often resulted in the generation of new FP variants for practical use. Last but not least, studies of FP-derived fluorescence in marine creatures suggest a number of previously unsuspected aspects of their physiology, ecology, and behavior (see sect. III).

The goal of this review is to summarize our current understanding of the structure, biochemistry, and evolution of this amazing protein family, and also to highlight the variety of biological techniques provided by FPs.

## II. SPATIAL STRUCTURE AND DIVERSITY OF CHROMOPHORES

### A. Structure

FPs and chromoproteins of GFP family consist of ~220–240 amino acid residues (25 kDa) (Fig. 3), which

fold into a barrel formed by 11 $\beta$ -sheets that accommodates an internal distorted helix (Fig. 3, A and B) (103, 162, 253, 324, 340, 346, 349, 465, 483, 500). The chromophore group is formed by a unique posttranslational modification of the three amino acid residues of the helix at positions 65–67 (numbering in accordance with *Aequorea victoria* GFP). While the side chain of the first chromophore-forming residue at position 65 can vary, Tyr66 and Gly67 are strictly conserved among all natural GFP-like proteins. The resulting chromophore is located in the very center of the  $\beta$ -barrel and therefore is well protected from contact with the solvent by the surrounding protein shell. In addition, the barrel of FPs is stabilized by multiple noncovalent interactions that ensure its extremely high stability to thermal or chemical denaturation as well as resistance to proteolysis (46, 435, 451).

Importantly, all GFP-like proteins have a more or less pronounced tendency to oligomerize. Even *Aequorea victoria* GFP, which is considered monomeric, forms dimers at high concentrations corresponding to physiological conditions in jellyfish (80). Some FPs exist as strong dimers, e.g., GFP from the sea pansy *Renilla* (253, 338, 472) or phiYFP from jellyfish *Phialidium* (383). Notably, nearly all FPs from nonbioluminescent Anthozoa and other taxa form very sta-

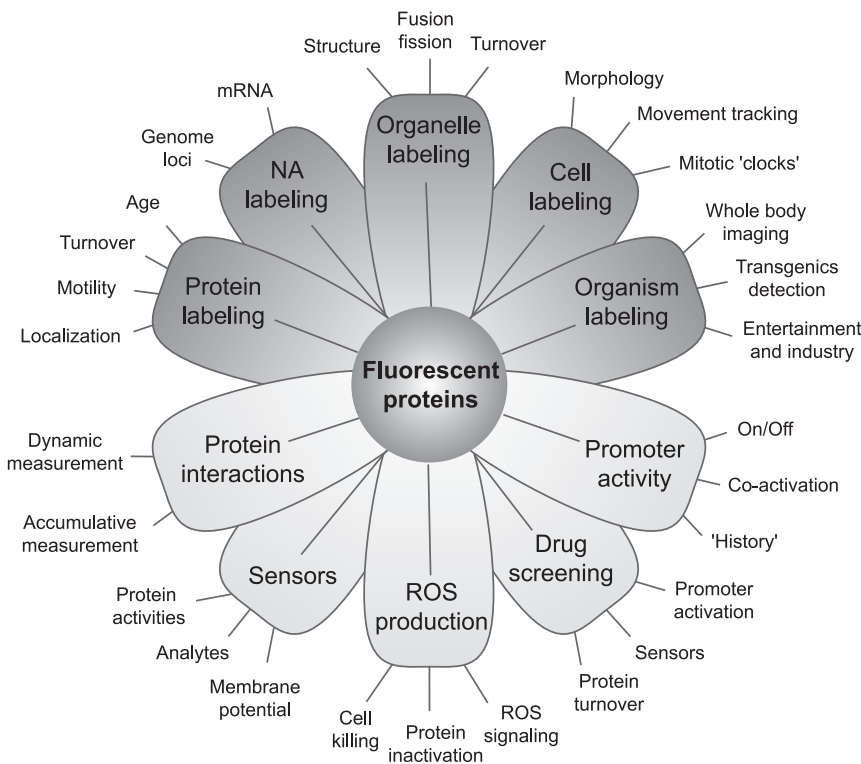


FIG. 2. Main areas of applications of fluorescent proteins. Dark gray and light gray petals show structural and functional studies, respectively, although boundaries between them are often quite fuzzy.

ble homotetramers even at very low (nanomolar) concentrations (26).

The tetrameric structure of FPs was first revealed by crystallographic studies of the red FP DsRed from *Drosophila sp.* (465, 500). Each DsRed monomer contacts the two adjacent protein molecules by two distinct interfaces (Fig. 4). The hydrophobic interface includes a cluster of closely packed hydrophobic residues surrounded by a set of polar side chains. The hydrophilic interface contains many hydrogen bonds and salt bridges between polar residues and includes buried water molecules. In addition, it is stabilized by an unusual "clasp" formed by COOH-terminal residues of each monomer. This tight tetrameric structure presented major difficulties for the early experimental use of red FPs (see sect. IV).

The side chains of amino acids buried inside the FP barrel play essential roles in chromophore formation and fine-tuning of spectral properties. The most important residues are located in the middle of the  $\beta$ -strands, close to the chromophore group. Therefore, each strand "controls" a chromophore from a particular direction as shown in Figure 5. Arg96 from strand 4 is the most critical catalytic residue (strictly conserved among FPs), which is in direct contact with the chromophore in mature FPs (Fig. 3C). Arg96 promotes protein backbone cyclization during FP maturation (244, 404, 405). Catalytic activity is also associated with the evolutionarily conserved Glu222 from strand 11 (244, 404, 405), although mutagenesis studies demonstrated that in some cases this residue can be

replaced with almost no deleterious effects on the maturation of the FP chromophore (101, 134). Inner residues from strands 7, 8, and 10 influence the FP spectra in a different way. Side chains of residues 148, 165, 167, and 203 are in contact with Tyr66 of the chromophore (Fig. 3D) and are the primary determinants of its protonation state (anionic or neutral), polarization, spatial conformation (*cis* or *trans*), and rotational freedom (19, 49, 70, 324, 340, 349, 352, 414, 459, 463). Variations of these side chains can dramatically alter the excitation and emission spectra, make the protein highly fluorescent or nearly completely nonfluorescent, or facilitate reversible photo-switching of the chromophore between two different states. Correspondingly, a number of interesting and sometimes extremely useful mutants have been obtained

by mutagenesis at these points. For example, widely used yellow variants of GFP (see sect. V) carry a key Thr203Tyr substitution that results in a red-shift of excitation and emission maxima (324). Substituting the same position for Ile or His, on the contrary, leads to stabilization of the protonated chromophore with a blue-shifted absorption at  $\sim 400$  nm, which is seen in such GFP variants as Sapphire (435, 512) and PA-GFP (334). A bright red FP DsRed was converted into a nonfluorescent chromoprotein state by substitutions Ser148Cys, Ile165Asn, Lys167Met, and Ser203Ala (51). Some FPs, such as asFP595 (256) or Dronpa (139), naturally possess pronounced reversible photo-switching characteristics that are largely determined by positions 148, 165, 167, and 203 (70).

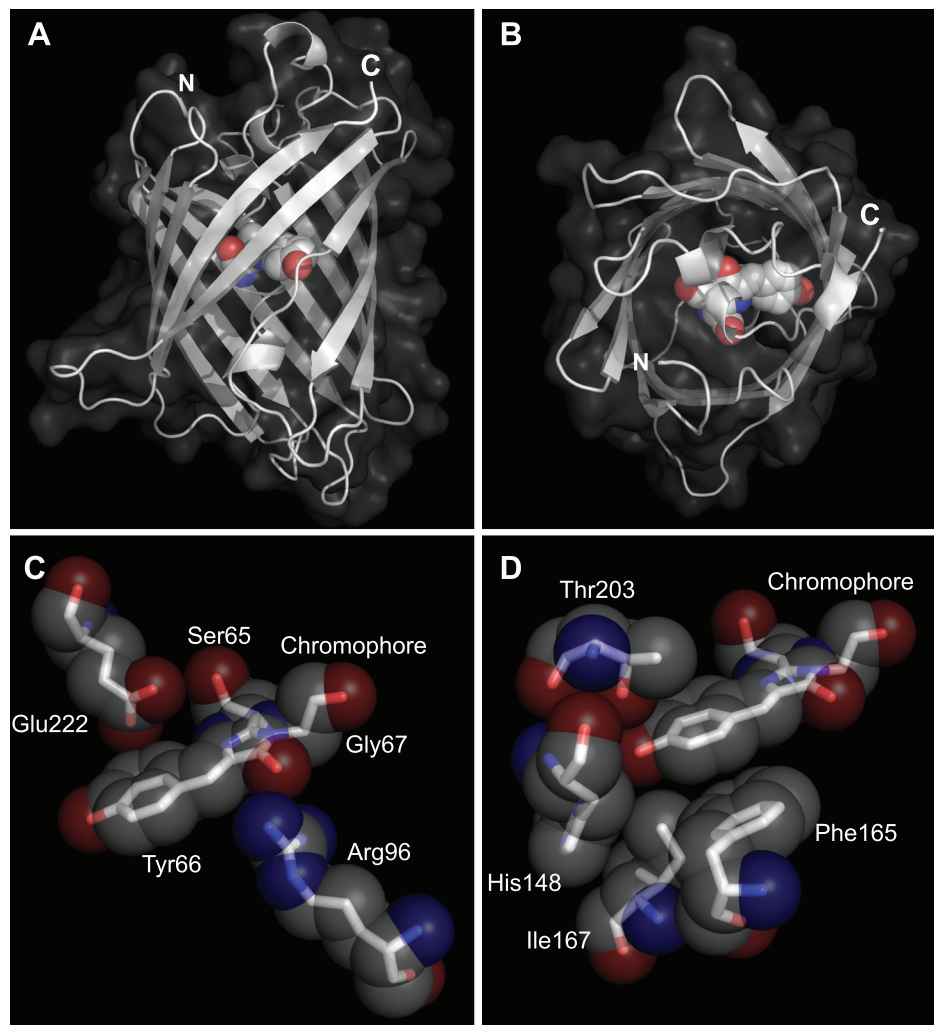


FIG. 3. Structure of GFP. A and B: overall structure of GFP  $\beta$ -barrel with semitransparent surface is shown from the side (A) and from the top (B). Chromophore is shown in a spacefill representation. C and D: GFP chromophore and selected nearby residues in sticks and semitransparent spacefill representation. Carbon atoms are gray, nitrogen atoms are blue, and oxygen atoms are red.

## B. Natural Diversity of Chromophores

The chromophore is arguably the most interesting part of an FP. Commonly, biosynthesis of pigments occurs through multiple sequential reactions catalyzed by several specific enzymes and involving low-molecular substrates and cofactors. In contrast, the barrel of FPs acts as a unique “enzyme” that modifies its own internal amino acids without any external cofactors and substrates except molecular oxygen. This property underlies all practical uses of FPs by ensuring fluorescence capability after expression in nearly any heterologous system.

Substantial efforts have been devoted to the study of chromophores of GFP-like proteins. These studies revealed chemical structures of the chromophores and suggested general mechanisms of their formation. However, the exact sequence of molecular events during chromophore maturation is still a matter of active debate, even for the most-studied GFP “green” chromophore, not to mention the more sophisticated red-shifted chromophores.

The GFP-like chromophore is formed by cyclization of the protein backbone at positions 65–67 (Ser-Tyr-Gly in *Aequorea victoria* GFP), followed by dehydrogenation of  $\text{C}\alpha\text{-C}\beta$  of Tyr66 with molecular oxygen (Fig. 6). These reactions result in a two-ring structure representing a conjugated  $\pi$ -system that is large, polarized, and planar enough to absorb and emit light within the visible range. The phenolic hydroxyl of the chromophore’s Tyr66 ionizes easily, which results in drastic changes in spectral characteristics. In the wild-type *Aequorea victoria* GFP, the chromophore is in equilibrium between protonated (neutral) and deprotonated (anionic) forms (473). Protonated GFP chromophore absorbs at  $\sim 400$  nm and can potentially give off blue light at  $\sim 460$  nm, as observed in PS-CFP (74), dual emission pH sensors (147, 280), and some permuted FPs (10). However, in most cases, the protonated GFP-like chromophores undergo the process called ESPT (excited state proton transfer): immediately after excitation, the chromophore loses one of its protons and becomes charged, thus dissipating a portion of the

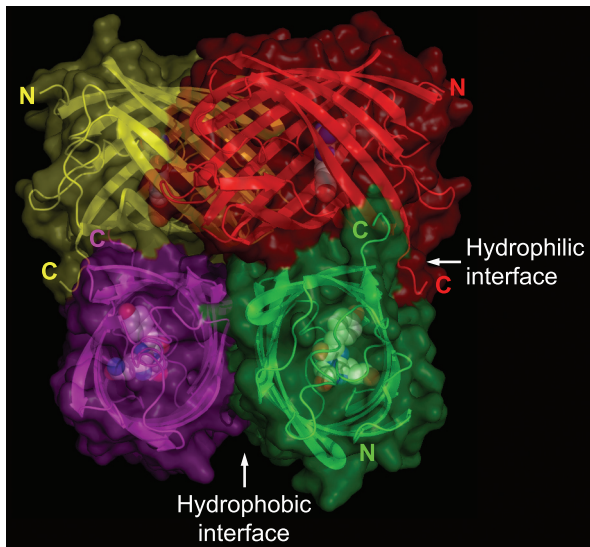


FIG. 4. Overall structure of DsRed tetramer. Monomers are shown in different colors. Chromophores are shown in a spacefill representation.

absorbed energy. Subsequently, it emits green fluorescence with an emission spectrum essentially identical to that of the initially charged form (49, 65). This effect was employed to generate the proteins with large Stokes shifts, characterized by a single excitation peak around 400 nm and a green fluorescent emission peak beyond 500 nm (6, 435, 512) (see sect. v).

Anionic chromophore absorbs at  $\sim$ 480 nm and emits green light at  $\sim$ 510 nm. The anionic form is often stable and is responsible for a single-peak excitation, as seen in one of the most popular green FPs, EGFP (77), as well as in numerous wild-type and mutant green FPs. In addition, excitation and emission spectra of the anionic GFP chromophore can be blue- or red-shifted by the influence of amino acid environment, from cyan such as amFP486 (275) to yellow FPs (see sect. v).

Although the typical GFP-like chromophore can already demonstrate dramatically different spectral properties depending on its molecular environment, its emission apparently cannot be red-shifted beyond 540 nm (yellow). To achieve a more substantial red shift, the basic GFP-like chromophore undergoes further covalent modification resulting in several other naturally occurring structures, among which the two most common ones are the red-emitting DsRed- and Kaede-like chromophores.

The chromophore of DsRed type is formed by additional oxidation (by molecular oxygen) of the  $\text{C}\alpha\text{-N}$  bond of a residue at position 65. This oxidation results in the appearance of an acylimine group that extends the conjugated  $\pi$ -system and leads to a dramatic bathochromic shift of excitation-emission spectra. Recent studies showed that formation of DsRed-like chromophore often occurs via a blue intermediate in which the central five-membered heterocy-

cle is conjugated to an acylimine group but not to the Tyr66 phenolic (Fig. 6) (415a, 419a). At the same time, in some fluorescent proteins, DsRed-like chromophore originates from a GFP-like precursor (326a). In some proteins, acylimine, which is a highly reactive group, undergoes further conversion. In particular, purple chromoprotein asFP595 from the sea anemone *Anemonia sulcata* carries an unusual chromophore consisting of a GFP-like core extended with a keto group; the protein backbone is broken just before the chromophore (Fig. 6) (352). This structure is most likely formed via a DsRed-like intermediate as a result of acylimine hydrolysis. In yellow FP zFP538 from the button polyp *Zoanthus*, the chromophore includes a third six-member heterocycle formed by the side chain of Lys65 so that the GFP-like core becomes extended with an additional conjugated C=N bond (Fig. 6) (135, 347, 359). This structure probably results from a transimination reaction in which a transiently appearing acylimine is attacked by the Lys65 terminal amino group, cleaving the protein backbone. Another unusual cyclization of a side chain was found in Kusabira-Orange (KO) from the stony coral *Fungia concinna* (200). Here, Cys65 forms a new five-member thioamide ring, which extends the GFP-like chromophore core (Fig. 6) (210). The appearance of a DsRed-like intermediate during maturation of the KO chromophore was proposed in this case as well.

Remarkably, instability of DsRed-related chromophores, together with technical problems and mistakes, led to considerable difficulties in ascertaining their exact chemical structures. For example, investigation of asFP595 was accompanied by an unprecedented number of wrong assertions noted even in publication titles. The article "Cracks in the beta-can: fluorescent proteins from *Anemonia sulcata* (Anthozoa, Actinaria)" described asFP595 as significantly shorter than other GFP-like proteins (476). This conclusion was refuted in the next paper entitled "Alternative cyclization in GFP-like proteins family. The formation and structure of the chromophore of a purple chromoprotein from *Anemonia sulcata*" (271), but the suggested unusual chromophore structure was in turn demonstrated to be incorrect by Zagranichny et al. in the article "Traditional GFP-type cyclization and unexpected fragmentation site in a purple chromoprotein from *Anemonia sulcata*, asFP595" (508). The same chromophore structure and the fragmentation site of the protein backbone were assumed in the published crystal structures of asFP595 variants (19, 484). However, the most recent crystallographic, chemical, and biochemical studies indicated that the protein in fact possesses a yet different chromophore structure and backbone fragmentation site (352, 433, 495). Similarly, only chemical synthesis of the zFP538 chromophore (493) explained its complex spectral transformations and resolved the controversy between biochemical (509) and crystallographic (347, 359) data.

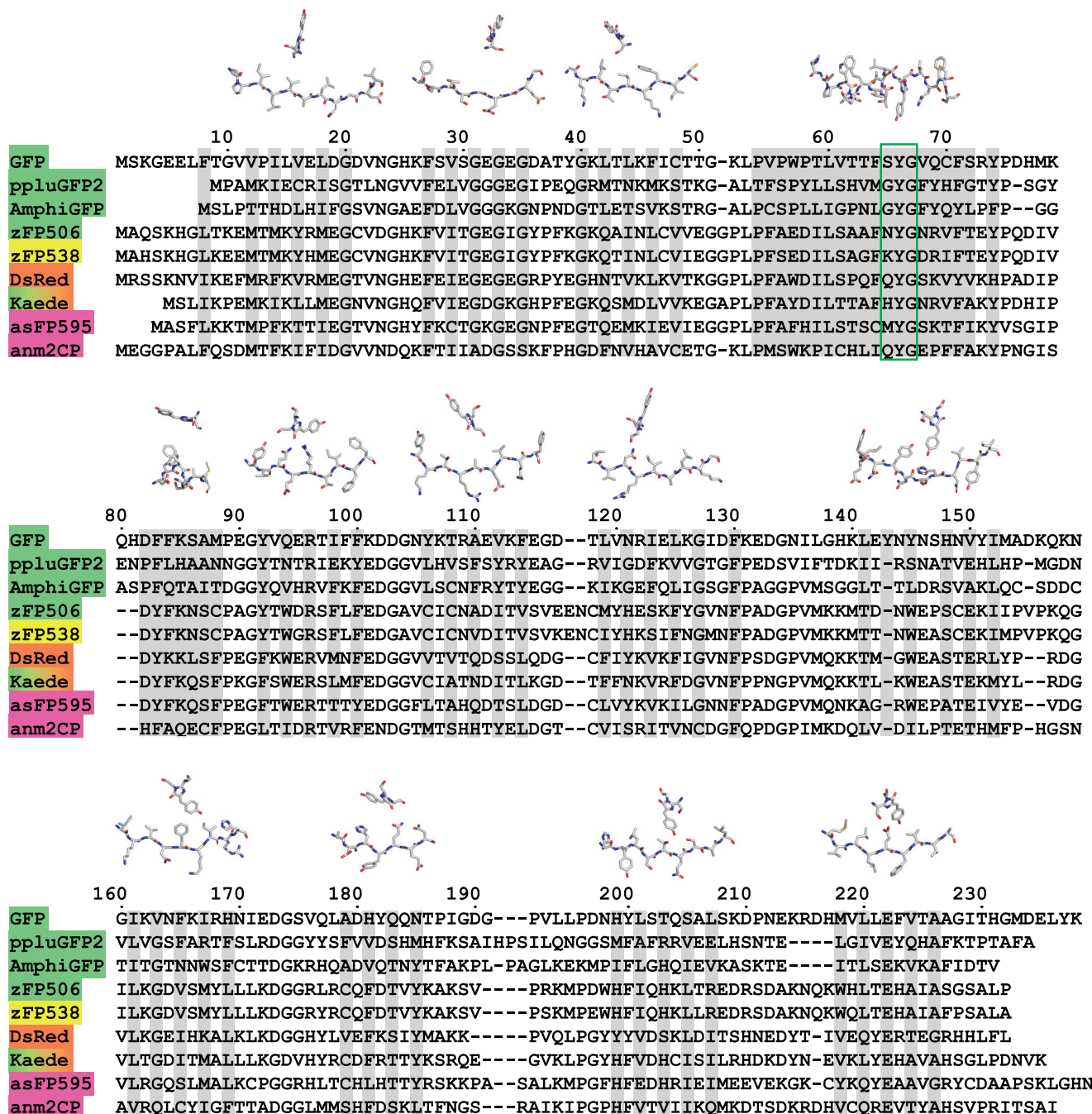


FIG. 5. Amino acid alignment of selected GFP-like proteins representing different taxa and color classes. GFP from jellyfish *Aequorea victoria*, ppluGFP2 from the copepod *Pontellina plumata*, AmphiGFP from lancelet *Branchiostoma floridae*, green zFP506 and yellow zFP538 from button polyp *Zoanthus*, red FP DsRed from mushroom anemone *Discosoma*, green-to-red photoconvertible FP Kaede from stony coral *Trachyphyllia geoffroyi*, and chromoproteins asFP595 from sea anemone *Anemonia sulcata* and anm2CP from an unidentified anthomedusa are shown. The numbering is in accordance with *Aequorea victoria* GFP. Introduced gaps are represented by dashes. The residues whose side chains form the interior of the  $\beta$ -barrel are shaded. The chromophore-forming triads are highlighted with a green rectangle. The spatial structure and positioning relative to the chromophore are shown for all  $\beta$ -strands and other selected regions above the corresponding amino acid sequences.

The green-to-red photoconvertible fluorescent protein Kaede demonstrates a principally different way of red chromophore formation. In contrast to DsRed, maturation of the Kaede-like red chromophore does not involve an oxidation step but requires light irradiation. All known

Kaede-like proteins carry His65, which appears to be indispensable for the formation of chromophore of this type. In the dark, Kaede matures to its green fluorescent form in which the GFP-like chromophore exists in equilibrium between protonated and deprotonated states. Ultravi-

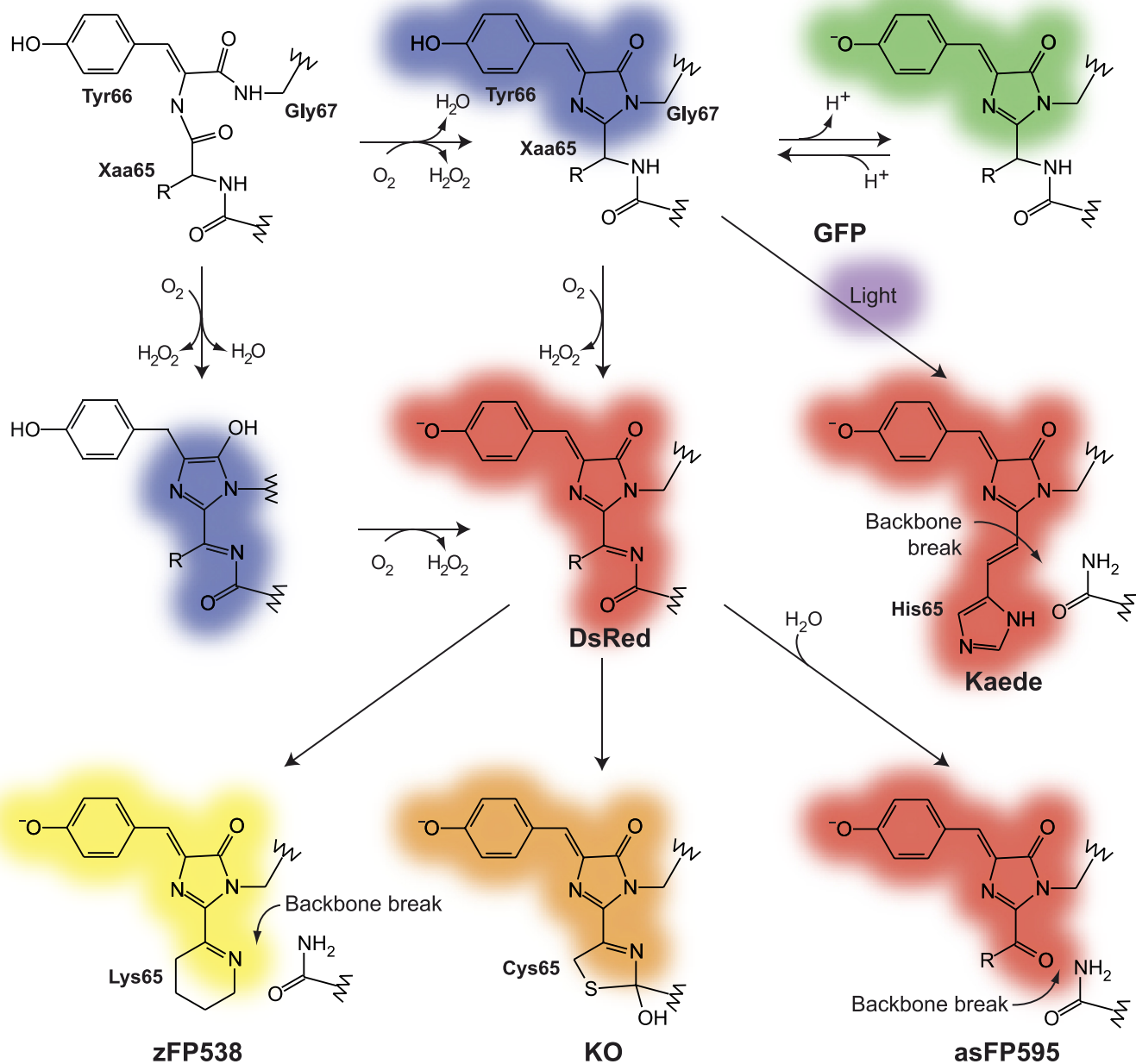


FIG. 6. Chemical structures and pathways of maturation of naturally occurring chromophores within GFP-like proteins.

olet (UV)-violet light illumination results in the conversion of the protonated chromophore into a mature red form. This conversion requires cleavage of the protein backbone between the C $\alpha$  atom and the amide N of His65 and formation of a double bond between the C $\alpha$  and C $\beta$  atoms of His65 (Fig. 6) (294). Kaede-like proteins became very popular as photoactivatable labels (see sect. VIII).

In addition to the diversity of chemical structures, crystallographic studies have revealed different conformational states of FP chromophores (Fig. 7). Most often, chromophores of FPs exist in a *cis* planar conformation.

However, some red FPs (285, 340) and all nonfluorescent GFP-like chromoproteins with known three-dimensional structures (270, 326, 349, 393) carry a *trans* nonplanar chromophore.

It is perhaps notable that the overwhelming majority of natural FPs features GFP-like chromophores in a deprotonated state. Protonated green chromophores are only rarely found, and the first FP characterized, *Aequorea victoria* wild-type GFP, is in fact very unusual in this regard. Among red-shifted proteins, DsRed-like chromophores are most common, determining spectral properties of not only red FPs but also most, if not all, chro-

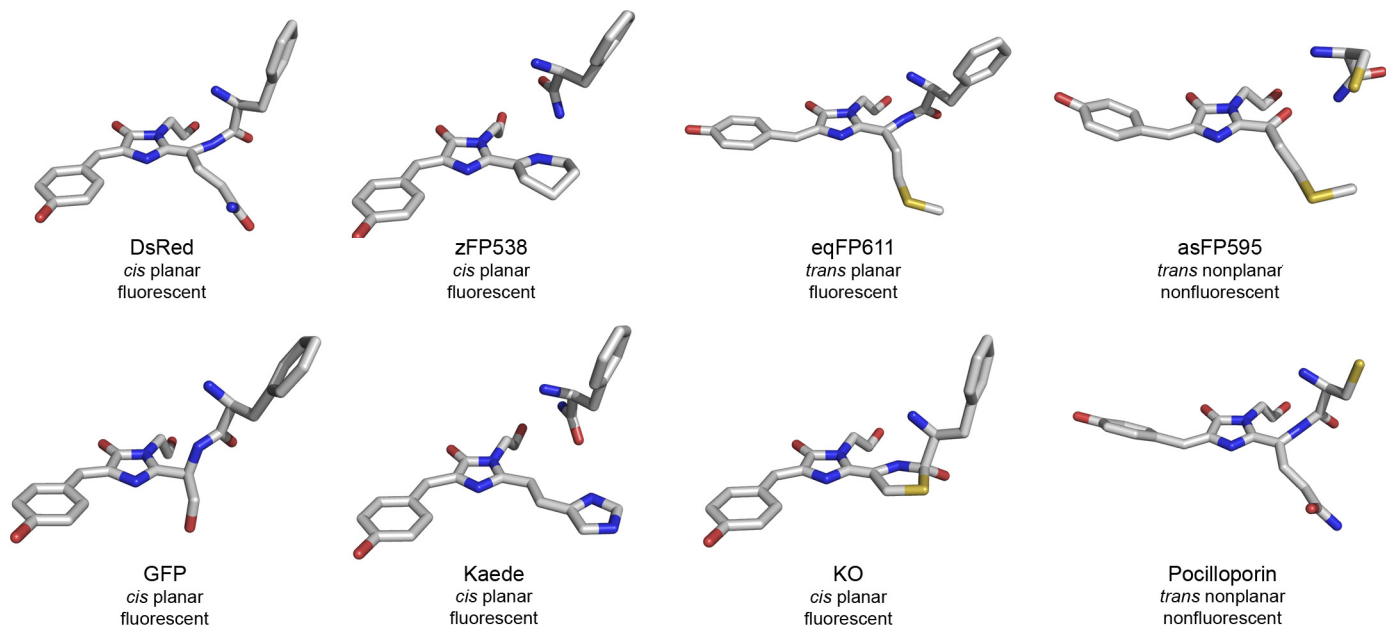


FIG. 7. Spatial structures of natural chromophores shown in stick representation. Carbon atoms are gray, nitrogen atoms are blue, oxygen atoms are red, and sulfur atoms are yellow.

moproteins (270, 326, 349, 393). Only a couple of groups within class Anthozoa opted for the green-to-red photoconvertible Kaede-like chromophore instead of a DsRed-like one for their red FPs; however, the chromoproteins of these Anthozoa are still DsRed-like (see sect. III). Other chromophore structures mentioned above have been only found once in nature thus far.

The diversity of chromophores along with the influence of their within-protein environment determines the wide spectral diversity of natural GFP-like proteins. The most commonly found spectral classes are cyan, green, red, and photoconvertible green-to-red FPs, as well as purple-blue nonfluorescent chromoproteins (Fig. 8) (239).

Cyan FPs possess relatively broad excitation and emission spectra peaking at ~450 and 485 nm, respectively (275). They contain GFP-like chromophores in which spectra are blue-shifted due to noncovalent interactions with nearby residues and buried water molecules (7, 135, 162). In addition, natural cyan FPs with protonated chromophores absorbing at ~400 nm were characterized recently (12).

Compared with cyan FPs, green FPs possess narrower and red-shifted spectra with excitation at 480–510 nm and emission at 500–520 nm. As mentioned above, GFP-like chromophores usually exist in the deprotonated state, although some proteins with a predominant neutral chromophore with absorption at 390–400 nm were found (239, 473).

Red FPs containing DsRed-like chromophores (in anionic state in all known natural proteins) possess excitation and emission maxima at ~560–580 and 570–610 nm, respectively. Some of the natural DsRed-like proteins

exhibit a “timer” phenotype (i.e., change fluorescent color over time) due to spontaneous green-to-red conversion in the process of chromophore biosynthesis (183, 239). This step of maturation of the DsRed chromophore can be enhanced by violet light irradiation (450).

Green-to-red photoconvertible Kaede-like proteins in their mature (photoconverted) red state fall into the same spectral region, but their emission spectra have a well-pronounced shoulder or even minor peak at 620–630 nm, a characteristic signature of His65 side chain incorporated into the chromophore (494).

Natural nonfluorescent chromoproteins of different hues possess a single absorption peak (at 560–610 nm for currently known proteins) that determines their color: purple for absorption maxima at 560–570 nm, lilac for 580–590 nm, and blue for >595 nm. Interestingly, examples of orange-red nonfluorescent coloration, which should correspond to an absorption peak at 480–520 nm, can be observed in coral species. Such chromoproteins likely will be characterized in the future.

Chemical modifications of DsRed-like chromophores described above are responsible for the appearance of yellow-orange FPs, zFP538 and KO, with excitation/emission maxima at 527/538 and 548/559 nm, respectively. Notably, among hundreds of natural FPs known to date, no other proteins have been identified with such spectral properties (except phiYFP, which carries GFP-like chromophore stacked with Tyr203) (12). The yellow-orange FPs and their respective chromophores thus appear to be curiosities rather than widespread biological phenomena.

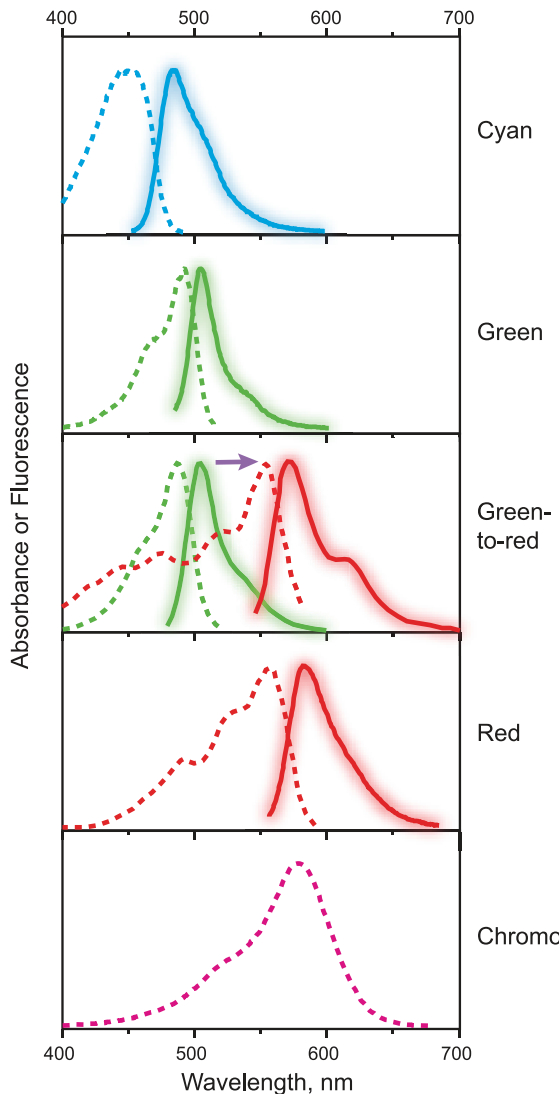


FIG. 8. Representative spectra of main spectral classes, which are widely encountered in natural GFP-like proteins. Excitation (dotted lines) and emission (solid lines) are shown for FPs. Spectra before (green lines) and after (red lines) photoconversion are shown for a Kaede-like green-to-red photoconvertible FP. Absorption spectrum is shown for a chromoprotein.

### C. Artificial Chromophores and Colors

The natural diversity of excitation-emission spectra was further extended via mutagenesis (see sect. v). Early attempts to mutate *Aequorea victoria* GFP revealed that Tyr66 of the chromophore can be substituted for aromatic side chains (Phe, His, or Trp), resulting in dramatically blue-shifted FPs (Fig. 9 and table in Fig. 10). Trp-based chromophores give off cyan fluorescence with an excitation/emission maxima at  $\sim 435/475$  nm, such as in the cyan FPs ECFP (155, 156), Cerulean (360), mTurquoise (122), and TagCFP (Evrogen JSC). His-based chromophores are characteristic of blue FPs such as EBFP (156, 361, 498), SBFP2 (230), EBFP2 (9), and Azurite (283) and have further blue-shifted excitation/emission peaks at 383/448 nm. Finally,

Phe66 provides the shortest wavelength fluorescence in GFP-like proteins with an excitation peak at 355 nm and emission peak at 424 nm, such as in the recently developed FP Sirius (430). None of these types of modification has ever been encountered in natural proteins, which invariably carry Tyr-based chromophores, for reasons yet unclear.

A textbook example of the influence of adjacent residues on spectral properties of GFP chromophore is yellow FP variant that carries the Thr203Tyr substitution. Tyr203 was inserted in GFP rationally based on the first crystal structure of GFP (324). A  $\pi$ - $\pi$  stack between Tyr203 and chromophore's Tyr66, confirmed by crystallography (463), results in significantly red-shifted spectra (excitation/emission maxima at 515/528 nm). In the following years, a number of improved yellow FP variants were developed and are currently used widely (see sect. v). It is remarkable that essentially the same chromophore environment was revealed in natural phiYFP, which was cloned much later (383).

Blue-shifted variants of DsRed-like chromophore were generated by mutation of Try66 (9, 384) or by stabilization of the blue chromophore which appears as an intermediate during normal maturation of the red chromophore (419, 419a) (Fig. 9). The introduction of Thr65 resulted in the DsRed variant mOrange, which displays orange fluorescence. X-ray studies showed that the chromophore of this protein is formed by cyclization of the Thr65 side chain (397) analogous to the above-mentioned cyclization of Cys65 in the natural orange FP KO (210).

A number of mutants in which Tyr66 was substituted for various nonaromatic residues were constructed and tested (30, 32–34, 366, 367). None of these mutants has immediate practical significance because they lack fluorescence, but they have provided valuable insights into the mechanisms of chromophore formation. Most importantly, it became clear that the chromophore biosynthesis does not require an aromatic residue at position 66 (366, 367). Also, structures that are believed to be intermediates during GFP chromophore formation were trapped, and unusual elimination and cross-linking reactions were revealed.

Extensive studies of naturally occurring FPs, along with mutagenesis-based efforts devoted to generation of their novel spectral variants, spawned the remarkable spectral diversity of FPs for practical use, described in section v.

### III. EVOLUTION OF GREEN FLUORESCENT PROTEIN-LIKE PROTEINS

Family of FPs originated very early in the evolution of Metazoa (multicellular animals) but appear to have been lost in many present-day lineages, perhaps in con-

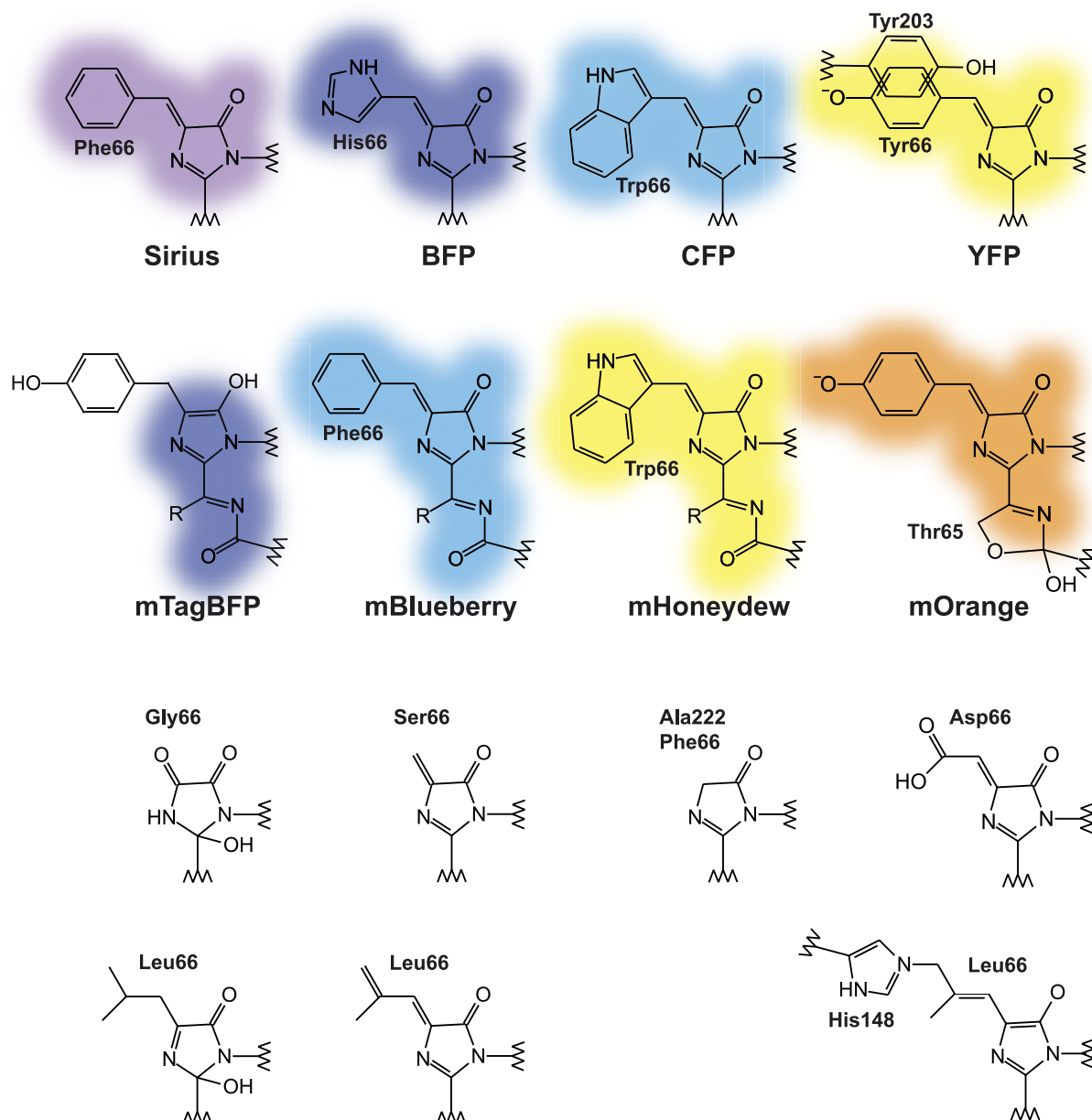


FIG. 9. Chemical structures of chromophores obtained in artificially mutated FPs. Top row: blue-shifted chromophores generated by substitution of GFP chromophore's Tyr66 by aromatic residues; also, a stacking of Tyr66 with Tyr203 utilized in YFP variants is shown. Middle row: blue-shifted modifications of DsRed chromophore obtained by stabilization of the blue acylimine-based chromophore, introduction of Phe or Trp residues instead of Tyr66, or by mutation Gln65Thr resulting in cyclization of Thr65 side chain analogous to that of Cys65 in KO. Bottom rows: colorless variants of GFP chromophore in Tyr66-substituted GFP variants.

nnection to their freshwater or terrestrial specialization. FPs exist in the host genome as a multigene family and have experienced frequent gene births and deaths, which may have facilitated their remarkable functional diversification in evolution. Due to the ease of their heterologous expression and phenotypic characterization, FPs represent an ideal model for studying the basic processes of functional diversification in protein families experimentally, using approaches such as the resurrection of ancestral proteins and evolutionary intermediates. However,

such studies have been held back by the lack of clear understanding of the actual biological function of FPs. This knowledge gap should be addressed through the experimental biology of FP-possessing organisms, such as corals, jellyfish, amphioxus, and copepods.

#### A. Where Do GFPs Come From?

Proteins sharing a GFP fold (“ $\beta$ -barrel,” consisting of 11  $\beta$ -sheets with a distorted helix threaded through the

| Protein     | Excitation peak, nm | Emission peak, nm | EC, M <sup>-1</sup> cm <sup>-1</sup> | QY   | Relative brightness | pKa  | non-comprehensive notes* | Reference(s)/Source |
|-------------|---------------------|-------------------|--------------------------------------|------|---------------------|------|--------------------------|---------------------|
| Sirius      | 355                 | 424               | 15,000                               | 0.24 | 0.11                | <3.0 | B-, pH++, Ps+            | (430)               |
| Azurite     | 383                 | 447               | 26,000                               | 0.55 | 0.43                | 5.0  | pH+, Ps+                 | (283)               |
| EBFP2       | 383                 | 448               | 32,000                               | 0.56 | 0.54                | 4.5  | pH+, Ps+                 | (9, 155, 156)       |
| TagBFP      | 402                 | 457               | 52,000                               | 0.63 | 0.99                | 2.7  | B+, pH++, Ps+, mat+      | (419)               |
| mTurquoise  | 434                 | 474               | 30,000                               | 0.84 | 0.76                | 4.5  | B+, pH+, Ps+             | (122)               |
| ECFP        | 434                 | 477               | 32,500                               | 0.40 | 0.39                | 4.7  | pH+                      | (155, 156)          |
| Cerulean    | 433                 | 475               | 36,000                               | 0.57 | 0.62                | 4.7  | pH+, Pi-                 | (360)               |
| TagCFP      | 458                 | 480               | 37,000                               | 0.57 | 0.64                | 4.7  | pH+, mat+                | Evrogen             |
| mTFP1       | 462                 | 492               | 64,000                               | 0.85 | 1.65                | 4.3  | B+, pH+, Ps+             | (7)                 |
| mUkG1       | 483                 | 499               | 60,000                               | 0.72 | 1.31                | 5.2  | B+, pH+                  | (436)               |
| mAG1        | 492                 | 505               | 55,000                               | 0.74 | 1.23                | 5.8  | B+                       | (201)               |
| AcGFP1      | 475                 | 505               | 50,000                               | 0.55 | 0.83                | -    |                          | (134)               |
| TagGFP2     | 483                 | 506               | 56,500                               | 0.61 | 1.05                | 5.0  | Ps+, pH+, mat+           | (419)               |
| EGFP        | 489                 | 509               | 55,000                               | 0.60 | 1.00                | 5.9  | Ps+                      | (77, 154, 497)      |
| mWasabi     | 493                 | 509               | 70,000                               | 0.80 | 1.70                | 6.5  | B+, pH-, Ps-             | (8)                 |
| EmGFP       | 487                 | 509               | 57,500                               | 0.68 | 1.19                | 6.0  | Ps-**                    | (79)                |
| TagYFP      | 508                 | 524               | 64,000                               | 0.62 | 1.20                | 5.5  | pH+, mat+                | Evrogen             |
| EYFP        | 514                 | 527               | 84,000                               | 0.61 | 1.55                | 6.5  | B+, pH-, Cl-             | (324)               |
| Topaz       | 514                 | 527               | 94,500                               | 0.60 | 1.72                | -    | B+                       | (79)                |
| SYFP2       | 515                 | 527               | 101,000                              | 0.68 | 2.08                | 6.0  | B+, Ps-                  | (231)               |
| Venus       | 515                 | 528               | 92,200                               | 0.57 | 1.59                | 6.0  | B+, Pi-, Ps-, mat+       | (304)               |
| Citrine     | 516                 | 529               | 77,000                               | 0.76 | 1.77                | 5.7  | B+, Ps-                  | (130)               |
| mKO         | 548                 | 559               | 51,600                               | 0.60 | 0.94                | 5.0  | pH+, Ps+, mat-           | (200)               |
| mKO2        | 551                 | 565               | 63,800                               | 0.57 | 1.10                | 5.5  |                          | (370)               |
| mOrange     | 548                 | 562               | 71,000                               | 0.69 | 1.49                | 6.5  | B+, pH-, Ps-             | (384)               |
| mOrange2    | 549                 | 565               | 58,000                               | 0.60 | 1.06                | 6.5  | pH-, Ps+, mat-           | (385)               |
| TagRFP      | 555                 | 584               | 100,000                              | 0.48 | 1.42                | <4.0 | B+, pH+                  | (285)               |
| TagRFP-T    | 555                 | 584               | 81,000                               | 0.41 | 0.99                | 4.6  | pH+, Ps+                 | (385)               |
| mStrawberry | 574                 | 596               | 90,000                               | 0.29 | 0.79                | <4.5 | pH+, Ps-                 | (384)               |
| mRuby       | 558                 | 605               | ~90,000                              | 0.35 | 1.06                | 4.4  | pH+, Ps-                 | (228)               |
| mCherry     | 587                 | 610               | 72,000                               | 0.22 | 0.48                | <4.5 | pH+, Ps+                 | (384)               |
| mRaspberry  | 598                 | 625               | 86,000                               | 0.15 | 0.39                | -    | Ps-                      | (468)               |
| mKate2      | 588                 | 633               | 62,500                               | 0.40 | 0.76                | 5.4  | Ps+, mat+                | (389)               |
| mPlum       | 590                 | 649               | 41,000                               | 0.10 | 0.12                | <4.5 | pH+, B-, Ps-             | (468)               |
| mNeptune    | 600                 | 650               | 67,000                               | 0.20 | 0.41                | 5.4  | mat-                     | (248)               |
| T-Sapphire  | 399                 | 511               | 44,000                               | 0.60 | 0.79                | 4.9  | pH+                      | (435, 512)          |
| mAmetrine   | 406                 | 526               | 45,000                               | 0.58 | 0.78                | 6.0  | Ps-                      | (6)                 |
| mKeima      | 440                 | 620               | 14,400                               | 0.24 | 0.10                | 6.5  | B-, pH-                  | (219)               |

FIG. 10. Selected monomeric FPs (updated 2009). The table includes monomeric FPs that are the best or the only one in their color class, the most popular, or the most recently published. \*\*Noncomprehensive\*\* means that absence of information does not imply any bad or good characteristics. \*\*Pronounced fast bleaching component (387). B-, low brightness; Ps-, low photostability; Pi-, strong reversible photoactivation; pH-, low pH stability; Cl<sup>-</sup>, sensitivity to Cl<sup>-</sup>; mat-, slow maturation; Ps+, high photostability; pH+, high pH stability; pH++, extreme pH stability; mat+, fast maturation; B+, high brightness.

middle) constitute a superfamily (383), uniting two protein families in which this fold is utilized for profoundly different functions. The family of GFP-like fluorescent proteins and chromoproteins is characterized by fluorescence and/or color enabled by the autocatalytic synthesis of the chromophore. The second family is composed of so-called G2F domains of nidogens, fibulins, and related multidomain extracellular matrix proteins from a variety of multicellular animals (276). In these proteins, the GFP fold serves as a protein-binding module (238). The only

two currently sequenced genomes that contain FPs, that of the starlet sea anemone *Nematostella vectensis* and the lancelet *Branchiostoma floridae*, also contain G2Fs, despite earlier claims to the contrary (37). In these genomes, G2Fs and FPs fall into their respective clusters within the superfamily tree, indicating that these two families resulted from gene duplication very early in the evolution of multicellular animals, as suggested earlier (383). G2F domains, therefore, constitute the most basal outgroup to GFP-like proteins, prompting the question of the function

of the common ancestor of these two families, which remains unclear. Unfortunately, the profound sequence dissimilarity despite nearly identical protein folds (177) between these two families precludes the most direct way of answering this question, which is through resurrection and characterization of the ancestral protein, since the reconstruction of such a sequence would be extremely ambiguous. Identification of a prokaryotic homolog of GFP would elucidate this problem to a great extent; however, to date, the only supposedly prokaryotic matches to GFP-like proteins in Genbank are either clear cases of GFP-coding vector contamination (such as GFPs from *Azotobacter*, *Azomonas*, and *Neisseria*, which are different from the GFP from *Aequorea victoria* by mere 2–5 nucleotide substitutions most likely due to sequencing errors) or the result of contamination of prokaryotic material with eukaryotic DNA, such as an intron-containing GFP-coding sequence from a marine environmental genomics dataset (Genbank accession no. AACY021567213). The only tentative functional similarity between FPs and G2Fs, which may be attributable to their common ancestor, is the molecular interface formed by the outward-facing side chains of the  $\beta$ -strands 1, 2, 3, and 11 of the fold (108, 276). In G2Fs, this is the experimentally determined protein-binding surface that is strongly conserved within the family (176). In contrast, in coral FPs this surface is hypervariable (Fig. 11), which was interpreted to be the result of diversifying positive selection driving the evolution of putative binding interface under the conditions of “evolutionary arms race” (108). It should be noted that,

whereas the protein-binding function of G2Fs is well characterized and constitutes the main function of these domains (e.g., Refs. 438, 482), for FPs it was postulated as a result of statistical phylogenetic analysis and, in the absence of direct evidence, remains highly speculative. To clarify this issue, an experimental investigation of protein-binding properties of natural FPs would be of considerable interest.

## B. FP Is an Ancient Metazoan Gene

FPs appear to be a protein family specific to Metazoa with a remarkably patchy distribution across phyla. To a significant extent, both Metazoa specificity and patchiness may be the result of incomplete and biased sampling; however, the fact that only two of the currently sequenced animal genomes contain FP genes clearly indicates that FPs are far from ubiquitous in Metazoa. Still, there are currently enough examples of FP-containing animals to conclude that the common ancestor of all Metazoa most likely possessed the FP gene (86, 383).

FPs are currently known to exist in four phyla of multicellular animals: Cnidaria, Ctenophora (comb jellies), Arthropoda, and Chordata (Fig. 12). Coincidentally, these four phyla provide a reasonably good sampling of the most basic partitions of the metazoan tree of life. Cnidaria and Ctenophora represent radially symmetrical animals (Radiata), which are, according to current views, not closely related (i.e., do not form a clade within the phylogenetic tree). Of these, Ctenophora split off the main stem of the metazoan tree of life especially early: it is generally accepted that comb jellies are a more ancient lineage than cnidarians, and one analysis even suggests that Ctenophora is the most basal phylum of all Metazoa (99). Arthropoda and Chordata belong to a group of bilaterally symmetrical animals (Bilateria) and represent the two major partitions, Protostomia and Deuterostomia, respectively. The discovery of FPs in all these taxa, therefore, strongly suggests that the FP gene was acquired very early during metazoan evolution (86, 383).

It should be noted, however, that the basal phylogeny of FPs (Fig. 12) does not fully match the currently accepted gross phylogeny of the host animals. Instead of constituting one of the basal lineages of the FP family, GFP from the ctenophore *Haeckelia beehleri* (143a) groups with Cnidaria, reminiscent of the now-dismissed grouping of cnidarians and ctenophores within the phylum Coelenterata. Moreover, even within the “Coelenterata” clade, the ctenophoran FP does not occupy a basal position but falls firmly into the clade of hydrozoan FPs. The easiest explanation for such a puzzling pattern is contamination of the ctenophore material with ingested hydrozoan medusae, which is quite likely since ctenophores of the genus *Haeckelia*

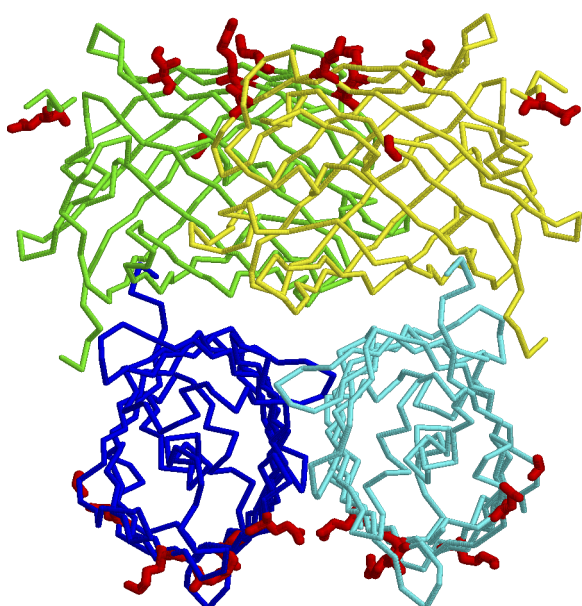


FIG. 11. Hypervariable amino acid positions (side chains rendered in red) mapped onto the structure of a typical coral FP tetramer. This pattern was interpreted as a binding interface requiring continuous readjustments through positive selection because of the “evolutionary arms race” against an unknown binding target. [From Field et al. (108).]

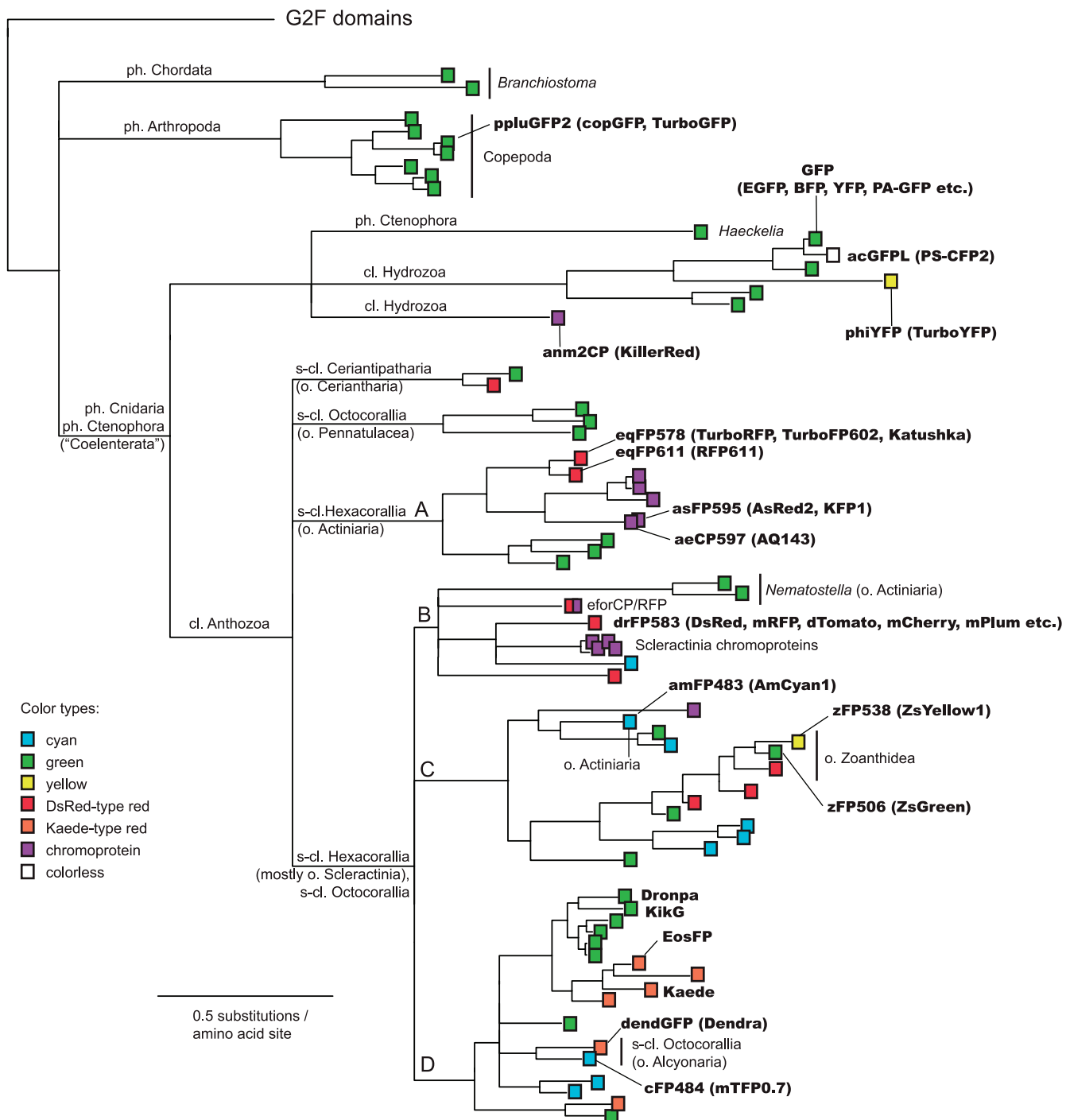


FIG. 12. Phylogenetic tree of representative FPs, reconstructed from the protein sequences using MrBayes 3.1 (181) under the “mixed” model. The branches with a posterior probability <0.95 are collapsed. Individual sequences are represented by boxes corresponding to their color type (see legend). Only the names of the proteins mentioned throughout the text of this review are shown, with their commercial names and/or mutant derivatives given in brackets. The systematic affinity of the host organisms is indicated. The clades designated A–D correspond to the groups originally reported in Ref. 239.

indeed specialize in preying on medusae (142). Otherwise, to reconcile the topology of the FP family with the currently accepted gross phylogeny of multicellular animals, one is forced to assume that Bilateria and Anthozoa inherited a different paralogous lineage of

FPs than Ctenophora and Hydrozoa and that these two paralogous lineages separated from each other perhaps even before the origin of multicellular animals. Unlikely as this sounds, given the peculiar birth/death dynamics of FP genes within a genome (see below), this possi-

bility is not entirely implausible. An alternative explanation may be the artifact of phylogenetic reconstruction known as the long branch attraction (106), since both ctenophore and hydrozoan FPs form long branches in the tree (Fig. 12). In that case, however, one would expect them to group with G2Fs, which form the longest branch. Improved sampling of diverse ctenophoran FPs will help resolve this issue.

It is tempting to attribute the lack of FPs in most model organisms with sequenced genomes to their terrestrial or freshwater origin, implying that the primary (frustratingly, still unknown) biological function of FPs is somehow related to the marine environment. Indeed, the current list of organisms harboring FPs consists exclusively of marine species. Among cnidarians, FPs are notably absent in the genome of the freshwater *Hydra* but are common in marine representatives of the same class (Hydrozoa) (134, 383, 392) and reach the highest known diversity in the exclusively marine class Anthozoa (12, 239, 275). Interestingly, representatives of the other three classes of Cnidaria, Scyphozoa, Cubozoa, and Staurozoa, all of which are large jellyfish of different kinds, despite also being exclusively marine, thus far have not yielded FPs and are not known to fluoresce, at least not in their adult forms (M. Matz, unpublished data). It would be interesting to look for fluorescence in the diminutive polyploid stage of the life cycle of these jellyfish.

Given these phylogenetic complications, it is reasonable to ask the following question: did fluorescence evolve only once in the FP family? A strong argument in favor of the single fluorescence origin is that, on the basis of spectroscopy (383), X-ray crystallography (103, 483), and patterns of sequence conservation (37, 86), it appears that in both cnidarian and bilaterian FPs follow the same structural solution to achieving fluorescence, which involves modification of Tyr66 and Gly67 to form a chromophore with the help of Arg96 and Glu222 side chains as key catalytic groups. Still, given the paucity of phyla that thus far have yielded FPs, as well as many unanswered questions concerning the mechanisms of the chromophore biosynthesis, the possibility of independent evolution of fluorescent FPs in different animal groups should not yet be discounted.

### C. Overview of Natural FP Diversity

Within Cnidaria, class Anthozoa contains the greatest diversity of FP colors (12, 239, 275) (it should be noted, however, that anthozoan FPs are also the best sampled). Multicolored FPs are found in all three subclasses of Anthozoa (Ceriantipatharia, Hexacorallia, and Octocorallia; Fig. 12).

A notable feature of the FP phylogeny of Anthozoa is that it fails to recapitulate the systematics of the host

organisms, which may be a consequence of a peculiar gene gain/loss pattern among anthozoan FPs, limited understanding of anthozoan phylogeny, or both (12, 239). The only “well-behaved” sequences are the two proteins from subclass Ceriantipatharia (cloned from tube anemones; Refs. 185, 477), which form a separate basal clade; however, it remains to be seen whether this grouping will hold when more representatives of this subclass are analyzed. Proteins from the other two subclasses (Octocorallia and Hexacorallia) are intermixed with each other, sometimes recapitulating individual orders (such as Pennatulacea, Alcyonacea, and Zoantharia), but generally do not follow a systematic pattern. The best-characterized group of all cnidarians, reef-building corals of the order Scleractinia, is represented by three diverse clades (clades B, C, and D of Ref. 239; Fig. 12). Of these, only the gene lineage represented by clade B is found in all corals, in the form of nonfluorescent chromoproteins. The other two lineages underwent sorting between coral groups so that a given coral species may contain FPs of either clade C or clade D, but not both (12). This was accompanied by independent evolution of the typical fluorescent color diversity within each lineage. In particular, within clade D, the origin of fluorescent color diversity clearly predated the separation of coral families represented there, which indicates that corals became colorful as early as the late Triassic-early Jurassic period, in the very beginning of the modern-type coral reefs (206). Also within clade D, a unique solution to red fluorescence was found in the form of the Kaede-like chromophore (294). All red proteins within clade D are Kaede-like, whereas in the rest of the tree, only DsRed-like red proteins are found (12).

Another class of Cnidaria, Hydrozoa, yielded the most divergent FP sequences; however, most of these proteins are green. There are two notable exceptions (383): the yellow fluorescent protein from *Phiallidium* sp., which nevertheless possesses the typical “greenlike” chromophore structure, and a purple chromoprotein from an unidentified anthomedusa, which was developed into the unique genetically encoded photosensitizer KillerRed (50) (see sect. x). It is also interesting to note a peculiar colorless FP, which was cloned from a nonfluorescent relative of the most famous jellyfish in the world [*Aequorea victoria*, the host organism of the original GFP (392), *A. coerulescens* (134)]. In this protein, following some Carroll-like nonsensical logic (61), fluorescence can be rescued by removing one of the side chains that is strictly conserved in FPs and is considered critical for chromophore formation (Glu222).

Thus far, the only taxon of protostome bilaterian animals that yield FPs is the class Maxillopoda, subclass Copepoda, which is part of phylum Arthropoda, subphylum Crustacea. Within copepods, FPs were cloned from representatives of two families, Pontellidae (383) and Aeteidae (273), both belonging to the same order (Cal-

anoida). GFP-like fluorescence was observed in at least one open-ocean representative of another order of copepods, Harpacticoida (Matz, unpublished data). All currently known Copepoda FPs possess typical GFP-like chromophores. Importantly, Copepoda FPs tend to exhibit several properties that are beneficial for their application in biotechnology: high brightness, low oligomerization tendency, and fast fluorescence development (103). It therefore may be interesting to survey copepods for FPs in a systematic fashion, primarily focusing on marine species from the open ocean.

Among deuterostomes, several FPs were recently found in two species of the lancelet (also known as amphioxus), genus *Branchiostoma* (phylum Chordata, subphylum Cephalochordata; Refs. 37, 47, 86). Other deuterostome genomes, even for marine species such as the sea urchin *Strongylocentrotus* or sea squirt *Ciona*, do not seem to contain FP genes (47). Some *Branchiostoma* FPs have a very high molar extinction coefficient ( $130,000\text{ M}^{-1}$ ) (37), suggesting that they may yield promising markers; however, their quantum yields have not been reported.

#### D. FPs Form Multigene Families in Host Genomes

The first indication that FPs are present in multiple copies in the host organism genome came from the fact that multiple FPs of different color could be cloned from the same organism (275). Later, an extensive analysis of FP sequences expressed in the great star coral *Montastrea cavernosa* demonstrated that multiple FP genes may correspond even to the same color of fluorescence: each of the principal fluorescent colors (cyan, green, and red) in this coral was determined by more than one gene, which now appears to be a typical situation for corals (12, 95, 206). Recent analysis of the fully sequenced genome of the lancelet *Branchiostoma floridae* revealed that this animal possesses 16 FP genes (37, 47). According to the results of heterologous expression of 15 of these proteins in bacteria, 14 of them encode GFPs. Of the remaining two, one was expressed in bacteria but failed to develop any color; for the other, expression was not attempted since its sequence contained a mutation that should have inhibited chromophore formation (Gly67-Ala). Only 3 of these 16 genes were abundantly expressed (47). The 16 lancelet FPs form 6 groups of closely related sequences, many of them produced by tandem duplications. Notably, the expansion of gene diversity within these groups appears to have occurred independent of another lancelet species, *Branchiostoma lanceolatum* (47). A quick glance at the genome and EST database of another FP-containing organism, the starlet sea anemone *Nematostella vectensis*, suggests a similar pattern: only two genes are expressed abundantly, while many more are encoded in the

genome, including partial genes and versions with deleted chromophore-forming sequences (Matz, unpublished data).

These observations suggest that frequent gene duplication and loss must be a key factor in the evolution of FPs. It is hardly surprising that the phylogeny of genes fails to follow the systematic position of the host organisms, since in most cases the genes from different species must be paralogs rather than orthologs. It is also tempting to speculate that frequent gene duplication may facilitate the evolution of color diversity. In general, FPs may provide a useful experimentally tractable model for studying the effects of gene duplication and loss on the evolution of functional diversity in protein families.

#### E. Color Evolution

Origins of different colors and associated chromophore types are arguably the most interesting aspects of the FP family evolution. In addition to the general interest for understanding the mechanisms of functional diversification in proteins, knowledge of the mutational pathways leading to different spectral properties and chromophore structures would be an important step toward the rational design of FP-like fluorescent labels ab initio, which would allow their precise tailoring for the needs of particular applications.

Of all the naturally occurring proteins, FPs are perhaps the most amenable to experimental studies of evolutionary modification, owing to their robust expression in bacteria and the ease of phenotypic characterization. Ugalde et al. (442) applied an ancestral reconstruction methodology to demonstrate that the common ancestor of the three fluorescent colors within clade D was green and that the complex Kaede-like red color (requiring one additional autocatalytic modification reaction to form the chromophore) evolved from it in a gradual fashion (Fig. 13). This result also implied that the red color within clade D appeared more than once. The general notion of pervasive convergent evolution of FP color diversity in corals was recently corroborated by reconstruction of the common ancestor of all three coral FP clades, which also turned out to be green (12). This study was taken further by Field et al. (108), who applied statistical phylogenetics to detect signatures of positive selection along the individual lineages leading to the new colors within clade D. This analysis demonstrated that the evolution of both cyan and red colors was facilitated by natural selection and identified the mutations involved. The key determinant of the cyan color turned out to be a mutation at site 167: it alone turns the ancestral green protein cyan, while its reversal in the extant cyan protein restores the ancestral green color. Likewise, the reversal of the three muta-

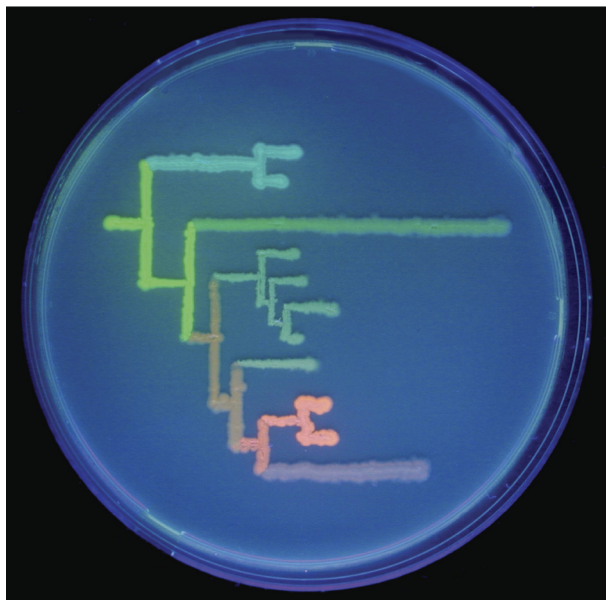


FIG. 13. Phylogenetic tree for a subset of clade D FPs, drawn on a petri dish using bacteria expressing extant and recreated ancestral proteins, under ultraviolet type A illumination. The more complex red fluorescent color evolves from ancestral green in a gradual fashion. [From Ugalde et al. (442).]

tions that were positively selected in the red lineage severely affects the efficiency of red chromophore maturation. The fact that the individual mutations that were under selection were critical for the new colors constitutes strong evidence for the biological role of FP colorfulness in reef-building corals. In the case of red color, however, introduction of the three candidate mutations into the green ancestor did not bring about even a trace of redness, indicating that mechanisms other than natural selection (such as neutral drift) must have been involved in assembling the necessary mutation combination. This combination was recently determined through analysis of a library of possible evolutionary intermediates between green and red proteins and was found to include a staggering 12 mutations (of a total 37 transitional mutations) (109). Most of these mutations could not have been predicted from purely structural considerations, since they affect sites that do not modify the chromophore environment directly. Instead, it appears that the evolution of additional chromophore modification capacity associated with the red color was enabled through adjustments of the overall protein fold, leading to subtle realignment of the chromophore and surrounding side chains. This hypothesis can be substantiated in the future by crystallography studies of resurrected ancestral proteins and evolutionary intermediates. It would also be very interesting to apply the same approach to other cases of color diversity evolution, such as independent evolution of Kaede-like red proteins within clade D and the origin of DsRed-like red proteins within clade C.

## F. Biological Functions of FPs

Despite the great interest in FPs from a biotechnology point of view and correspondingly numerous works devoted to their structure, mutation analysis, and adaptation to various labeling applications, their biological function remains highly controversial. Multiple hypotheses have been proposed based on laboratory studies of cloned proteins, but none of these has been verified in actual experiments with host organisms, such as corals or jellyfish. At the moment, it is not even clear whether the primary function of FPs is related to their fluorescent ability or whether fluorescence is simply a side effect of some other functional activity.

The suggested fluorescence-related functions can be grouped into two classes: photosynthesis modulation and optical communication. The first applies to reef-building corals that host algal symbionts ("zooxanthellae"): it has been suggested that the presence of FPs may scatter photosynthetically active radiation and thus either dissipate its excess in high light, providing photoprotection (204, 371), or deliver the unabsorbed light back to the zooxanthellae under low light conditions (371). Indeed, there is a correlation between fluorescence and stress resilience in morphs of the same species (371), and FP expression is upregulated by high light, especially by the blue light that is the most photosynthetically relevant (83). However, there are numerous counter-arguments, and we list only three that seem the most compelling. First, FP fluorescence in corals is typically not strong enough to make any appreciable impact on the light field experienced by zooxanthellae (279). Second, FP colors other than green are suboptimal or even completely unsuitable for photoprotection or photoenhancement due to mismatch with the photosynthesis action spectrum, yet the color diversity is relevant for coral survival, as demonstrated by statistical phylogenetic analysis (108). Third, numerous anthozoans do not contain symbionts yet display bright and often multicolored fluorescence (184, 378).

The visual communication function is most commonly associated with green FPs from bioluminescent organisms, such as jellyfish *Aequorea victoria* or sea pansy *Renilla reniformis* (194, 392, 474). In these animals, green FP is associated with the light-producing enzyme (aequorin or luciferase) and converts its inherently blue emission into green through a nonradiative energy transfer mechanism (300, 301, 474). This association sometimes results in the improvement of the overall bioluminescence quantum yield (474), but not always (for example, not in *Aequorea victoria* bioluminescent system; Refs. 124, 301), prompting the search for an explanation related to the blue-to-green color conversion. This need is most commonly attributed to the fact that green light in greenish coastal water is less attenuated than blue

(191) and thus would be visible over longer distances (299). There is a problem with this explanation, however, since the luminescence in jellyfish is initiated by mechanical stimulation (e.g., Refs. 150, 164) and does not have to travel far to the eye of the attacker; besides, green luminescent species are found not only in coastal waters, but also in the open ocean that is the most transparent in the blue, rather than green, region of the spectrum (143). Another explanation, which appears more likely to us, is that the green color is more visible since it better fits the spectral sensitivity of the eyes of potential predators (268, 331, 332). We would like to suggest one additional possibility: that green rather than blue luminescence may be an adaptation for better signal visibility in the presence of light (during the day at shallow depths), since green luminescence would produce a stronger contrast against the blue background of the ocean water. This possibility is supported by the abundance of green-fluorescent, but nonbioluminescent medusae in the well lit open ocean, in which FPs may serve as a “daytime analog of bioluminescence” (383).

Localization of green fluorescence in tentacles and oral appendages of many hydrozoans, including medusae and siphonophores (Matz, unpublished data) (143), immediately suggests the prey attraction function; however, the obvious may not be true in this case. An alternative explanation for such localization, as previously mentioned, is that localization of fluorescence in these retractable body parts provides the possibility of generating a deterring “fluorescence flash” in response to mechanical stimulation, resulting from a concentration of fluorescence within a small volume as a result of rapid retraction of the previously extended fluorescent body part (383). To verify these hypotheses, experiments with live fluorescent jellyfish are required, where the jellyfish would be exposed to potential prey and predators under different light conditions (either improving or diminishing the visibility of fluorescence).

What types of prey might be attracted to the green fluorescence of jellyfish and corals? For the large predatory flower hat jelly *Olindias formosa*, which possesses strong green fluorescence in the tentacles, it may be small fish (S. H. D. Haddock, personal communication). For corals and a plethora of smaller jellyfish, one possibility is diverse larvae of marine invertebrates, most of which show positive phototaxis with one of the sensitivity maxima in the green region (111). It is conceivable that, even despite the fact that larvae cannot form visual images and navigate to the tentacle from a distance, the green fluorescence in the tentacle in close proximity may induce the larva to change its swimming trajectory sufficiently to increase the chance of its capture. Corals also sometimes exhibit patterns of fluorescence that suggest a role in prey attraction. For example, the area immediately surrounding the polyp’s mouth is very commonly brightly fluores-

cent green (but sometimes, red), and tentacles may also show green fluorescence. For corals in particular, there is an interesting qualitative observation (173) that free-swimming dinoflagellate algae of the genus *Symbiodinium*, the ones that form symbiosis with corals, seem to be attracted to the green light. If so, green fluorescence of tentacles and oral region in coral polyps may serve as an attractor for potential symbionts.

Another visual function of green fluorescence may be realized in pontellid copepods, in which it has been suggested to serve as a mate recognition signal (383). This idea is supported by species-specific pattern (383) and the sexual dimorphism of fluorescence (Matz, personal observation). However, this hypothesis would be difficult to test experimentally.

In corals, fluorescent and nonfluorescent coloration derived from FPs seem to be suitable for eliciting strong visual responses from fishes inhabiting the reef, so corals are indeed colorful in the ecological sense of the word (277). The role of such signaling remains unclear but may include aposematic (warning) function to advertise the coral’s unpalatability. Another curious function that was suggested by an analysis of the ability of fish to discern coral colors is that in some cases fluorescence seems to mask the presence of symbiotic algae in the coral tissues, thereby perhaps hiding the algae from the eyes of herbivorous fishes. Both signaling and “algal camouflage” functions wait to be substantiated by behavioral experiments with reef fishes *in situ*.

Several functions unrelated to fluorescence directly have been suggested as a result of exploring additional activities of heterologously expressed FPs. The GFP from *Aequorea victoria* has been shown to transport protons across its globule as a result of its complicated photocycle (4, 5), which for corals prompts a hypothesis of FP involvement in regulating the deposition of calcium carbonate skeleton, a process that is highly pH dependent. Although most green coral FPs have permanently anionic chromophores (12) and therefore do not feature the GFP-like photocycle, their occasional accumulation in the coral tissue responsible for skeleton deposition (calicoblastic ectoderm, Ref. 267) provides support for such an idea. Induction of chromoproteins and red fluorescent protein in the immunocompromised coral tissues suggested their role in coral immunity (329, 330), which is corroborated by *in vitro* demonstration that FPs can scavenge reactive oxygen species (47, 48). It would be interesting to explore whether red coral FPs and chromoproteins exhibit scavenging activity as well.

Arguably the most intriguing alternative FP function was suggested by the recent finding that green FPs can act as light-driven electron donors in concert with appropriate electron acceptors, including biologically relevant ones (45). This was found to be a common feature of GFPs of different origins, including jellyfish, anthozoans,

copepods (45), and lancelets (K. A. Lukyanov, unpublished data). Interestingly, electron transfer can be mediated only by FPs with a natural Tyr66-based chromophore, while mutants with artificial Trp66- or His66-based chromophores are inactive in this regard. This observation provides an indirect indication of the biological significance of this phenomenon and a plausible explanation of absolute conservation of Tyr66 in natural FPs. For example, FP-mediated redox reactions may participate in diverse cellular processes such as light sensing or the production of reductive equivalents.

At the same time, the light-induced transfer of two electrons from an FP to an oxidizer *in vitro* results in irreversible inactivation of the FP, which makes the prospect of using FPs as electron donors *in vivo* rather wasteful and therefore not very likely. The only possible exception may be sensory function (45), since it does not require massive electron transfer. It is easy to imagine that an FP *in vivo* may be simultaneously accepting electrons from somewhere to prevent its inactivation and thereby functions as a true light-dependent electron pump. If such an activity is demonstrated, the role of FPs in animals will have to be completely reconsidered. For example, it would be tempting to speculate that the original role of GFP in bioluminescent systems was photoregeneration of spent luciferin, coelenterazine, during the daytime.

#### IV. KEY CHARACTERISTICS FOR PRACTICAL USE

The natural diversity of FPs has provided scientists with a rich palette of variants with different biochemical and spectral characteristics, which represent a huge source of potentially powerful molecular tools for numerous applications in the study of complex biological systems. However, the properties of wild-type FPs are determined by their natural function(s) (as yet unknown; see sect. III). The purpose of natural evolution could differ essentially or even contradict that of researchers employing FPs in fluorescent microscopy and other fluorescent techniques.

Below we will consider, one by one, the key characteristics of FPs that might be important for their practical use. These considerations, however, cannot be comprehensive since each particular assay or experimental setup may require a specific choice or optimization of an FP.

##### A. Brightness: QY and EC

Sensitivity and signal-to-noise ratio of any fluorescence detection technique clearly depend greatly on the brightness of the fluorophore employed. For fluorescent labeling in living systems, high brightness of an FP provides additional advantages. In particular, the brighter

FPs require a lesser dose of excitation light, and thus lower phototoxic effects occur. It is also important that a bright FP or its fusion construct can be used in lower amounts, minimizing intervention in natural processes.

Many of the naturally occurring FPs are characterized by high brightness determined both by a molar extinction coefficient exceeding  $100,000 \text{ M}^{-1} \cdot \text{cm}^{-1}$  and a fluorescence quantum yield approaching the theoretical limit of 1. Also, for the enhancement of artificially derived FP variants (such as monomerized FPs), brightness is the easiest parameter to improve, through mutagenesis followed by screening of expression libraries for brighter clones. The mutants may be generated *in vitro* by random or site-directed mutagenesis, which is the most common way, or using somatic hypermutation approach (468, 469). The palette of FPs is therefore rich in bright variants (see the next section).

Along the visible spectrum, the obtainable brightness seems to be maximal for those FPs that have a peak emission at  $\sim 500\text{--}530 \text{ nm}$  (green and yellow FPs) and decreases toward its limits (blue and far-red FPs). This apparent trend is likely due to the physical properties of the GFP-like chromophore, which is the predecessor of all FP chromophores, and by its surrounding formed by a homotypic  $\beta$ -barrel structure. Nevertheless, recent efforts have resulted in development of substantially brighter variants with emission peaks in the blue and far-red regions, indicating that some progress is still possible (see tables in Figs. 10 and 14).

However, enhancement of an FP brightness during its optimization can happen at the expense of other characteristics, such as its monomeric nature and pH- and photostability. Meanwhile, FP of lower brightness but higher photostability can result in better signal-to-noise ratio, especially for experiments involving long time series. Therefore, brightness should not be the only parameter considered while choosing an FP for a particular application.

It should also be kept in mind that fluorescent brightness measured for an FP sample *in vitro* cannot be directly extrapolated to its actual brightness *in vivo*. Indeed, the resulting signal brightness generated by an FP expressed in living cells is determined not only by its intrinsic spectral characteristics, but also by such parameters as transcription and translation efficiency, mRNA and protein stability, and chromophore maturation rate (see below). These parameters can differ for various FPs and their fusion constructs. Importantly, at the single molecule level, an FP can demonstrate much higher brightness than that measured for the ensemble of FP molecules in a sample (413).

##### B. Maturation Rate

FP fluorescence appears after protein folding and chromophore maturation, which includes several consecutive covalent modifications that are especially extensive for orange and red FPs (see sect. II). Usually, chromo-

| Protein           | Excitation peak, nm | Emission peak, nm | EC, M <sup>-1</sup> cm <sup>-1</sup> | QY   | Relative brightness | pKa | Non-comprehensive notes*   | Reference/Source |
|-------------------|---------------------|-------------------|--------------------------------------|------|---------------------|-----|----------------------------|------------------|
| AmCyan1           | 458                 | 489               | 39,000                               | 0.75 | 0.89                | -   | T                          | (275, 499)       |
| Midori-Ishi Cyan  | 472                 | 495               | 27,300                               | 0.90 | 0.74                | 6.6 | D, B+, pH-                 | (200)            |
| copGFP (ppluGFP2) | 482                 | 502               | 70,000                               | 0.60 | 1.26                | 4.3 | T, B+, pH+, Ps+, Mat+, Ag- | (383)            |
| TurboGFP          | 482                 | 502               | 70,000                               | 0.53 | 1.12                | 5.2 | D, B+, pH+, Ps+, Mat+      | (103)            |
| ZsGreen           | 493                 | 505               | 43,000                               | 0.91 | 1.19                | -   | T, B+                      | (275, 499)       |
| TurboYFP          | 525                 | 538               | 105,000                              | 0.53 | 1.69                | 5.9 | D, B+, Ps+, Mat+           | (383)            |
| ZsYellow1         | 529                 | 539               | 20,000                               | 0.65 | 0.39                | -   | T                          | (275, 499)       |
| TurboRFP          | 553                 | 574               | 92,000                               | 0.67 | 1.87                | 4.4 | D, B+, pH+, Mat+           | (285)            |
| dTomato           | 554                 | 581               | 69,000                               | 0.69 | 1.44                | -   | D, B+, Ps+                 | (384)            |
| DsRed2            | 563                 | 582               | 43,800                               | 0.55 | 0.73                | -   | T, B+                      | (275, 499)       |
| DsRed-Express     | 555                 | 584               | 38,000                               | 0.51 | 0.59                | -   | T, Ps+, Mat+               | (42)             |
| DsRed-Express2    | 554                 | 591               | 35,600                               | 0.42 | 0.45                | -   | T, Ps+, Mat+               | (415)            |
| DsRed-Max         | 560                 | 589               | 48,000                               | 0.41 | 0.60                | -   | T, Ps-, Mat+               | (415)            |
| AsRed2            | 576                 | 592               | 61,000                               | 0.21 | 0.39                | -   | T                          | (275)            |
| TurboFP602        | 574                 | 602               | 74,400                               | 0.35 | 0.79                | 4.7 | D, B+, pH+, Mat+, Ps-      | EvoGreen         |
| RFP611            | 555                 | 606               | 120,000                              | 0.48 | 1.75                | -   | T, B+, Ps-                 | (227)            |
| Katushka          | 588                 | 635               | 65,000                               | 0.34 | 0.67                | 5.5 | D, B+, pH+, Ps+, Mat+      | (388)            |
| Katushka2         | 588                 | 633               | 69,000                               | 0.37 | 0.77                | 5.5 | D, B+, pH+, Ps+, Mat+      | (389)            |
| AQ143             | 595                 | 655               | 90,000                               | 0.04 | 0.11                | -   | T, B-                      | (394)            |

FIG. 14. Selected dimeric and tetrameric FPs (updated 2009). \*\*“Noncomprehensive” means that absence of information does not imply any bad or good characteristics. T, tetrameric; D, dimeric; B-, low brightness; Ps-, low photostability; pH-, low pH stability; Ag-, aggregation; Ps+, high photostability; pH+, high pH stability; mat+, fast maturation; B+, high brightness.

mophore maturation is the rate-limiting step for the FP to become fluorescent. Depending on the particular FP, oxygen concentration, and temperature, maturation can take from several minutes (103, 304) to hours or even days, as in the case of Timer FPs (418, 425) (see sect. vi).

For practical use, the maturation rate should be reasonably fast to obtain a high and stable fluorescent signal. Most FPs in use have a maturation half-time from ~40 min to 1–2 h, which is sufficient to label cells, organelles, and proteins of interest and to perform various quantitative experiments. However, for some applications, such as early detection of promoter activation, labeling proteins of interest with a short lifetime, or monitoring single translational events, FPs with very fast maturation are needed. For example, fast-maturing yellow FPs allowed the direct observation of the production of a single protein molecule in real time (503).

At the same time, the quantitative measurement of an FP maturation rate is not a trivial task, especially for fast maturing proteins. Probably the most accurate approach to measure the FP maturation rate requires the denaturation of an FP and reduction of a chromophore using dithionite (103, 304, 357). This approach is commonly used to follow fluorescent protein maturation starting from the native polypeptide, but it is only applicable to green and yellow FPs, since dithionite reduction often leads to irreversible destruction of red FPs (our observations). Alternatively, maturation can be traced in living bacteria (230, 231) or for the proteins rapidly purified after expression under anaerobic conditions that prevent chromophore maturation (285, 384). Finally, a rough com-

parison of FP maturation rates can be performed in living eukaryotic cells. However, this latter approach can give results quite different from in vitro data, due to differences in FP expression efficiency, turnover rates, etc.

In general, the diversity of techniques employed to measure maturation rates still does not allow for accurate comparisons of all FPs. A comprehensive study is needed to compare maturation rates of the most popular FPs in a single assay. Nevertheless, measurements performed using the same system in the same laboratory (or strictly following the same criteria) make it possible to assess the relative maturation rate for at least some of the FPs. In this paper, we mark fast maturing proteins as “Mat+” (tables in Figs. 10 and 14).

### C. Photostability and Undesirable Photoconversions

Photostability of FPs is one of the cornerstones of a successful imaging experiment and becomes the key factor for the long time series, for gathering weak fluorescent signals, and for quantitative measurements, including FRET techniques. The chromophore of FPs is protected from the environment by the protein shell. This largely determines the generally high photostability and low phototoxicity of wild-type FPs, which is probably important for their natural function in sea creatures. Low phototoxicity is also inherited by most mutant variants of natural FPs known to date, except KillerRed (see sect. x). Successful mutant variants also preserve naturally high photo-

tostability of wild-type FPs. At the same time, there are plenty of “enhanced” variants that have lost high photostability of their parent wild-type proteins in the course of optimization of green FPs; development of blue, cyan, and yellow FPs; and monomerization of red FPs.

The appropriate choice of a photostable FP (tables in Figs. 10 and 14) is often crucial for a successful experiment. This choice, however, can be rather complicated, since the photostability of any given FP in a living cell depends on many parameters that are not yet well understood. In particular, light source (laser scanning, wide-field, or spinning disk), intensity of light, and frequency of light pulses, as well as employed excitation wavelengths, determine the photobehavior of an FP to a great extent. For example, mRaspberry surpasses mPlum in photostability in confocal microscopes, but this is not the case under widefield irradiation (389).

Several approaches for evaluating photostability in FPs exist, all with their own advantages and drawbacks. The simplest way is to compare FPs of similar spectral characteristics side by side under the same excitation light. This allows for direct selection of the most photostable variants for a given experimental system. However, this approach does not provide absolute physical characteristics that would make it possible to compare FPs of various spectral properties requiring different excitation wavelengths.

To compare FPs of different colors, it is common practice to calculate the photobleaching halftime required to reduce the emission rate to 50% from an initial emission rate of 1,000 photons/s per fluorescent protein (384–386, 389). This comparison, however, requires complex calculations based on ensemble brightness of an FP measured for a protein sample in vitro and a number of assumptions potentially leading to accumulated errors. Notably, the resulting photostability value ends up correlated with the protein’s brightness so that the brighter protein always appears more photostable just because of its higher photon output and thus appears even more desirable as a marker. In addition, in practice, this approach cannot be universally applied to various experiments performed in living cells and tissues. Such factors as cell state, composition of the cell medium (44), and compartmentalization of fusion FPs within the cell also play a role. Moreover, fusion with a cellular protein can substantially influence the photobehavior of an FP, probably due to the restriction of FP motility (our unpublished data).

Photostability can be also measured at the single molecule level, providing an estimation of photobleaching quantum yield (480). However, it should be noted that the photobehavior of a single FP molecule may be very different from that at the ensemble molecule level.

In addition to irreversible photobleaching, it is important to take into account possible reversible photoconversions resulting in temporary quenching or “kindling” of flu-

orescence, which is actually quite common among FPs. Notable reversible quenching is characteristic for various *Aequorea*-GFP-based cyan, green, and yellow FPs, as well as for some red FPs (358, 385, 403). Kindling of fluorescence is pronounced for mKate (388, 389) and can be seen in mCherry, Katushka, mKate2, etc., under certain irradiation conditions (usually low irradiation intensity). Clearly, pronounced reversible changes in fluorescence intensity and/or excitation/emission spectra can drastically distort the expected results of quantitative experiments.

The possibility of irreversible photoconversions should be kept in mind as well. Such photoconversions are observed for many FPs upon intense irradiation under the appropriate conditions, for example, green-to-red conversion of EGFP and other green FPs (45), red-to-green conversions of some orange and red FPs under high power of excitation light or two-photon excitation (123, 232, 264), yellow-to-cyan conversion of some yellow FPs (214, 232, 353, 444), and possibly other yet undescribed effects. While photoactivation effects have been successfully exploited in many applications (see sect. viii), they can be disastrous for quantitative analysis, leading to erroneous interpretation of experimental data.

Due to all these reasons, we do not provide a comparison of FP photostabilities in absolute numbers, but only label proteins as having high or low photostability when there is sufficient information (tables in Figs. 10 and 14).

To conclude, the guidelines for choosing a photostable FP can be summarized as follows.

To choose an FP for an experiment requiring high photostability and consistent photobehavior of a fluorescent label, literature data can be used as a general guide, but attention should be paid to the fact whether the imaging systems that was used to evaluate the FPs is similar to the one that is going to be used for the study. Preferably, several FPs of a desirable color should be initially evaluated, and experiments to control for any unexpected photobehavior should be performed before starting any large-scale quantitative experiments. To avoid undesirable photoconversions, intensity and duration of excitatory illumination should be minimized as much as possible.

## D. Oligomeric Nature and Aggregation

Being genetically encoded, FP can be cloned in frame with a protein of interest, thus allowing for its direct tracking in a living system. However, for the labeling of most proteins, an FP must be monomeric (see also sects. v and vi). Otherwise, oligomerization of a chimeric construct would interfere with the normal function and localization of the studied protein. Moreover, if the protein of interest is an oligomer itself, the fusion construct with a dimeric or tetrameric FP may form a network of interacting proteins leading to aggregation (71, 386, 452).

It was rather serendipitous that the first fluorescent protein discovered, *Aequorea victoria* GFP, turned out to be a natural monomer. This property, inherited by its artificially generated descendants, enables wide use of this group of FPs for labeling of various proteins of interest as in-frame fusion to the COOH or NH<sub>2</sub> terminus or even as an insert within a flexible loop. Minor dimerization of *Aequorea victoria* GFP derivatives at high concentrations is negligible for most applications and can be eliminated by a point mutation A206K (507).

As described above, the spectral characteristics of the GFP chromophore can vary greatly, depending on the protein environment. Chromophores can be modified by substituting Tyr66 for His, Trp, or Phe, which results in the blue-shifted spectral variants (see sect. II). Extensive mutagenesis of *Aequorea victoria* GFP produced a series of monomeric FPs of a variety of colors: blue (155, 156), violet (430), cyan (155, 156, 231, 360), green (77, 154, 497), and yellow (324). This palette enables multicolor labeling of proteins of interests and FRET-based techniques (see sects. V–VII). Improved monomeric markers derived from FPs cloned from *Aequorea spp.* are still being developed, gradually achieving better brightness, photo- and pH-stability, maturation rate, etc. (8, 9, 79, 130, 134, 231, 283, 304, 419).

However, there are no reports on green FP modifications thus far that would succeed in shifting its emission peak beyond 540 nm without further covalent modification of the chromophore, which, in turn, seems difficult to achieve using available mutagenesis and screening techniques. Although we have reported a partially red mutant of EGFP, no useful purely red variant was generated (288).

Breakthrough in the red fluorescent field occurred only after the discovery of DsRed and other red fluorescent and chromo proteins in Anthozoa species (95, 256, 275, 476). These discoveries opened the way for the development of orange, red, and far-red FPs with emission peaks located as far as 655 nm (394).

However, the vast majority of natural FPs and chromoproteins cloned from various species during the past 10 years are tetramers, such as FPs from Anthozoa (95, 256, 275, 476) and Copepoda (103, 383), or dimers, such as anm2CP and phiYFP from Hydrozoa (383). FPs recently described in *Branchiostoma* (lancelets) (37, 47, 86; patent application WO2007142582) are still poorly characterized, but their amino acid similarity with Copepoda FPs and first gel-filtration experiments (patent application WO2007142582) suggest their oligomeric state.

Most importantly, oligomerization is common for all orange and red GFP-like fluorescent proteins discovered, including DsRed (275) and other Anthozoa FPs (285, 480), anm2CP (50, 383), and probably red FPs from lancelets (patent application WO2007142582). Engineering of the red monomeric FP has become one of the most challenging tasks for FP developers. Although crystallography

studies (103, 315, 340, 347, 352, 416, 465, 481, 485, 500) have suggested ways to disrupt the tetramers through rational site-directed mutagenesis, such mutagenesis most often leads to structural changes impairing the fragile mechanism of the red chromophore maturation. All monomeric orange, red, and far-red FPs available to date were obtained after laborious mutagenesis of dimeric or tetrameric Anthozoa FPs, which aimed to shatter oligomerization interfaces of these proteins, but to retain successful maturation and fluorescence of the red chromophore.

The challenge of generating a monomeric red FP was finally met by Tsien and co-workers (59, 384, 468) and other groups (200, 228, 285, 388, 416), although extensive efforts are still being devoted to optimization of the red monomers (370, 385, 389). Today, the palette of monomeric FPs covers the whole visible spectrum (see next chapter) and allows for multicolor labeling of proteins of interest (see sect. VI), complex FRET experiments (see sect. VII), and other multiparameter imaging experiments.

For some applications, dimerization or tetramerization of FPs could be potentially employed as a useful feature. In particular, minor dimerization can provide more effective FRET, as is the case for the enhanced FRET pair CyPet-YPet (321, 457). Weak dimerization of Superfolder GFP due to the characteristic mutation A206V apparently facilitates the solubility of its fusions with relatively insoluble proteins (337). Indeed, we have observed this “superfolder” property for other dimeric and tetrameric FPs as well (our unpublished data). In principle, natural tetramerization of FPs can be made useful to form fluorescent complexes for various assays, for example, multivalent recombinant fluorescent antibodies.

It is also important to note that application of FPs for the labeling of cellular organelles, whole cells, and tissues, as well as visualization of promoter activity (see sect. VI), does not necessarily require monomeric FPs. Often, dimeric and tetrameric FPs demonstrate advantageous spectral and biochemical properties compared with their monomeric counterparts and may be preferable for applications not involving molecular tagging (table in Fig. 14).

Unfortunately, in addition to tetramerization, many natural FPs are prone to aggregation at high concentrations, which can be toxic for living cells, hindering work with cell cultures and making it impossible to generate stable cell lines and healthy transgenic animals. One of the most remarkable examples of toxic aggregation is the formation of huge needle-like crystals by wild-type copGFP (ppluGFP2), which can physically destroy eukaryotic cells in several hours (103). At the same time, copGFP is one of fastest maturing, pH stable, and brightest FPs that can be used to track the early stages of promoter activation (103). Some FPs have a tendency to accumulate in lysosomes (202), forming dotlike struc-

tures that can merge into larger and potentially cytotoxic agglomerations. Potential aggregation problems should always be kept in mind, especially for the expression of FPs in transgenic animals. The positive service record of an FP, including successful generation of stable cell lines and application in living organisms, should be taken into account when choosing an appropriate nonaggregating FP.

### E. pH Stability

The key parameter that is usually employed to compare pH stability of FPs is  $pK_a$ , which is the pH value at which the brightness of fluorescence for a given FP equals 50% of the maximal brightness measured at an optimal pH. Fluorescence of FPs typically increases at higher pH and reaches its maximum at pH 8–9. A further increase in pH commonly does not alter fluorescence until reaching alkaline values of 10–13, which lead to protein denaturation and/or degradation of the chromophore.

For most FPs developed to date, fluorescence brightness depends on pH changes in the physiological range, with a typical  $pK_a$  from 5.0 to 7.0. Generally, pH dependence of FPs is most pronounced for yellow FPs ( $pK_a$  from 5.5 to 6.5) and to a lesser extent for the green FPs ( $pK_a$  from 5 to 6), while blue, red, and far-red variants are often much less sensitive to pH, with  $pK_a$  values as low as 2.7 for TagBFP (419) and 3.8 for TagRFP (285). Such pH-stable FPs can be visualized in acidic organelles such as endosomes, lysosomes, and Golgi and provide more reliable readouts for quantitative assays.

In general, since substantial pH changes are common during many physiological processes (410), the pH dependence of an FP fluorescence can notably distort the results of quantitative experiments. Therefore, pH stability is an important parameter for the choice of an FP for quantitative measurements, especially for ratiometric dual- or multicolor imaging and for FRET techniques. Control experiments and appropriate calibration may be necessary for quantitative imaging. Also, we recommend using FPs with similar pH dependence for quantitative dual color labeling and FRET (see sect. vii).

As usual, there is a flip side to the pH stability problem: dependence of FPs on pH can be efficiently exploited to monitor pH changes and vesicular transport in living cells (see sect. ix).

## V. MODERN PALETTE OF FLUORESCENT PROTEINS

### A. Monomeric FPs

Today, after a long struggle against the natural tendency of FPs to form oligomers (see previous section),

color diversity of monomeric FPs covers almost the whole visible spectrum, from violet (emission peaking at 424 nm) to far-red (emission peaking at 650 nm) (table in Fig. 10 and Fig. 15). This palette is additionally enriched by a number of FP variants with a large Stokes shift of more than 100 nm. The only notable gap remains in the near-infrared region, and development of a bright monomeric FP with emission maximum peaking at 660–700 nm would be a great advancement both for multicolor labeling and whole body imaging (see sect. vi).

The current palette of monomeric FPs enables multicolor protein labeling experiments with as many as six colors (219) and potentially more. In our hands, the combination of available monomeric FPs allows for straightforward five-color imaging using an Olympus FV1000 confocal microscope equipped with standard filter sets, without the need for spectral deconvolution (Fig. 16). Options for multicolor labeling can be potentially expanded to more than 10 colors by adding large Stokes T-Sapphire and mKeima (see below) and reversibly photoactivatable Dronpa (16), Padron (17), and RsCherrys (413) (see sect. viii).

The abundance of monomeric FPs of various spectral characteristics opens new possibilities for multiparameter imaging of structures and processes in living systems. Below we summarize the properties of the best monomeric FPs developed to date, in the order of their emission color, starting from the shortest wavelength.

#### 1. Violet FP (excitation/emission peaking at 355/424 nm)

Weak violet-blue emission is characteristic of the FP variants carrying a Tyr66Phe mutation of the chromophore-forming triad (78, 435). In 2009, the first practically usable “ultramarine” FP of this type was reported, named Sirius (430), which has an emission peak at 424 nm, the shortest wavelength of all known FPs. Due to its high photo- and pH stability, Sirius tolerates prolonged exposures and can be targeted to acidic organelles. Sirius was successfully applied as a FRET donor within a blue-cyan sensor for caspase-3 activity in dual FRET experiment and is expected to become a valuable addition to the common-use FP list. However, its low brightness (Fig. 15), along with the tendency of living cells to autofluoresce in the violet part of the visible spectrum and general toxicity of violet and UV light (412), will likely limit applicability of Sirius in its present form. Brighter versions of Sirius and its like are necessary to mitigate these problems.

#### 2. Blue FPs (excitation/emission peaking at ~380–400/450 nm)

Until recently, the only FP variant available in blue was EBFP (156, 361, 498), the Tyr66His mutant variant of

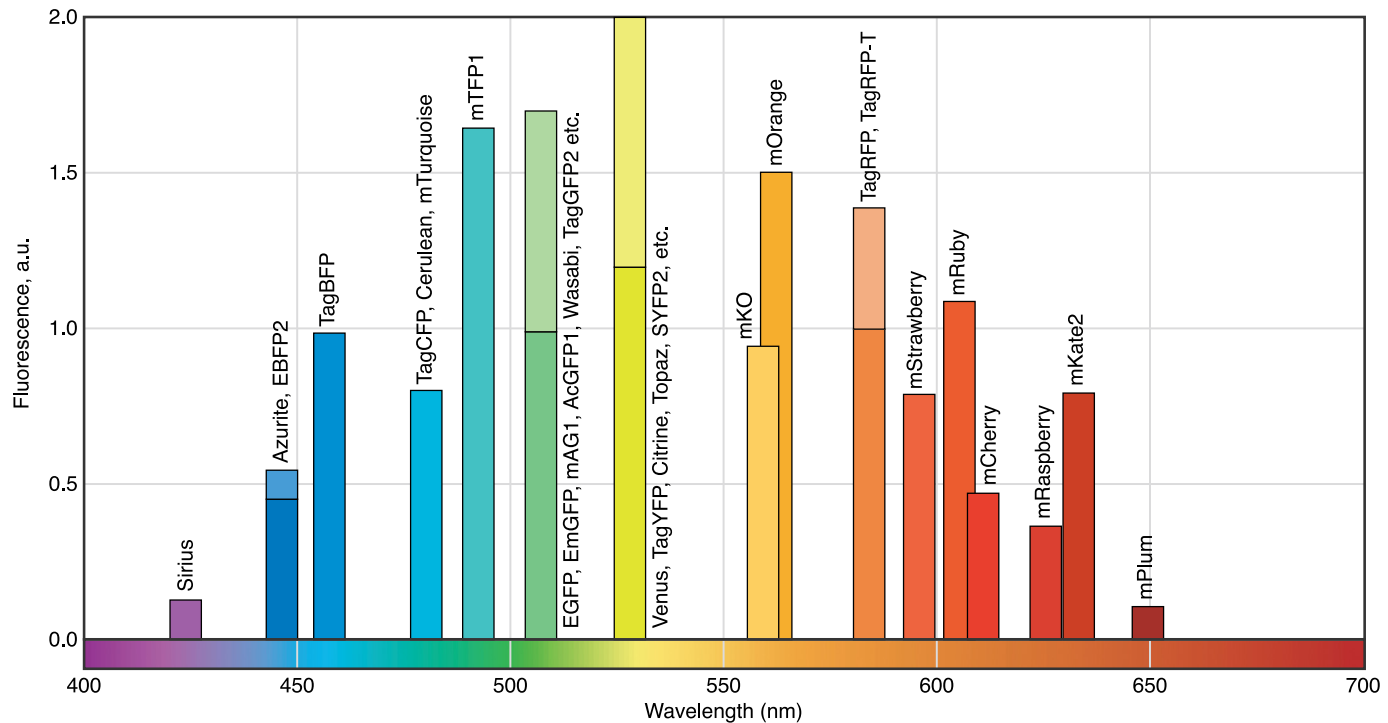


FIG. 15. Spectral diversity of available monomeric FPs. Columns show positions of emission maxima and relative brightness of representative monomers. Fluorescence brightness values were calculated as a product of molar extinction coefficient and fluorescence quantum yield taken from original publications for each protein and normalized per EGFP brightness (extinction coefficient  $55\,000\text{ M}^{-1}\cdot\text{cm}^{-1}$ , quantum yield 0.6).

*Aequorea victoria* GFP. As a spectrally favorable FRET donor for EGFP, EBFP was used in a number of FRET-based sensors (156, 292, 336, 361). However, EBFP has low brightness and very poor photostability and thus has not become a popular tag. Fortunately, these detrimental qualities turned out not to be inherent to the histidine-

containing chromophore. Recent publications reported dramatic progress in further modification of EBFP, resulting in proteins named SBFP2 (230), Azurite (283), and EBFP2 (9). All these blue FPs have the monomeric nature of *Aequorea victoria* GFP and work properly in fusion with various proteins (9, 230, 386). In particular, EBFP2 and Azurite are characterized by enhanced photostability and are clearly much better than EBFP for any application (table in Fig. 10).

Nevertheless, in the end, His66-based blue FPs may yield to the emerging class of blue FPs carrying the “original” Tyr66-containing GFP-like chromophore (9). In particular, the recently reported TagBFP (419) demonstrates superior brightness and high photostability and is a strong competitor of classical blue FPs (Fig. 15).

In general, it can be stated that today’s blue FPs, unlike the earlier versions, are on par with other colors in terms of brightness and stability and can be widely applied for techniques such as multicolor, FRET, and FCCS, which should lead to rapid growth of their popularity in the coming years.

### 3. Cyan FPs (excitation/emission peaking at ~430–460/480–490 nm)

In contrast to His66-based EBFP, cyan fluorescent ECFP (155, 156) with a Trp66-containing chromophore and excitation/emission peaks at 434/477 nm has become popular for use in FRET (see sect. vii) and dual-color

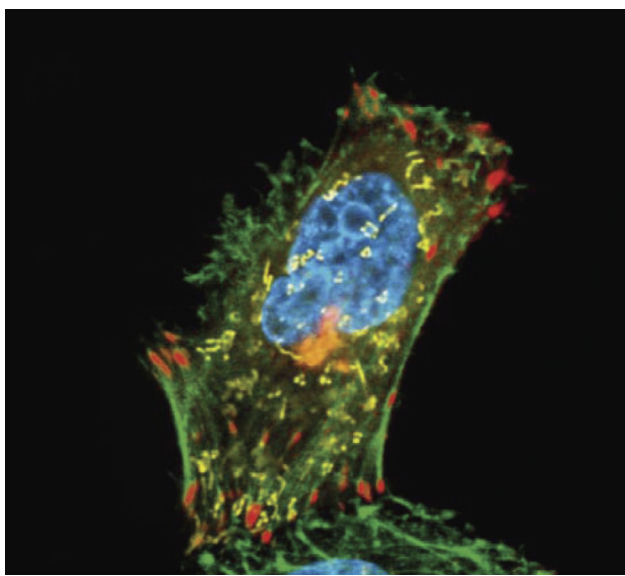


FIG. 16. Multicolor labeling, living HeLa cells, Olympus FV1000 confocal microscope. TagBFP-H2B (blue), TagGFP2-actin (green), mYFP-mito (yellow), TagRFP-golgi (orange), mKate2-zyxin (red).

labeling in combination with yellow FPs. Directed evolution of ECFP resulted in substantial progress, with the best variants reported being Cerulean (360) SCFPs (231), TagCFP (Evrogen JSC), and mTurquoise (122), all characterized by enhanced brightness and/or maturation rate (table in Fig. 10).

However, similar to blue FPs, the palette of cyan FPs was recently enriched with a monomeric FP carrying a natural GFP-like Tyr66 chromophore but demonstrating cyan fluorescence emission. This protein, named mTFP1 (“monomeric Teal FP,” Ref. 7), is a monomeric mutant developed from the tetrameric protein cFP484 from the soft coral *Clavularia* sp. (275). Compared with Cerulean, mTFP1 possesses higher brightness and photostability. The narrower emission spectrum of mTFP1 can reduce cross-talk in multicolor and FRET experiments (6). On the other hand, the fluorescence emission peak of mTFP1 is closer to that of green FPs, which may complicate its spectral separation from yellow FPs.

#### 4. Green FPs (excitation/emission peaked at ~490/510 nm)

Historically and due to natural abundance, numerous green FPs have been discovered and developed, and a number of good monomeric green FP labels are available today (table in Fig. 10). However, it should be pointed out that one of the first enhanced variant obtained, EGFP (77, 154, 497), already combined most of the desirable characteristics. Novel green FP variants that should be mentioned are as follows: 1) mEGFP carrying a point mutation A206K, which makes *Aequorea victoria* GFP derivatives fully monomeric even at high concentrations (507); 2) mWasabi, which is brighter at the expense of some photo- and pH stability (8); 3) Emerald (EmGFP), which has faster maturation (79); 4) Superfolder GFP, which supports the solubility of fused proteins but presumably possesses stronger dimerization due to the mutation A206V (337); 5) TagGFP2, which has high pH stability and fast maturation (half-time of fluorescence development at 37°C is 11 min) (419).

#### 5. Yellow FPs (excitation/emission peaked at ~515/530 nm)

A bathochromic shift in both the excitation and the emission spectra characteristic of yellow FPs is due to stacking of the GFP-like chromophore with Tyr203 (324) (see sect. II). One of the first enhanced yellow FPs reported, EYFP, is characterized by low pH stability and high sensitivity to halide ions, and therefore in most applications is going to be replaced by further enhanced versions, such as Citrine (130), Venus (304), Topaz (79), and TagYFP (390) (table in Fig. 10). One of the brightest yellow FPs reported to date is YPet, which also demonstrates enhanced FRET with co-optimized cyan FP CyPet

(311). However, the problem of the latter pair is increased tendency to form homo- and heterodimers (321). The spectral gap remains at an emission wavelength between 530 and 555 nm that has yet to be filled with monomeric FP variants (Fig. 15), while dimeric and tetrameric FPs of these wavelengths already exist (table in Fig. 14).

#### 6. Orange FPs (excitation/emission peaking at ~550/560 nm)

The list of orange and red monomeric FPs is much more modest compared with the short wavelength palette. However, several bright variants with rather good characteristics are already available to choose from. In particular, the orange segment is represented by mKO (monomeric Kusabira Orange; Ref. 200) and mOrange (384), both developed from Anthozoa tetrameric FPs.

Enhanced versions were reported recently for both proteins, although tradeoffs remain: faster maturation of mKO2 seems to be accompanied by lower pH stability (370), and photostable mOrange2 matures slower than the original protein (385). Nevertheless, all four orange FPs described have reasonably high and generally balanced characteristics and are suitable for protein labeling and multiple fluorescent applications (table in Fig. 10).

#### 7. Red FPs (excitation/emission peaking at ~560–590/580–610 nm)

The nomenclature for FP colors is a bit confusing, for which our team is largely to blame. Indeed, fluorescence emission of many FPs that are called red, such as DsRed (275), TagRFP (285), TurboRFP (285), and others, actually look orange-red, and chemical fluorescent probes (such as TRITC) of this emission wavelength are usually designated as orange. Currently, in this orange-red segment, five monomeric FPs seem to be preferable for most applications (table in Fig. 10). The brightest one is TagRFP (285), which still yields to enhanced TagRFP-T in photostability (385). Closer to the red edge of the segment, similarly, mStrawberry and mRuby (228) win in brightness but lose in photostability to mCherry (384). Although optimization of red monomers is still ongoing, the available variants generally satisfy the demands of most applications. Importantly, high extinction coefficients of the FPs of this class make them excellent FRET acceptors for yellow donors. It can be expected that yellow/red FRET pairs will soon challenge traditional cyan/yellow pairs (see sect. VII).

#### 8. FarRed FPs (excitation/emission peaking at ~590/630–650 nm)

Longer excitation wavelengths can penetrate deeper into biological tissues, causing less background autofluorescence and less phototoxicity. These advantages, along

with requirements of FRET and multicolor labeling techniques, have spurred the development of more and more red-shifted FPs of higher brightness.

To date, the list of useful monomers in this part of the spectrum includes four FPs: mRaspberry (468), mPlum (468), mKate2 (389), and mNeptune (248). Characteristics of mKate2 combine high brightness and photostability; at the moment, mKate2 is probably the preferable FP of this color class for most applications, including protein labeling in living tissues. Still, mNeptune can be preferable for multicolor labeling in combination with orange-red FPs due to the more red shifted excitation and emission spectra that can be therefore better separated.

This field is rapidly developing, and the appearance of enhanced far-red FPs is expected in the near future. However, bright far-red fluorescence is not a natural property of FPs. Moreover, the Gaussian-like shape of the brightness histogram (Fig. 15) suggests a physical limit for known FP chromophores. For this reason, future development of essentially red-shifted FPs will likely be limited by this barrier, unless a principal innovation breaks through it.

#### 9. FPs with increased Stokes shift

FPs characterized by increased ( $>100$  nm) distance between excitation and emission maxima (Stokes shift) open several unique possibilities. In combination with regular FPs they can be used for visualization of two emission colors at a single excitation wavelength that is optimal for both proteins, visualization of two FPs with similar emission but different excitation optima, fluorescence cross-correlation spectroscopy (FCCS) (220), and construction of effective FRET pairs (see sect. vii).

Large Stokes FPs contain protonated chromophores (either GFP-like or DsRed-like), which undergo excited state proton transfer (see sect. ii), resulting in rapid chromophore transition into the charged form and emission in the longer wavelength (49).

Thus green fluorescent Sapphire (101, 155) and its enhanced mutant variant T-Sapphire (512), as well as the recently reported yellow FP mAmetrine (6), are characterized by violet excitation peaks (table in Fig. 10). Both T-Sapphire and mAmetrine are efficient FRET donors for orange-red FPs (6, 152) (see sect. vii).

Similarly, red fluorescent mKeima (named after the Japanese chess piece), which was developed from *Montipora* stony coral, demonstrates the largest known Stokes shift among FPs, with a blue excitation peak at 440 nm and red emission peak at 620 nm. The relatively weak characteristics of mKeima limit its application, and development of an enhanced Keima-like FPs is highly desirable. Nevertheless, even in its present form, mKeima can be used for FCCS and multicolor labeling (219, 220).

It can be concluded that the currently available variety of bright monomeric FPs is quite sufficient for multicolor labeling, FRET, and other microscopy techniques. Still, their spectral and biochemical properties could be further optimized. The main remaining objectives include higher photostability and better performance in fusions with “capricious” proteins (see sect. vi).

#### B. Tandems

Although monomerization of FPs is arguably the best way to their successful application as protein fusion tags, alternative solutions were also proposed (53, 59, 112, 243), including generation of tandem versions of dimeric FPs, in which two copies of an FP gene are fused head-to-tail via a short flexible linker (59, 112). Upon expression, tandem FPs form intramolecular dimers that generally behave as a monomer of twice the size, thus avoiding interaction with other FP molecules in solution.

This approach was proposed in 2002 and successfully implemented to generate tandem versions of far-red FP HcRed (112) and a dimeric variant of DsRed (59). One of the most popular tandems employed today is tdTomato, which demonstrates very high brightness and photostability (384). Recently, tandem versions were also reported for the large Stokes Keima (220), red TurboRFP and far-red Katushka2 (389), RFP611 (228), RFP639 (228), and photoactivatable EosFP (312).

Tandem FPs usually demonstrate satisfactory performance in “noncapricious” fusions and thus can be applied for the labeling of fusion proteins. Still, the larger size of a tandem FP is more likely to cause disruption of function in fused proteins, and therefore true monomeric FPs are generally preferable for reliable protein labeling (281).

#### C. Dimeric and Tetrameric FPs

For uses other than as a fused molecular tag, the monomeric state of an FP is generally not required (see sect. vi). Therefore, the choice of an appropriate fluorescent label is not restricted to monomers and tandems, but also includes dimeric and tetrameric FPs that are often characterized by advantageous characteristics. The table in Figure 14 summarizes the best dimeric and tetrameric FPs available to date. Among these proteins, several deserve special mention: 1) tetrameric wild-type ppluGFP2 from *Pontellina plumata* (commercial name copGFP) demonstrates excellent characteristics, including fast maturation, high brightness, and photostability. The drawback of copGFP is that it is prone to form needlelike aggregates in mammalian cells after 2 days of expression (103). However, it still can be used in various applications that do not require prolonged visualization in living systems.

2) ZsYellow1 and TurboYFP (enhanced version of phiYFP; Ref. 383) are the only two “true yellow” FPs available. Both proteins demonstrate high brightness, photostability, and fast maturation and can be recommended for cell labeling in various assays. Being a weak dimer, TurboYFP can be also applied for fusion protein labeling for a limited set of proteins of interest.

3) DsRed-Express2 and DsRed-Max were reported to have lower toxicity in long-term expression than other red FPs (415), useful for constructing transgenic lines.

4) Katushka (commercial name TurboFP635) exhibits the highest emission brightness beyond 650 nm among all FPs and therefore can be the FP of choice for whole body imaging (see sect. vi) (388, 389).

Other considerations are summarized as “noncomprehensive notes” in the table in Figure 14.

## VI. BASIC APPLICATIONS OF FLUORESCENT PROTEINS

FPs can be applied in a large variety of studies related to various aspects of living systems, and the range of these applications is continuously expanding. In this section, we briefly summarize the basic applications of FPs and describe particularly well-developed fields in more detail in subsequent sections. Our goal is to provide a general overview to inspire novel ideas and future work. Each of the mentioned applications, however, deserves a separate comprehensive review to summarize all the information relevant for rational experimental planning.

### A. Protein Labeling

Cloning a gene of interest in frame with an FP results in a genetic construct that can be transferred into cells and organisms to highlight localization of the expressed protein of interest, as first demonstrated in 1994 (470). Today, protein labeling is one of the most popular applications of FPs for visualizing protein expression, localization, translocations (see sect. ix), interactions (see sect. vii), and degradation (see sect. viii) in living systems in real time.

When fused to a protein of interest, good natural FP monomers derived from *Aequorea* species (see sects. ii, iv, and v) usually do not affect its proper localization and function. Monomeric mutant variants of naturally tetrameric FPs also work well in a fusion with most proteins of interest (386). It should be mentioned, however, that occasionally some of the latter cause problems, presumably due to the residual weak dimerization or nonspecific interactions of exposed hydrophobic interfaces. To control for these possible artifacts, one should preferably try several FPs of a desired color class for capricious fusions

and compare the localization pattern with those visualized with a trustworthy natural monomer such as EGFP, as well as by antibody staining of endogenous proteins in fixed cells.

In many cases, fusion to one of the termini of the protein is preferable due to involvement of another terminus in specific interactions or its essential role in determining the protein’s localization. In this respect, literature data describing successful performance of a fusion of interest with one particular FP can be roughly extrapolated to other monomeric FPs. In some cases, performance of a fusion can be improved by inserting a flexible Gly-rich linker of several amino acid residues between the FP and the protein of interest, which may prevent potential steric conflicts. Occasionally, the importance of both termini of a studied protein or other considerations may prompt insertion of an FP inside the protein chain, which has been successfully achieved in a number of cases (25, 298, 364).

Many factors can influence the apparent expression level of a fusion construct, including efficiency of transcription, mRNA stability, efficiency of translation, FP maturation rate, and stability of the protein chimera. The stability issue is particularly important since the inherent turnover rate of the targeted protein often determines the half-life of the whole construct in a cell.

The desirable expression level of a fusion construct is balanced between sufficient signal for reliable imaging and minimal interference with the biochemistry of a living cell. This tolerable level is unique for each protein of interest, depending on its functional role in the protein ensemble and also on the properties of a fused FP. In some cases, deletion of one or several domains of a studied protein may be necessary to avoid deleterious effects on overexpression (370).

Expression levels are particularly important for multicolor imaging of several proteins of interest, where the cumulative effect of several overexpressed proteins must not be disruptive to the living cell, but at the same time, all fusions should be bright enough for reliable detection. Moreover, expression of these fusions should be at comparable levels; otherwise, the dominant one would bleed through into other spectral channels. One way to achieve a desirable balance of expression levels is by adjusting concentration of vectors used for transient transfection. In general, in transient transfections, the expression level usually varies considerably among the transfected cells, and so optimally expressing cells (producing a relatively low but still easily detectable signal) should be chosen from the population. However, for the quantitative long-term experiments and high reproducibility of the results, it is preferable to generate stable cell lines.

## B. Photobleaching Techniques

While photobleaching is generally an undesirable phenomenon that may complicate the visualization of a fluorescent label, it can be exploited to study the mobility of fluorophores, including proteins of interest fused to FPs. Any functional fusion construct of an FP and a protein of interest can be used to estimate the protein's mobility in living cells, as well as to investigate the influence of external factors on its mobility, using photobleaching techniques (250). This information is extremely valuable, since protein movement within a cell is tightly connected with its functional activity and interaction with other molecules.

The most widely used techniques are as follows: 1) fluorescence recovery after photobleaching (FRAP), which consists in bleaching a small region of interest (ROI) by intense light irradiation followed by monitoring of the rate of fluorescence recovery. This rate is determined by rate of migration of unbleached protein into the photobleached patch from other regions of the cell. 2) Fluorescence loss in photobleaching (FLIP), where the rate of fluorescence signal decay is monitored within ROIs adjacent to the repeatedly bleached region (see Ref. 250 for a detailed review).

Photobleaching techniques have several limitations, including difficulties with monitoring fast protein movement, side-effect phototoxicity due to high-power light, and complex photobehavior of some FPs, such as reversible photoconversion. However, these techniques are well established and provide a way to reliably measure or at least compare protein mobilities, assuming that all the necessary corrections and controls are performed, and an FP with well-characterized photobehavior is used. Indeed, photobleaching techniques involving FPs have provided invaluable insights into the dynamic behavior of proteins in living cells. A remarkable example is the high motility of nuclear proteins that has become evident through FRAP, which dramatically changed the prevailing views of the architecture of nuclear processes (341).

A potentially more straightforward and sensitive alternative to photobleaching techniques is tracking the mobility of photoactivated proteins, enabled by the recently developed photoactivatable FPs, as discussed in section VIII.

## C. Subcellular Localizations

The distribution of proteins within a cell is well organized, and protein trafficking is accurately controlled by consensus peptide sequences that serve as subcellular address labels. An FP or FP-based sensor construct may be thus targeted to various subcellular compartments, enabling organelle visualization, studies of fusion-fission

events, and local monitoring of cellular parameters. Some of the most popular signal motifs that can efficiently target a construct of interest to a desirable compartment are presented in Table 1. In some cases, duplication of a signal may be necessary to achieve reliable targeting (327). Importantly, the data presented in Table 1 can be used not only to target a protein of interest to a particular compartment, but also to avoid undesirable targeting of a designed nontargeted construct. In this case, such "address label" sequences should be avoided when designing linkers or modifications of the NH<sub>2</sub> and COOH termini; otherwise, the engineered protein may be (and quite commonly is) inadvertently targeted to the nucleus (by K/R-rich sequences), peroxisomes (by the COOH-terminal sequence XKL), etc.

## D. Promoters Tracking

Cloned under the control of a promoter of interest, an FP can highlight promoter activity in a given genetic environment, in particular cells and tissues, in particular time, and in response to an external influence (63, 344). Compared with enzyme-based assays, this approach has lower sensitivity but enables *in vivo* visualization without exogenous intervention, and multicolor fluorescent imaging of several promoters using distinct FP reporters.

Two key factors should be considered when selecting an FP reporter for promoter activity tracking: the FP's maturation rate and its half-life in the cell (turnover rate). The maturation of an FP is a time-limiting step that can substantially delay the appearance of a detectable fluorescent signal (see sect. IV). It is important to note that the monomeric state of an FP is not necessary for promoter activity tracking (unless the FP aggregates and leads to toxicity; see sect. V). Therefore, fast-maturing tetrameric FPs can be successfully used for this purpose. The maturation half-time of some of these is as short as several minutes (tables in Figs. 10 and 14).

Each FP has a characteristic turnover rate in a given expression system. Therefore, inactivation of a promoter does not lead to immediate disappearance of the reporter's fluorescent signal, which can be stable for many hours or even days (76). However, FP lifetimes can be modulated by fusing appropriate domains or destabilization signals (245). Destabilized FPs have faster turnover rates, and their fluorescence disappears soon after promoter inactivation (245). Therefore, fast maturing and fast-degrading FPs show the closest coupling to actual promoter activity. With such reporters, one can monitor sequential activation as well as inactivation of promoters of interest and thus infer the mechanisms underlying gene regulatory networks and cyclic processes in living systems.

So-called split FPs, i.e., FPs divided into two halves that can reconstitute to produce functional protein, rep-

TABLE 1. Some popular signal motifs used to target fluorescent proteins, fusion constructs, and genetically encoded sensors to subcellular compartments

|                        | Targeting Signal Motifs  | Source                        | Reference Nos.           |
|------------------------|--|-------------------------------|--------------------------|
| Nucleus                | COOH terminus: PKKKRKVEDA<br>COOH terminus: DPKKKRKV<br>COOH terminus: DPKKKRKVDPKKKRKVDPKKKRKGSTGSR<br>In general, various KR-rich sequences close to the COOH terminus can lead to more or less efficient protein localization to the nucleus or nuclear membrane  | NLS<br>NLS of SV40 TAg        | 93, 115, 292<br>196, 241 |
| Cytosol                | COOH terminus: LALKLAGLDI  | NES                           | 475                      |
| ER lumen               | NH <sub>2</sub> terminus: MLLSVPLLLGLLGLAAAD and COOH terminus: KDEL   | Calreticulin                  | 292, 328                 |
| Mitochondrial matrix   | NH <sub>2</sub> terminus: MSVLTPLLLRLGTGSARRLPVPRAKIHSLGDP   | Cytochrome-c oxidase          | 327                      |
| Mitochondrial membrane | NH <sub>2</sub> terminus: MVGRNSAIAAGVCGALFIGYCIYFDRKRRSDPN  | Tom20                         | 13, 115                  |
| Golgi lumen            | NH <sub>2</sub> terminus: MAIQQLRSLFPLALPGMLALLGWWWFSSRKK  | DAKAP1a                       | 93                       |
| Golgi membrane         | NH <sub>2</sub> terminus: 81 amino acids of the human $\beta$ 1,4-galactosyltransferase  | 1,4-Galactosyltransferase     | 121                      |
| Plasma membrane        | NH <sub>2</sub> terminus: MGNLKSVAQEPGPPCGLGLGLGLCGKQGPA<br>NH <sub>2</sub> terminus: MGCIKSKRKDNLNDDGVDMKT  | eNOS<br>Lyn kinase            | 13, 115<br>115, 235, 327 |
| Peroxisomal matrix     | Myristoylation and palmitoylation<br>COOH terminus: KKKKKSKTKCIVM<br>Farnesylation<br>COOH terminus: KLNPPDESGPGCMSCKCVLS<br>Farnesylation<br>NH <sub>2</sub> terminus: MLCCMRRTKQVEKNDEDQKI<br>Double palmitoylation<br>COOH terminus: SKL<br>COOH-terminal sequence XKL can also determine notable targeting to the peroxisomal matrix | K-ras4B<br>v-Ha-Ras<br>GAP-43 | 93<br>153<br>153<br>125  |

Adapted from VanEngelenburg and Palmer (449).

resent an alternative approach that can be applied for the tracking of simultaneous activity of two promoters (Fig. 17A). Fluorescent signals produced by such complementary FP halves driven by two different promoters of interest highlight cells expressing both genes (516). Moreover, by combining several FP halves carrying point mutations leading to spectral differences, one can potentially resolve the combination of promoters that are active in a particular system (179).

## E. Timers

A whole range of possibilities, which thus far remain largely unexplored, is provided by so-called Timer FPs that change fluorescence color with time and thus allow the determination of their temporal expression in retrospect. Importantly, different timer FPs are characterized by various maturation rates (from minutes to hours and even days) and thus are suitable for investigations of processes on a variety of time scales.

The first Timer FP named DsRed-E5 was reported in 2000 (425). DsRed-E5 produces green fluorescence within several hours after synthesis, but later converts to a red fluorescent form. These fluorescent changes occur since some of the chromophores within a tetramer mature to the green GFP-like form instead of red, and their green

fluorescence dominates until slower maturing red chromophores appear and “steal” the excitation energy away from the green ones through a hyperefficient intratetrameric FRET (450). Therefore, tissues, cells, or cellular organelles that are colored green signify recent production of DsRed-E5, while red fluorescence marks regions that have already expressed the protein at least several hours ago. The ratio of red to green fluorescence is proportional to the age of expressed protein and thus can indicate the time since corresponding promoter activation. In practice, this provides means to monitor the dynamics of gene expression in various tissues (287), to separate cells that have recently activated a promoter of interest from the cells characterized by permanent promoter activity (289), to analyze the age-dependent distribution of organelles (98, 406), and to study protein trafficking (82, 225, 247).

However, tetrameric FPs are generally not suitable for fusion with other proteins. Therefore, the recent development of monomeric mCherry-based Timers named fast-FT, medium-FT, and slow-FT, which change fluorescent color from blue to red within time periods from several hours to a day, is an important contribution (418). Monomeric Timers simultaneously track localization and age of proteins of interest in living cells and thus reveal the pathways of trafficking of newly produced proteins.

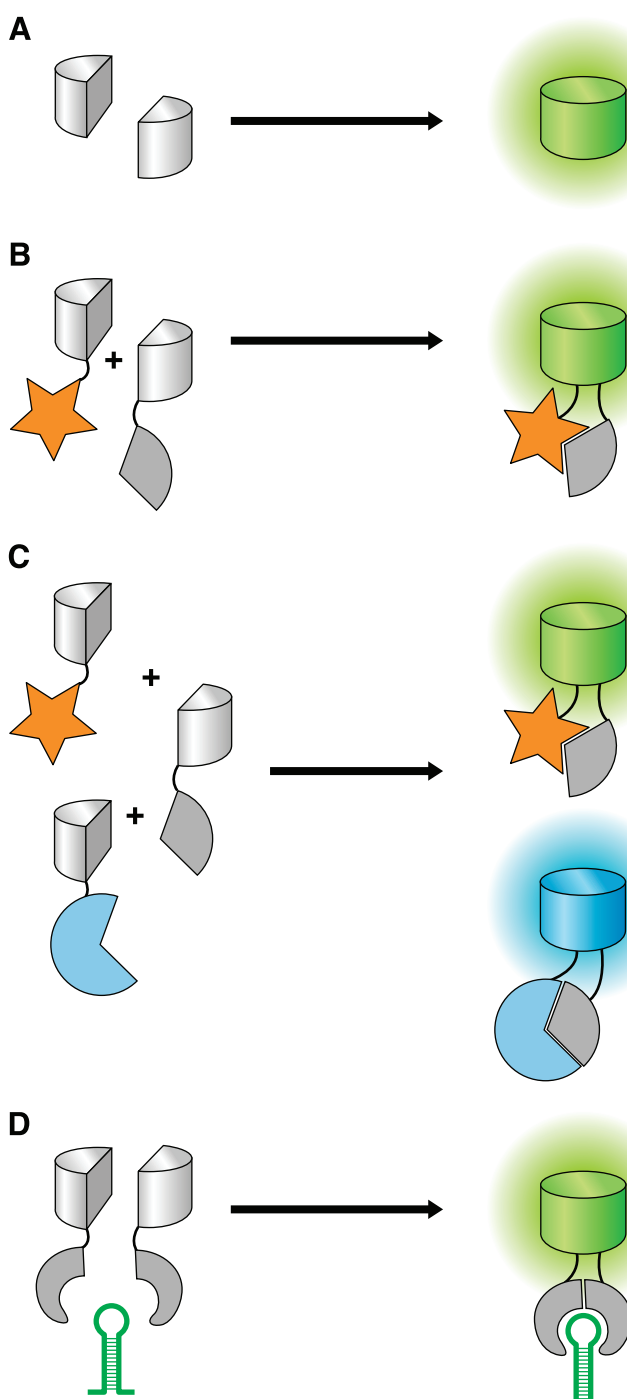


FIG. 17. Main modes of applications of split FPs. Split FPs are shown as gray halves of a barrel (in fact, sizes of NH<sub>2</sub>- and COOH-terminal FP parts are usually quite different); reconstituted FPs, as colored barrels; fusion partners, as gray geometrical figures of different shapes. *A*: self-associating split FPs allow the detection of a simultaneous presence of FP halves in a cell or cell compartment. *B* and *C*: non-self-associating split FPs fused to proteins of interest make it possible to determine whether target proteins interact with each other (*B*) and also to compare the relative strengths of protein-protein interactions (*C*). *D*: RNA-binding domains fused to FP halves enable detection of appearance and localization of target RNA molecules.

## F. Cell and Tissue Labeling

Under the control of a specific promoter in an appropriate genetic context, an FP can help visualize particular cell types in whole animals, organs, tissues, and cell cultures. This possibility is particularly important in such fields as immunology (145, 282), neurobiology (168, 251, 420, 456, 502), development (68, 333, 425), transplantology (113, 319, 467, 488), and carcinogenesis (170, 171, 439, 496, 504, 505).

Multiple FPs can be combined to visualize locations of different cell types in living systems. Moreover, it was recently reported that a mixture of several FPs obtained by random recombination enables multicolor cell labeling with more than 100 hues distinguishable by fluorescence microscopy. This was demonstrated in one of the most beautiful applications ever developed with the use of FPs, Brainbow (251). Brainbow employs *Cre*-mediated recombination to generate a random mix of several FPs expressed in individual neurons, which is expected to greatly help in deciphering complex neuronal circuits (Fig. 18).

Similar to promoter tracking, rational engineering of degradation motifs can be a powerful approach to visualize changes in molecular ensembles of living cells. A vivid example of this is the technique developed for the real-time monitoring of cell cycle progression in living tissues, named Fucci (370). This technique employs green and red FPs fused to appropriate protein domains that cause their rapid degradation at particular stages of a cell cycle (Fig. 19). As a result, red and green fluorescent signals oscillate in antiphase: all cells in the G<sub>1</sub> phase are labeled red and those in the S/G<sub>2</sub>/M phases are labeled green. This technique works well in transgenic animals and in time-lapse imaging, allowing the identification of dividing cells in studies of development, tumor progression, and other processes employing division and redistribution of living cells.

The major difficulty of fluorescent imaging of proteins, cells, and tissues within whole animals is the light absorption by melanin and hemoglobin, as well as light scattering (223). Both absorption and scattering become less pronounced as the light wavelength increases. The optimal “optical window,” which is most transparent for the visualization in living tissues, is considered to be between 650–700 and 1,100 nm (223). Therefore, development of bright far-red or near infrared FPs should help to increase sensitivity of the whole body imaging techniques employing a genetically encoded label. At the moment, one of the preferable FPs for use in whole body imaging is Katushka, a far-red FP with an emission profile that peaks at 635 nm and extends far beyond 700 nm to the infrared part of the spectrum (388). Beyond 650 nm, Katushka demonstrates superior brightness compared with any other FP reported to date and therefore should

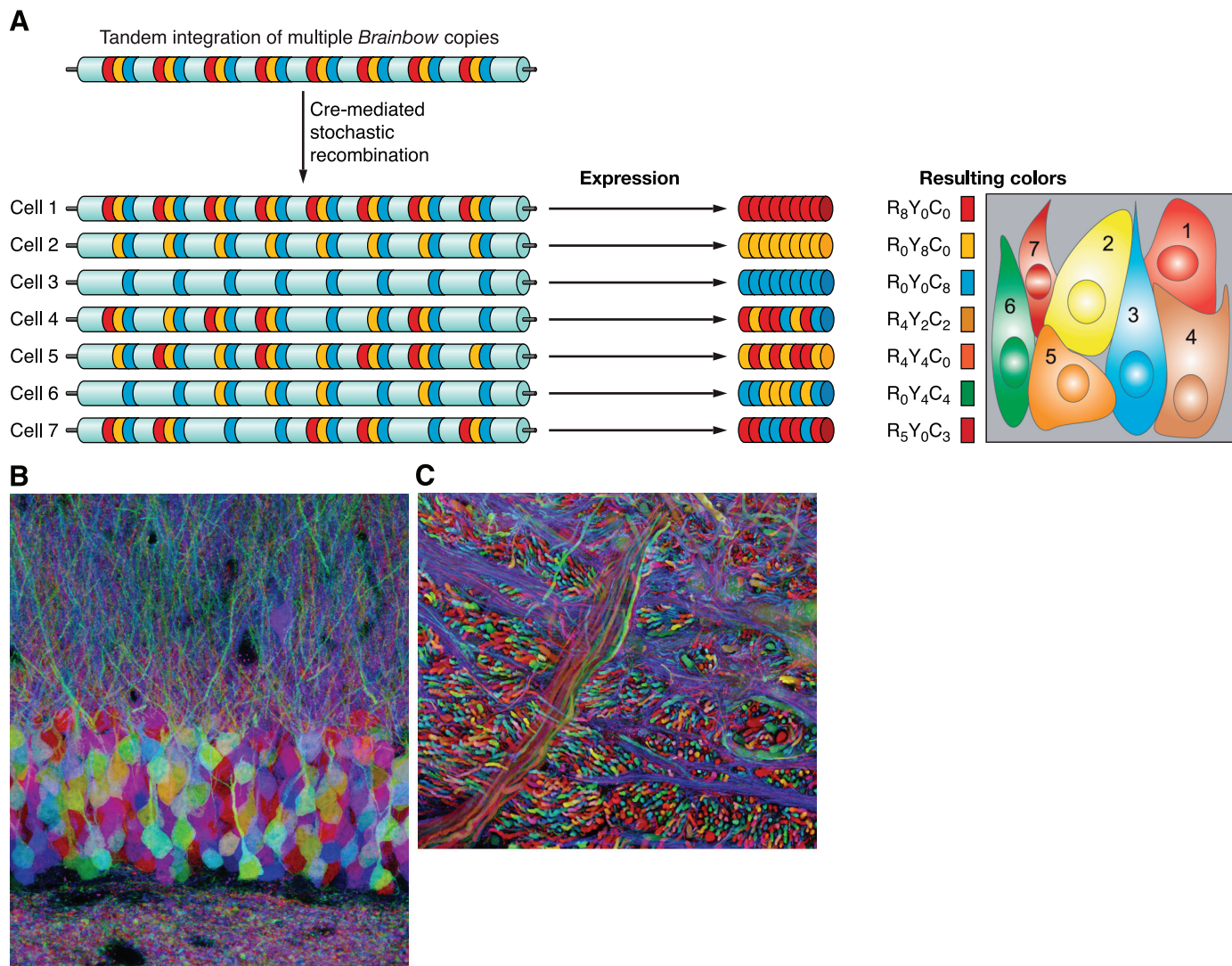


FIG. 18. A: schematic representation of multicolor cell labeling using Brainbow technology. One possible variant is shown where a cassette of three FPs of different colors (red, yellow, and cyan) separated by different *lox* sites under control of a single promoter is inserted into the genome in multiple tandem copies (8 in this case). Transient activation of Cre recombinase results in stochastic recombination events so that each cell expresses different amounts of each FP and is colored individually (7 combinations among many potentially possible are shown). B and C: Brainbow examples, transgenic mouse: dentate gyrus, three FP variants (B); brain stem, four FP variants (C). (Images kindly provided by Prof. J. Lichtman.)

provide the best sensitivity (87, 169, 388). However, the excitation maxima of available far-red FPs, including Katushka, are still located within the suboptimal wavelength range: 590 nm and lower. Therefore, a significant bathochromic shift of FP absorbance is still highly desirable to provide efficient excitation by 633 nm laser line or other deeply penetrating far-red light sources. In this respect, recently reported mNeptune with excitation maximum peaked at 600 nm can be a possible choice (248). Alternatively, efficient excitation in living tissues can be achieved via two-photon excitation that employs infrared wavelengths (96).

Generation of a bright FP emitting in infra-red would probably be the best solution for whole body imaging. However, infrared appears to be a rather unattainable

peak for FP developers. An alternative solution for semi-genetically encoded infrared labeling on the basis of bacterial phytochromes was recently developed (396). In spite of low brightness of the reported label and requirement of injection of a cofactor biliverdin, this approach in general is very promising for fluorescent imaging in whole tissues.

A number of advanced imaging techniques have been developed for enhanced imaging of FPs in living tissues. The most recent example is a remarkable technique utilizing FPs as contrasting labels for the multispectral optoacoustic tomography (MSOT) for deep high-resolution imaging in living tissues (356). The technique combines photoacoustic imaging tomography (137, 471) and selective-plane illumination microscopy (SPIM) (182) to recon-

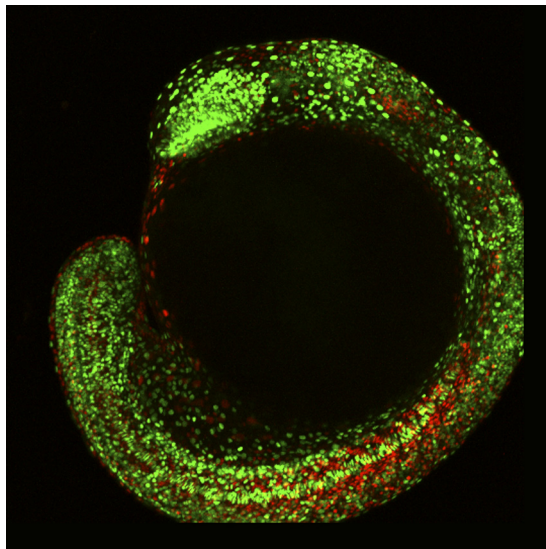


FIG. 19. Monitoring of cell cycle progression inside the developing zebrafish embryo with zFucci technique. [Image kindly provided by Prof. A. Miyawaki; from Sugiyama et al. (421).]

struct FP distribution in a thick sample, making it possible to identify individual FP-labeled cells at a depth of several millimeters.

#### G. DNA and RNA Labeling

In vivo imaging of mRNAs production, localization, and dynamics is a crucially important tool for live cell studies. Several techniques for real-time mRNA labeling and tracking were proposed with the use of FPs (see Ref. 440 for the detailed review). These techniques allow direct fluorescent labeling of specific mRNA molecules in living cells. Moreover, since both mRNA and FP constructs are genetically encoded, these techniques can be potentially applied within stable cell lines and transgenic animals.

In the most straightforward scheme, an FP is fused to the RNA-binding domain, and the corresponding RNA motif recognized by this domain is fused with a target mRNA. Multiple copies of the RNA motif can be introduced to amplify the signal. If the RNA-binding domain is highly sequence specific, and if its target RNA motif is naturally absent in the studied cells, this approach results in target mRNA labeling with high sensitivity and specificity. The first appropriate domain-mRNA pair proposed was the bacteriophage coat protein MS2 binding to a specific hairpin of the phage RNA (38, 40). This pair was successfully employed in a number of applications (351, 365). Combining this one with another recently introduced domain-mRNA pair (84) enabled simultaneous dual color labeling of two mRNAs (242). The key limitation of this approach is the high background signal produced by unbound FP molecules. This problem can be partially

solved by low expression levels of FP or its targeting to the nucleus (114). An alternative solution is the application of split FP halves that reassemble into a functional FP only in the presence of RNA containing the two motifs that bring them together (Fig. 17D). The feasibility of this approach was demonstrated in several works (325, 354, 443).

Still, all these approaches imply the introduction of RNA motifs recognized by a protein domain. Just as the fusion of an FP to a studied protein can potentially disrupt the protein's function, the introduction of specific RNA motifs into natural mRNA can alter its behavior in living cell. This important issue represents the general concern for RNA labeling techniques and should be kept in mind when designing mRNA constructs and interpreting the results.

Several techniques have been also developed to exploit FPs to monitor chromosomal dynamics in living cells. These techniques employ the fusion of an FP with DNA-binding domains, such as natural transcription factors that bind to the introduced recombinant DNA locus carrying several specific binding sites (118, 203, 278, 363) or zinc finger DNA-binding domains recognizing specific DNA sequences (249). The fusion of an FP with proteins present in chromatin, such as histones (197) or centromere binding domains (163), can be helpful for visualizing chromosomal dynamics.

### VII. STUDYING PROTEIN-PROTEIN INTERACTIONS USING FLUORESCENT PROTEINS

Information concerning protein interactions is vitally important for understanding the function of molecular ensembles in living cells. FPs can be employed in at least three principal ways to identify, confirm, or disprove the dynamic or stable interactions of proteins of interest: Förster resonance energy transfer (FRET), FCCS, and complementation of split FPs, which are described in this section. It is also conceivable that in the future super-resolution microscopy techniques may enable direct visualization of interacting proteins; this theoretical possibility is discussed in connection with photoactivatable FPs in the next section.

#### A. FRET

The measurement of energy transfer efficiency between two FP molecules is currently one of the most commonly used approaches to monitor protein-protein interactions in living cells (343) and is also utilized in genetically encoded sensors (see sect. IX). This approach is based on the fact that excited chromophore of a higher energy (i.e., operating in a shorter excitation-emission

wavelength range) can transfer some of its excitation energy to an acceptor chromophore of a longer wavelength range, through a nonradiative dipole-dipole coupling mechanism termed FRET (110).

The principle of protein interaction detection using FRET is as follows. Two proteins of interest are fused correspondingly to a donor and acceptor FPs. When the two proteins interact, FRET between their FP tags can be detected, assuming that the interaction brings the FPs into sufficient proximity and allows for their favorable orientation with respect to each other. The distance between the two chromophores plays by far the most important role: the efficiency of FRET decreases with distance following inverse sixth power law and should be typically shorter than 10 nm to result in detectable energy

transfer. This makes FRET very useful for detecting molecular interactions by microscopy, spectroscopy, and flow cytometry analysis of living cells (343, 402).

Efficiency of FRET (i.e., the quantum yield of the energy transfer) between any two FPs also depends on a number of other parameters: spectral overlap of donor emission and acceptor absorption spectra, quantum yield of donor fluorescence, and extinction coefficient of the acceptor. For each pair of donor and acceptor chromophores, the measure of FRET efficiency integrating over these factors is Förster distance ( $R_0$ ), defined as the distance at which FRET efficiency is 50% of its maximal value. The theoretical Förster distance can be calculated and is typically 4–6 nm (the more the better) for the best FP pairs reported (table in Fig. 20).

| FRET pair            | Donor excitation peak, nm | Donor emission peak, nm | Acceptor excitation peak, nm | Acceptor emission peak, nm | Donor QY | Acceptor EC, M <sup>-1</sup> cm <sup>-1</sup> | Forster radius (R <sub>0</sub> ), nm | comments   | References |
|----------------------|---------------------------|-------------------------|------------------------------|----------------------------|----------|---|--------------------------------------|--|------------|
| EBFP2-mEGFP          | 383                       | 448                     | 489                          | 509                        | 0.56     | 57,500  | 4.8                                  |  | (152)      |
| TagBFP-TagGFP2       | 402                       | 457                     | 483                          | 506                        | 0.63     | 56,500  | 5.3                                  |  | (419)      |
| PS-CFP2-phiYFP       | 400                       | 468                     | 525                          | 537                        | 0.20     | 130,000                                       | 6.1                                  | Very good spectral separation. phiYFP is a weak dimer. | (409, 510) |
| GFP2-YFP             | ~400                      | ~510                    | ~515                         | ~530                       | 0.55     | 84,000  | -                                    | Good spectral separation                               | (517)      |
| T-Sapphire-DsRed     | 399                       | 511                     | 563                          | 582                        | 0.60     | 43,800  | -                                    | Very good spectral separation. DsRed is a tetramer.    | (430)      |
| T-Sapphire-TdTomato  | 399                       | 511                     | 554                          | 581                        | 0.60     | 138,000                                       | -                                    | Very good spectral separation. tdTomato is a tandem    | (6)        |
| E0GFP-mCherry        | 400                       | 508                     | 587                          | 610                        | 0.60     | 72,000  | 5.1                                  | Very good spectral separation.                         | (11)       |
| mAmertine-TagRFP     | 406                       | 526                     | 555                          | 584                        | 0.58     | 100,000                                       | -                                    | Very good spectral separation.                         | (6)        |
| mAmertine-tdTomato   | 406                       | 526                     | 554                          | 581                        | 0.58     | 138,000                                       | -                                    | Very good spectral separation. tdTomato is a tandem    | (6)        |
| ECFP-EYFP            | 434                       | 477                     | 515                          | 527                        | 0.40     | 83,400  | 4.9                                  |  | (116, 336) |
| CyPet-Ypet           | 435                       | 477                     | 517                          | 530                        | 0.51     | 104,000                                       | 5.1                                  | enhanced dimerization                                  | (311, 321) |
| mTFP1-mCitrine       | 462                       | 492                     | 516                          | 529                        | 0.85     | 64,000  | -                                    |  | (6)        |
| mECFP-cp157Venus     | 434                       | 477                     | 515                          | 528                        | 0.40     | 92,200  | 5.1                                  |  | (7)        |
| mCerulean-cp157Venus | 433                       | 475                     | 515                          | 528                        | 0.62     | 92,200  | 5.3                                  |  | (7)        |
| mTFP1-cp157Venus     | 462                       | 492                     | 515                          | 528                        | 0.85     | 92,200  | 5.7                                  |  | (7)        |
| mTFP1-mOrange        | 462                       | 492                     | 548                          | 562                        | 0.85     | 71,000  | 5.7                                  | Good spectral separation                               | (7)        |
| MiCy-mKO             | 472                       | 495                     | 548                          | 559                        | 0.90     | 51,600  | 5.3                                  | Good spectral separation. MiCy is a dimer              | (200)      |
| mUKG-mKO             | 483                       | 499                     | 548                          | 559                        | 0.72     | 51,600  | -                                    | Good spectral separation                               | (436)      |
| TagGFP-TagRFP        | 482                       | 505                     | 555                          | 584                        | 0.59     | 100,000                                       | 5.7                                  | Very good spectral separation                          | (390)      |
| EGFP-mCherry         | 489                       | 509                     | 587                          | 610                        | 0.60     | 72,000  | 5.1                                  | Very good spectral separation.                         | (152)      |
| Venus-tdTomato       | 515                       | 528                     | 554                          | 581                        | 0.57     | 138,000                                       | 5.9                                  | tdTomato is a tandem                                   | (152)      |
| Venus-mCherry        | 515                       | 528                     | 587                          | 610                        | 0.57     | 72,000  | 5.7                                  | Very good spectral separation.                         | (152)      |
| mCitrine-mKate2      | 516                       | 529                     | 588                          | 633                        | 0.57     | 62,500  | -                                    | Very good spectral separation.                         | (303)      |
| Venus-mPlum          | 515                       | 528                     | 590                          | 649                        | 0.57     | 41,000  | 5.2                                  | Very good spectral separation. Plum is dim.            | (152)      |
| TagRFP-mPlum         | 555                       | 584                     | 590                          | 649                        | 0.48     | 41,000  | -                                    | Plum is dim.   | (127)      |

FIG. 20. Selected FRET pairs of fluorescent proteins.

FRET can be detected in several ways, based on changes of a number of fluorescence parameters that can be measured by the methods of modern fluorescence microscopy (343, 379). These changes include the following: 1) decreased fluorescence brightness (fluorescence quantum yield) of the donor; 2) increased fluorescence brightness of the acceptor upon excitation of the donor; 3) decreased donor fluorescence lifetime; and 4) loss of emission light polarization.

One of the most commonly used methods for imaging FRET is sensitized emission, where the intensity of the acceptor fluorescence is registered upon excitation at a wavelength that is optimal for the donor FP. Sensitized emission is relatively easy to measure but requires multiple controls to reliably establish the presence of FRET, due to substantial cross-talk between excitation and emission spectra of most FP pairs (see below). Image processing necessary to account for this cross-talk may lead to the loss of weak FRET signals (343, 447).

Another FRET detection technique, called acceptor photobleaching, registers an increase in donor fluorescence upon irreversible photobleaching of the acceptor. This technique is more robust than sensitized emission but cannot be used for repeated measurement of the same molecules (188). Importantly, minor photoconversions of FPs, including yellow-to-cyan conversions of some yellow FPs (214, 232, 353, 444) and red-to-green conversions of some red FPs (123, 232, 264), can lead to false-positive results in acceptor photobleaching and should be controlled for. In the future, so-called photochromic FRET employing reversibly inactivated acceptor (see sect. viii) may become a powerful alternative to the acceptor photobleaching method.

One of the most reliable techniques for quantitative FRET measurements is fluorescence lifetime imaging microscopy (FLIM) (35, 148, 446). Its primary advantages are independence of protein concentration and little or no sensitivity to cellular parameters. FLIM, however, requires expensive instrumentation that is not yet widely available.

FRET signals are usually quite weak, making quantitative measurements of changes in FRET efficiency challenging and prone to errors (343, 460). Rigorous FRET experiments require a number of controls and very conservative data interpretation. Specifically, it is important to evaluate, and/or control for, the following potential problems: 1) cross-talk between the FRET partners. On the one hand, acceptor may be excited at the donor excitation wavelength; on the other hand, donor emission may bleed into the acceptor detection channel. Therefore, it is preferable to use FRET partners that are as spectrally separate as possible, but at the same time, donor emission and acceptor excitation should overlap as much as possible. Large Stokes shift FPs, such as UV-excited green

FPs, or some green/red pairs of FPs may help to achieve the desirable compromise (see table in Fig. 20).

2) Undesirable photobleaching or photoconversion (reversible or irreversible) of the donor or acceptor during visualization (see sect. iv): control experiments and appropriate corrections are necessary.

3) Different sensitivities of donors and acceptors to pH and other intracellular parameters: it is generally preferable to use FRET partners with similar pH stability.

4) Difference in stoichiometric ratios of donor and acceptor molecules, or excess of natural cellular partners for the studied recombinant FP-fused proteins, which leads to higher background fluorescence of molecules that are not undergoing FRET: in transient transfection experiments, concentrations of DNA used for transfection can be adjusted to mitigate this problem.

5) Difference in brightness of the donor and acceptor, which can lead to a significant contribution of noise to the fluorescence of a dimmer fluorescent partner: it is preferable to use FRET partners of comparable brightness (343).

6) Unfavorable orientation or large distance between FRET partners within the formed protein complex can diminish the FRET signal, even though the proteins of interest are interacting. Alternative positioning of fused FPs may be necessary to obtain sufficient FRET in such situations (293).

7) Weak interaction may be possible between some donor and acceptor FPs, which may result in two types of effects. On the one hand, the interaction of FPs may increase background FRET signal in the absence of interaction of studied proteins of interest. On the other hand, the weak interaction of FPs may enhance FRET efficiency after the interaction of proteins of interest (321, 457). Depending on the balance between these effects, detection may be either improved or hindered.

In general, it is beneficial to shift the operational wavelengths toward the red part of the spectrum, since it reduces autofluorescence and increases FRET efficiency (123, 229). A palette of novel orange, red, and far-red monomeric FPs (see sect. v) has dramatically expanded the number of potential genetically encoded FRET pairs. Some of these pairs can provide better spectral separation of the donor and acceptor fluorescence and still yield high FRET efficiency. Moreover, the detection of triple interactions by FRET has now become possible, where the acceptor of a donor fluorescence would simultaneously play a role of a donor for the second acceptor (116). In addition, it is now possible to monitor the interaction of two pairs of proteins of interest simultaneously using two pairs of FPs (6, 430).

In practice, the choice of a preferable FRET pair is dictated predominantly by available microscopy solutions, as well as by the limited information on the performance of different FRET pairs. Here we provide an in-

complete list of FRET pairs chosen among the best and most popular ones reported (table in Fig. 20). Förster radius and specific comments found in the table in Figure 20 can guide preliminary comparison of these pairs, but the reader is referred to the original manuscripts for the technical details and potential limitations.

## B. FCCS

An alternative method for detecting protein-protein interactions is based on fluorescence correlation spectroscopy (FCS). FCS detects fluorescence intensity fluctuations at the single molecule level within a limited volume and so allows the measurement of average concentrations and diffusion rates of molecules quantitatively in the living cell.

In dual-color FCCS, the fluctuation of signals is recorded simultaneously for two different fluorophores (24, 381). The cross-correlation is a degree to which the two signals fluctuate together, which allows one to estimate the interdependence of diffusion rates of two types of molecules due to their interaction in living cells (24, 209, 213).

Dual-color FCCS based solely on FPs was first utilized in the work of Kohl et al. in 2002 (221), in which a caspase-3 cleavage site was introduced between a DsRed and green FP and the activation of caspase-3 was monitored. Later on, dual-color FCCS with fused FPs was successfully applied to monitor protein-protein interactions in a number of applications (36, 211, 212).

To provide efficient excitation of two different fluorophores, two laser lines should be used, which must be aligned to the same confocal spot. This can be technically difficult. An alternative solution is to combine two FPs, one with a small and another with a large Stokes shift (see sect. iv), which fluoresces differently but can be excited at the same wavelength. The first application of this idea with FPs was implemented using the mKeima, which has a large Stokes shift, paired with cyan FP (219). Although the low brightness of mKeima limits its wide application for *in vivo* imaging, its success in FCCS is encouraging, and development of enhanced Keima-like FP variants is expected. In the violet part of the spectrum, the combination of blue Azurite (283), EBFP2 (9), or TagBFP (419) with the large Stokes shift T-Sapphire (512) or mAmetrine (6) should theoretically enable dual-color FCCS using a single excitation wavelength (see table in Fig. 10). Another alternative is to employ a two-photon light source that is relatively efficient for excitation of various FPs in dual-color FCCS (211, 212, 221).

The most important difference between FRET and FCCS for studying protein interactions is the distance allowed between the detected fluorophores within a complex. In contrast to FRET, in which close proximity and

favorable orientation of fluorophores are required, FCCS does not depend on a certain distance between the FPs and therefore gives much more freedom with respect to construct design. It is also important to note that FCCS does not require high expression levels and thus minimizes interference with normal cellular biochemistry. Another advantage of FCCS is that monitoring of two fluorophores is concurrent, which makes the readout generally independent of cellular motility, unless the movement of labeled cellular structures introduces undesirable fluorescence fluctuations. At the same time, cell motility can distort data acquired by sequential imaging using FRET techniques (24).

## C. Fluorescence Complementation (Split Fluorescent Proteins)

A powerful method to study protein-protein interactions is the bimolecular fluorescence complementation (BiFC) assay based on split FPs (see more detailed reviews in Refs. 207, 208). We have previously discussed the application of self-assembling variants of split FPs to detect the simultaneous activation of two target promoters (see sect. vi). Such self-assembling split FPs (55–57) are also useful to assess the topology of integral membrane proteins, i.e., to determine the location of their NH<sub>2</sub> and COOH termini and internal hydrophilic loops in particular cell compartments (cytosol, endoplasmic reticulum, etc.) (511). In contrast, studying protein-protein interactions is based on split FP fragments that ideally do not associate with each other spontaneously. Such FP halves are fused to the two proteins of interest. If the target proteins interact, they bring the split FP halves into contact, resulting in reconstitution of FP and fluorescence appearance (178, 208) (Fig. 17B). This provides a technically straightforward and relatively easy way to determine whether two selected proteins interact and where this interaction occurs in the cell. In contrast to FRET measurements discussed above, the BiFC assay is unsuitable for real-time detection of target protein interactions. Indeed, after reassociation of the split FP fragments, it takes time (minutes to hours) to form a mature fluorescent chromophore (208) (there is an EGFP split variant that appears to have a preformed chromophore in the NH<sub>2</sub>-terminal half, but even in this case fluorescence develops within several minutes after complementation) (89). Thus fluorescence development is considerably delayed from the moment when the protein-protein interaction occurs. In addition, the association of FP halves is irreversible in most cases (208), although some examples of partial reversibility of the split FP assembly were documented (89, 133, 443), so breakup of the complex between the target proteins does not quench the fluorescence signal. Notably, trapping the target protein complex forced by an FP

can potentially affect cell physiology. At the same time, even very weak interactions can be detected using BiFC due to signal accumulation (260). Therefore, the sensitivity of BiFC appears to be higher compared with FRET.

A number of efficient split variants were developed for blue (EBFP), cyan (ECFP, Cerulean, SCFP3A), green (EGFP), and yellow (EYFP, Venus, Citrine) mutants of *Aequorea victoria* GFP (178, 179, 398, 462). Moreover, FPs of other origins were used recently to construct their split variants including red and far-red FPs mRFP1 (187), mCherry (105), DsRed-monomer (218), and mKate (67).

A very important step forward was the multicolor BiFC assay (179). Complementary fragments representing color mutants of the same FP (e.g., *Aequorea victoria* GFP) can yield cross-associated species with distinct spectral properties (Fig. 17C). This approach makes it possible to study competition between two or more proteins for binding with a common partner (131, 179). In addition, one can use two split FPs of different origins and distinct colors (e.g., split variants derived from *Aequorea victoria* GFP and DsRed mutants) that do not form hybrids with each other. This approach enables simultaneous visualization of two independent pairs of interacting proteins (105, 218). Finally, a combination of the two above-mentioned approaches, i.e., the use of the cross-associated BiFC system (e.g., Cerulean plus Venus splits) together with a distinct non-cross-associated BiFC system (e.g., mKate split), provides the opportunity to simultaneously detect three pairs of protein-protein interactions in the same cell (67).

To study ternary protein complexes, a combined use of BiFC with FRET or BRET was suggested (117, 399, 400). In these approaches, a red-shifted (e.g., yellow) FP split system acts as an acceptor for FRET/BRET from a blue-shifter donor FP or a luciferase. Thus the interaction of three target proteins can be analyzed: two proteins (A and B) fused to split FP halves and a third protein (C) fused to the donor FP or luciferase (it can be the same target protein in all fusions if its homo-oligomerization is studied; Ref. 117). However, the results of such assays should be treated with caution, because BiFC produces a delayed and irreversible signal, as discussed above. Thus energy transfer to the reconstituted FP acceptor does not necessarily mean that simultaneous interaction of all three native target proteins occurs *in vivo*. Indeed, a situation where protein A transiently interacts with protein B, and then protein B interacts with protein C, will be mistakenly detected as a ternary A-B-C complex by the BiFC-FRET assay.

Further progress in the development of BiFC-based assays for protein-protein interactions will make this approach more efficient and informative. A panel of thermo-tolerant split FP variants of different colors is highly desirable. Split FP variants of different colors and divergent sequences will allow the simultaneous detection of

three or more independent pairs of interacting proteins, while split FPs of different colors generated from one parental FP would be useful to study the competitive interactions of several proteins. Also, the development of a BiFC system with fast fluorescence development and with the capacity for easy and fast dissociation of FP halves would enable the BiFC assay to be applied to study the dynamics of protein-protein complexes in real time.

### VIII. PHOTOACTIVATABLE FLUORESCENT PROTEINS

Photoactivatable fluorescent proteins (PAFPs) represent a distinct class of FPs whose fluorescent properties can be turned on by a pulse of light of a specific wavelength. Kindling from the dark state or switching from one color to another, PAFPs can serve as selective photolabels of proteins, organelles, cells, and tissues. It is possible to choose which fraction of the PAFP molecules to activate, as well as when and within which region of interest. Activated PAFP molecules can be visualized in a separate spectral channel, rendering nonactivated molecules invisible. This property introduces unique possibilities for precision labeling and tracking of objects of interest in living systems, enhancement of signal-to-noise ratio, and super-resolution fluorescence imaging.

#### A. Structural Basis for the Photoactivation

The tight surrounding of a chromophore within GFP-like proteins can stabilize it in various conformations and dramatically influence its spectral properties by determining its protonation state, extinction coefficient, and fluorescence quantum yield, as well as precise positioning of the excitation/emission peaks. Therefore, *cis-trans* transitions of the chromophore, accompanied by conformational changes of neighboring amino acids, can result in reversible light-induced photoconversions that greatly change the spectral properties of a protein (2, 18, 19, 70, 160, 313, 352, 414).

Irreversible changes of spectral characteristics become possible if the energy of absorbed photon leads to a chemical reaction within a particular FP, such as cleavage of the protein backbone within the chromophore (15, 294) or decarboxylation of the Glu222, which plays a key role in the hydrogen network formed around the chromophore (161, 448). Besides, irreversible photoconversions that occur under particular conditions were recently described for the FPs that were not originally considered photoactivatable. In particular, we have reported the oxidative reddening characteristic for apparently all green FPs, including EGFP (45). Red-to-green or orange-to-far-red photoconversions upon intense or two-photon excitation were reported for DsRed, mKate, mKO, and mOr-

ange, the mechanism of which remains unclear (123, 232, 264). Some of these photoconversions may find practical application in the future.

## B. Key Properties of PAFPs

Similar to common FPs, for practical use of a PAFP it is important to consider such parameters as brightness, photostability, pH stability, maturation rate of the initial form at 37°C, turnover of PAFP or its fusion construct in living cells, and absence of additional minor photoconversions (besides the key photoswitching event), both for the initial and for the activated states of the PAFP. Regardless of visualization techniques and the experimental task, monomeric PAFPs are required for applications involving molecular tagging, due to the reasons described in section IV.

An additional specific characteristic of PAFPs is the maximal contrast obtainable after photoactivation, i.e., the brightness of the activated form relative to the initial one. The contrast determines the signal-to-noise ratio and thus sets the primary limit to any application of a PAFP.

The intensity of light required for the photoactivation of a PAFP is also an important parameter. If the required activating light intensity is too high, it can be harmful to living cells and can photobleach other FPs used in multi-color experiments. It may also require prolonged irradiation for effective photoactivation, which is undesirable for fast tracking experiments. On the other hand, activation that is too easy is also undesirable, since it makes visualization of the initial nonactivated form difficult, complicates precise control of photoactivation, and may lead to increased background signal.

Successful photoactivation often depends on the light source and many other parameters, including light continuity (differing for the confocal versus widefield microscopy), light intensity, light wavelength, zoom, irradiated field, protein motility, and temperature (72, 73, 255, 335, 479), as well as hypothetically on the redox potential of the environment (45). Therefore, each new PAFP requires thorough testing and fine-tuning of photoactivation parameters for a particular live system and a microscope.

## C. Reversible PAFPs

Reversible increase or decrease of fluorescence brightness is a widespread phenomenon among FPs. For example, red fluorescent proteins mKate and mCherry demonstrate a 5–15% increase in fluorescence brightness upon irradiation by green light. At the same time, many FPs demonstrate more or less pronounced reversible “quenching,” which can exceed 50% of initial brightness under appropriate irradiation conditions, as demonstrated for Venus, Cerulean, Emerald, mApple, etc. (233, 385). Moreover, depending on the parameters of the irradiating light,

the same protein can demonstrate either kindling or quenching photobehavior (385).

In extreme cases, reversible changes may involve the switching of a protein from an essentially nonfluorescent state to a bright fluorescent state (“kindling”) or from a bright fluorescent to a nonfluorescent (“quenching”) state. Fluorescence characteristics of such reversible PAFPs can be controlled by light irradiation of a specific wavelength, intensity, and duration. Moreover, fluorescence of reversible PAFPs can be switched on and off multiple times (hundreds of times for the good variants).

Reversible PAFPs reported to date include none-to-red activatable “kindling” coral protein asFP595 (256), along with its mutant variants (KFP1 and others; Refs. 68, 70), green-to-none “quenchable” Dronpa (16, 139, 140) and a number of its enhanced versions and modifications (14, 17, 414, 486), cyan-to-none “quenchable” mTFP0.7 and its modifications (160), and none-to-red activatable rsCherry and rsCherryRev (413).

An additional characteristic specific to reversible PAFPs is the relaxation half-time, which is the time period required for 50% of the photoactivated or quenched protein to spontaneously return to the initial state. The relaxation half-time can vary from several seconds to hours for different reversible PAFPs and also depends on the temperature. For some of the reversible PAFPs, immediate reverse transition is possible by irradiation of light of another wavelength. For example, nonfluorescent asFP595 (also known as asulCP and asCP) “kindles” into the bright red form upon intense green light irradiation (which coincides with the excitation optimum), but can be “quenched” immediately by weak blue (450 nm) light irradiation. Green fluorescent Dronpa demonstrates the opposite behavior: it can be “quenched” by intense blue light irradiation (which coincides with the excitation optimum), but can be immediately “kindled” back to the bright fluorescent state by relatively weak violet light irradiation.

The PAFP field is rapidly developing. New PAFP variants appear every few months, and many of them at the moment remain poorly characterized. Among these proteins, Dronpa is currently the best-tested reversible PAFP that is monomeric, has high brightness, and can be switched on and off multiple times with high contrast (85). A brief overview of the characteristics of reversible PAFPs is provided in the table in Figure 21.

Reversible photoconversions of FPs can be implemented for a number of unique techniques for precise imaging.

### 1. Repeated tracking of protein movement

A portion of PAFP fused to a protein can be selectively photoactivated within a region of interest of a live cell, and the rate of distribution of the activated fluorescent signal can be tracked. In such a way, PAFPs can help

| PAFP                                   | Kindling FPs<br>(asFP595,<br>asFP595-148G,<br>KFP1, etc.) | Dronpa and its<br>variants           | Padron                               | mTFP0.7 and<br>its variants         | rsCherry                            | rsCherryRev                         |
|--|---|--------------------------------------|--------------------------------------|-------------------------------------|-------------------------------------|-------------------------------------|
| Oligomeric state                       | Tetramer  | Monomer                              | Monomer                              | Monomer                             | Monomer                             | Monomer                             |
| Activating light                       | Green or<br>yellow  | UV-Violet                            | Blue, max at<br>~490 nm              | UV-Violet                           | Yellow                              | Blue, max at<br>~450 nm             |
| Quenching light                        | Blue, max at<br>~450 nm                                   | Blue, max at<br>~490 nm              | UV-Violet                            | Blue                                | Blue, max at<br>~450 nm             | Yellow                              |
| On-state color,<br>ex/em peaked at, nm | Red,<br>580/600-615                                       | Green,<br>503/518                    | Green,<br>503/518                    | Cyan                                | Red,<br>572/610                     | Red,<br>572/610                     |
| Fluorescence changes,<br>fold          | 70-100  | n.d. (high)                          | n.d. (high)                          | 14                                  | 7                                   | 20                                  |
| Brightness of the<br>fluorescent form  | medium  | high                                 | low                                  | n.d.                                | Low<br>(high at single<br>molecule) | Low<br>(high at single<br>molecule) |
| Source organism<br>(Class of organism) | <i>Anemonia</i><br><i>sulcata</i><br>(Anthozoa)           | <i>Pectiniidae</i> sp.<br>(Anthozoa) | <i>Pectiniidae</i> sp.<br>(Anthozoa) | <i>Clavularia</i> sp.<br>(Anthozoa) | <i>Discosoma</i> sp.<br>(Anthozoa)  | <i>Discosoma</i> sp.<br>(Anthozoa)  |
| References                             | (68, 70, 256)   | (14, 16, 17,<br>139, 414,<br>486)    | (17)                                 | (160)                               | (413)                               | (413)                               |

FIG. 21. Selected reversibly photoactivatable FPs.

tracking protein motility, similar to the photobleaching techniques discussed in section vi. However, the PAFP approach is more straightforward: instead of inferring the protein movement from the change in average fluorescence, it can be used to directly observe the redistribution of the photoactivated protein molecules. This approach is more informative and can be applied for tracking very fast protein movement. In contrast to the irreversible PAFPs (see below), reversible ones can be applied to track movement of a fused protein of interest repeatedly within the same cell, to generate multiple spatial and temporal points. This allows the identification of differences in protein motility in various parts of the same cell and the monitoring of changes in motility or transport direction of a protein in response to the particular external influence or caused by internal changes of the cell state (16).

## 2. Enhanced imaging of fast protein movement: “protein rivers”

By averaging multiple tracking series, it is possible to obtain low-noise time series of protein redistribution within a cell. In this approach, reversible photoactivation is used to collect information for identical time series obtained after multiple photoactivation rounds. Averaging of the data results in high signal-to-noise ratio imaging of rapid protein movement (69).

## 3. Reliable FRET detection: photochromic FRET

Photochromic FRET (PC-FRET) is based on the use of a FRET acceptor that can be reversibly photoswitched

between two states that are substantially different in their absorbance spectra and/or molar extinction coefficient. Such a light-controlled acceptor can serve as an intrinsic control of FRET (see sect. vii). Indeed, if a fluorescent donor is in close proximity to the acceptor (PAFP), then the intensity or lifetime of the donor fluorescence must be affected by photoswitching of the acceptor. PC-FRET has been described with organic dyes (120), and we anticipate that analogous PAFP-based methods will appear in the near future. The only requirement for the technique is the development of monomeric reversibly photoactivatable FP that would substantially change absorbance characteristics in the orange-red part of the spectrum upon photoconversion.

## 4. Enhancement of signal-to-noise ratio

Optical control allows the switching of reversible PAFP between the fluorescent and nonfluorescent states, while other signals remain constant. Therefore, a specific fluorescence signal can be distinguished from the background by selective registration of the modulated fluorescence of a reversible PAFP. This approach results in high-contrast images of specific structures on high background levels (266).

## 5. Dual-color imaging within the same channel

Similar to the previous application, reversible PAFPs can be detected not only despite high background levels, but also in the presence of another flu-

orescent dye of the same color. For example, green EGFP can be combined with green Dronpa in dual-color labeling experiments.

### 6. Super-resolution imaging

Probably the most exciting application of reversible PAFPs is super-resolution imaging based either on reversible saturable optical fluorescence transitions (RESOLFT; Refs. 172, 380) or on photoactivated localization microscopy (PALM) techniques (see below).

## D. Irreversible PAFPs

Switching of irreversible PAFPs leads to profound one-time photoconversion from a nonfluorescent state to bright green or red fluorescence, from cyan fluorescence to green, from green fluorescent to red, etc. This activated signal can be bleached but cannot be reverted to the initial state of the protein, and thus photoactivation cannot be repeated multiple times for the same protein molecule. Irreversible PAFPs open a different range of opportunities for *in vivo* photolabeling and visualization techniques, since they enable the accumulation of contrasting activated signals and ensure their stability over time.

To date, multiple irreversible PAFPs of various spectral characteristics have been developed (table in Fig. 22).

The first one reported, PA-GFP, switches from a weakly green fluorescent state excited by violet light (~400 nm) to a bright green fluorescent state excited by blue light (~480 nm) (334). Photoactivation requires violet light irradiation of relatively low intensity and results in a 100-fold increase of blue-light-excited green fluorescence, making it possible to visualize the activated protein with high contrast. Initial violet-light-excited green fluorescence can be visualized as well but photoconverts rapidly. Therefore, it is rather difficult to obtain an image showing the initial location of PA-GFP without undesirable activation of the whole field. This drawback hampers the rational choice of the region of interest for further photoactivation. Nevertheless, due to its monomeric nature, high contrast and high brightness of the activated form, PA-GFP is one of the most powerful PAFPs and has gained popularity in a variety of applications (29, 66, 88, 91, 144, 161, 165, 258, 269, 272, 274, 297, 320, 335, 377, 426, 427, 461).

A similar protein, named PS-CFP, as well as its enhanced version, PS-CFP2 (Evrogen), switches from the cyan to green fluorescent state with high contrast in response to irradiation by a 405-nm laser line (72, 74). Compared with PA-GFP, PS-CFP2 gives lower brightness of the activated signal. However, its key advantage is that the initial cyan form can be visualized without significant photoactivation, especially using an arc lamp source (491).

| PAFP                                | PA-GFP                              | PS-CFP2                                 | Kaede                                     | tdEos                                    | mEos2                                    | KikGR                         | mKikGR                        | Dendra2                              | PA-mCherries                    |
|-------------------------------------|-------------------------------------|---|---|--|--|-------------------------------|-------------------------------|--------------------------------------|---------------------------------|
| Oligomeric state                    | Monomer                             | Monomer                                 | Tetramer                                  | Tandem                                   | Monomer                                  | Tetramer                      | Monomer                       | Monomer                              | Monomer                         |
| Activating light                    | UV-Violet                           | UV-Violet                               | UV-Violet                                 | UV-Violet                                | UV-Violet                                | UV-Violet                     | UV-Violet                     | UV-Violet or blue                    | UV-Violet                       |
| Initial color, ex/em, nm            | Green*, 400/515                     | Cyan, 400/468                           | Green, 508/518                            | Green, 506/516                           | Green, 506/519                           | Green, 507/515                | Green, 507/515                | Green, 490/507                       | Dark, Abs. at 400               |
| Switched color, ex/em peaked at, nm | Green, 504/517                      | Green, 490/511                          | Red, 572/580                              | Red, 569/581                             | Red, 573/584                             | Red, 583/593                  | Red, 580/591                  | Red, 553/573                         | Red, 570/596                    |
| Fluorescence changes, fold          | ~200                                | >2,000                                  | 2,000                                     | nd                                       | nd                                       | >2,000                        | 560                           | 4,500                                | 3,000-5,000                     |
| Brightness of the initial form      | low                                 | medium                                  | high                                      | high                                     | high                                     | high                          | high                          | high                                 | na                              |
| Brightness of the activated form    | medium                              | medium                                  | high                                      | high                                     | high                                     | high                          | high                          | high                                 | medium                          |
| Source organism (Class of organism) | <i>Aequorea victoria</i> (Hydrozoa) | <i>Aequorea coerulescens</i> (Hydrozoa) | <i>Trachyphyllia geoffroyi</i> (Anthozoa) | <i>Lobophyllia hemprichii</i> (Anthozoa) | <i>Lobophyllia hemprichii</i> (Anthozoa) | <i>Favia Favus</i> (Anthozoa) | <i>Favia Favus</i> (Anthozoa) | <i>Dendronephthya sp.</i> (Anthozoa) | <i>Discosoma sp.</i> (Anthozoa) |
| References                          | (334)                               | (74)                                    | (15)                                      | (312, 478)                               | (281)                                    | (437)                         | (141)                         | (136)                                | (417)                           |

FIG. 22. Selected irreversibly photoactivatable FPs. \*Initial weak green fluorescence of PA-GFP can be visualized using violet excitation, but rapidly leads to photoconversion.

A specific class of irreversible PAFPs is comprised by Kaede-like proteins. Kaede (“maple leaf” in Japanese) is the founder of this group, which rapidly changes its color from green to red upon violet light irradiation (15). Photoactivation of Kaede-like proteins is based on the cleavage within the first amino acid of the chromophore, His65, which results in  $\pi$ -electron conjugation of Tyr66 to the imidazole ring of His65 and thus leads to the dramatic batochromic shift (294, 314).

Photoactivation of Kaede generates high contrast, and spectral characteristics of both initial and activated forms of the protein are favorable. Importantly, the non-activated green fluorescent protein can be monitored using blue (488 nm) light excitation without any photoactivation.

Kaede has been successfully applied as a very efficient marker for photolabeling and tracking of organelles in cells and cells in living tissues (376, 431). However, Kaede, as well as several other proteins of the same type, including mcavRFP (239), rfloRFP (239), dendGFP (239), EosFP (478), and engineered KikGR (437), were all cloned or developed from Anthozoa species and are inherently tetrameric, just as all other Anthozoan FPs. To overcome this limitation, significant efforts were devoted to develop monomeric Kaede-like proteins, resulting in a series of markers (136, 141, 281, 312, 478), the best of which are currently mEos2 (281) and Dendra2 (3, 136) (see table in Fig. 22). These proteins are extensively used in various techniques, including protein tracking (29, 81, 104, 422) and super-resolution microscopy (107, 126, 236, 281) (see below).

Dendra2 is notable due to its ability to be photoactivated not only by violet, but also by less damaging blue light irradiation using an arc lamp (see table in Fig. 22). However, to achieve such blue-light-mediated activation on a confocal microscope, very careful adaptation of irradiation parameters is required. This conversion is easy to achieve in Leica SP2 confocal microscopes equipped with a “beam expander” hardware option (72, 73).

Another emerging class of irreversible PAFPs is represented by none-to-red activatable proteins based on monomeric red FPs. While the first reported protein of this type, PA-mRFP1, was characterized by rather dim fluorescence (453), significantly enhanced variants named PAmCherry1, -2, and -3 were reported recently (417). PAmCherries are characterized by faster photoactivation, higher contrast, and better photostability and may become a valuable addition for super-resolution imaging in two-color PALM.

IrisFP is a remarkable protein of the most complex photobehavior reported to date among FPs (2), demonstrating both reversible and irreversible types of photo-transformation. This protein is a mutant version of EosFP (478) and is capable of irreversible photoconversion from a green to a red fluorescence state, whereas both initial

green and activated red fluorescent forms are also capable of reversible photoswitching.

Applications of irreversible PAFPs include the following.

### *1. Redistribution of a protein of interest*

Protein movement in living cells can be visualized with irreversible photoactivation as described above for reversible PAFPs. Irreversible photoactivation does not allow for repeated photoactivation and tracking events, but instead produces a stable signal that can be tracked for a long period of time. Therefore, irreversible PAFPs represent a strong alternative to traditional kinetic microscopy of protein motility in living cells, based on photobleaching effects (250) (see sect. vi).

### *2. Organelle labeling and tracking*

With the use of a specific localization signal (see sect. vi), PAFP can be targeted to any organelle of a living cell. Individual organelles can then be labeled with irreversible photoactivation to track their motility, direction of movement, and interaction with other organelles in fusion-fission events (297). In addition, motility of proteins within organelles and proteins exchange between cellular compartments can be tracked.

### *3. Cell labeling*

Irreversible PAFP can be used to photolabel individual cells within cultures, living tissue, or whole organisms to track the movements of these cells during development, cancerogenesis, and inflammation (255, 376, 431). For example, with PS-CFP2 it is possible to track the photolabeled cell of interest in a living organism for up to several days (411).

### *4. Protein degradation*

Irreversible PAFPs can be used to track the degradation of a fusion protein of interest. In contrast to the fluorescence intensity of a common FP, the photoactivated signal is independent of the rate of novel protein synthesis. Therefore, photoactivation generates a fluorescent signal that depends only on the degradation rate of the construct (provided that potential photobleaching effects are avoided or appropriately corrected for). This technique allows precise and direct monitoring of protein degradation in living cells (515).

### *5. Super-resolution microscopy*

Similar to reversible PAFPs, arguably the most powerful and therefore rapidly developing application of irreversible PAFPs is the imaging of fluorescence at a resolution beyond the diffraction barrier (see below).

### E. Super-resolution Microscopy

Spatial resolution in optical microscopy is limited by the diffraction of light. Due to diffraction, any point source of light is always observed as a blurred spot when visualized in optical microscopy, as demonstrated by Abbe as early as 1873 (1). The resulting profile of the observed blurred spot is described by point spread function (PSF), which depends on the NA (numerical aperture) of the objective. The PSFs generated by two fluorophores separated by too short distance will overlap and will become impossible to resolve as two point sources of light. Thus PSF limits the resolution of the optical microscope. It can be expressed as a full width at half maximum (FWHM) of a PSF, which is physically limited to  $\lambda/(2NA)$  for the focal plane ( $xy$ ) and to  $2\lambda\eta/(2NA)^2$  for the optical axis ( $z$ ). Since objective lenses have an NA of  $<1.5$ , this results in a maximal 150–200 nm lateral and 500 nm axial resolution that can be theoretically obtained by optical microscopy (158).

This resolution is clearly insufficient for detailed studies of cellular structures, many of which require resolution at the nanometer scale. In addition, it is very desirable to achieve sufficient resolution to enable direct visualization of interaction between two proteins in living cells. Although electron microscopy provides a very high resolution (224), it cannot visualize live cells. Moreover, low labeling efficiency in electron microscopy makes visualization of molecular interactions extremely difficult.

A number of techniques have been developed to improve the resolution of optical microscopy, including optical sectioning by confocal microscopy (62) and multi-photon excitation (90, 97), improvement of axial resolution by two objective lenses employed in 4Pi (159) and I<sup>5</sup>M (138).

Still, axial resolution was not significantly improved, and optical microscopy remained limited by the diffraction barrier. The recent development of “super-resolution” microscopy, which is able to resolve objects separated by several nanometers in living cells by fluorescent microscopy, was therefore a long-anticipated breakthrough.

In the past 20 years, several super-resolution techniques were proposed, either avoiding significant diffraction (near-field super-resolution imaging) or overcoming the diffraction limit by modulating the molecular states of a fluorophore that narrows the PSF or precise localization of individual fluorophore molecules through processing of the blurred images (107, 157). The combination of the latter idea with PAFPs has revolutionized fluorescent in vivo imaging by introducing a technique named PALM. PALM [and the like: PALMIRA (100), FPALM (165, 166)] goes beyond the diffraction barrier in fluorescence microscopy in living cells and currently represents one of the most promising super-resolution approaches.

PALM is based on gradual and statistically random photoswitching of a pool of photoactivatable probes in a sample, using light of a power insufficient to activate all the molecules at once. A stack of images representing random samples of fluorophore molecules is accumulated through repeated cycles of photoactivation followed by exhaustive photobleaching. These images can be processed according to single molecule techniques, such that each molecule can be localized with high precision by determining its center of fluorescence emission. This position is calculated by fitting the measured photon distribution from an individual molecule to the ideal PSF. Therefore, the precision of localization directly depends on the number of detected photons per activated molecule and thus on the fluorescence quantum yield and photostability of the photoactivated form of a PAFP. The best systems report up to 10 nm localization precision for the FPs in cells.

A number of monomeric photoactivatable fluorescent proteins have been developed that are well suitable for PALM, including both irreversibly photoactivatable proteins and reversible ones (41). To date, successful PALM imaging has been demonstrated for PA-GFP (165, 166), Dronpa (395), PS-CFP2 (395), mEos2 (281), Dendra2 (281), and PA-mCherry1 (417). Some of the photoactivatable proteins can be combined to obtain a two-color PALM. One of the favorable solutions reported is the combination of PS-CFP2 with green-to-red photoconvertible protein (395), as tdEosFP, mEos2, or Dendra2. In principle, two-color PALM should allow the visualization of protein-protein interactions directly, which is one of the most important goals of super-resolution imaging.

## IX. GENETICALLY ENCODED SENSORS

### A. Power of Genetically Encoded Sensors

FPs represent a unique basis for development of fully genetically encoded sensors (GES) that can be used to visualize and quantify the enzymatic activity or conformational state of a protein of interest, changes in concentrations of particular molecules, and various physiological events in vivo, including living cells, tissues, or whole organisms.

On a whole organism scale, GES allow the visualization of signaling pathways between different cells, such as neuronal activities, interactions of cells in development, and communication of immune cells. Arguably the most promising application is to image the responses from individual neurons in vivo in transgenic animals with calcium GES (263, 428). On a cellular scale, GES have been adopted for a variety of tasks and can be used to decipher the complex network of interacting proteins, nucleic acids, and other molecules through both time and space (60, 129, 290, 408, 449, 513).

The unique nature of GES makes them quite different from the chemically synthesized sensitive fluorescent dyes, in terms of both their development and their application. The first key difference is that the GES are delivered as genetic materials by either transient transfection or transgenic techniques and are subsequently produced by cells themselves. Transgenic organisms expressing GES can be created to monitor analyte concentrations, the activity of proteins of interest, and cell states *in vivo*, including tissues and cells that cannot be loaded with fluorescent dyes. Tissue-specific, stage-specific, and inducible promoters and regulatory genetic elements can drive GES expression selectively in chosen cells and in a temporally controlled manner.

The protein nature of GES allows their targeting to virtually any cellular compartment or microcompartment through fusion with an appropriate signal domain, or by adding a few extra amino acid residues to one of the protein's termini that form appropriate signal motif. Some of the commonly used signal motifs are summarized in Table 1 (see sect. vi).

In contrast to chemical dyes, GES do not require external injection and are not prone to leakage during long-term experiments. Also, stably transfected cell lines can be used to standardize high-throughput and high-content screening assays.

Arguably the most important principal advantage of GES is that they can incorporate naturally evolved protein sensor domains, which can provide ultimate sensitivity and specificity for virtually any molecular or physiological event or an analyte of interest. Practically any process in a living cell involves proteins, so a suitable sensor domain that generates some readout (such as change in conformation or protein-binding affinity) upon binding of a specific analyte, covalent modification, mechanical influence, redox potential, membrane potential, etc. can potentially be found in nature. Accordingly, sensitive genetically encoded constructs can be designed by nimble manipulation of these domains and FP(s), either utilizing the conformational changes of fused domains to influence spectral properties of a single FP, or based on changes in distance and dipole orientation between two FPs capable of FRET (see sect. vii). This approach has resulted in a great number of FP-based sensors for monitoring specific physiological events in living cells and tissues by means of fluorescent microscopy, spectroscopy, and flow cytometry analysis (129, 195, 290, 408, 449, 513).

However, the natural origin of such sensor domains can also be their drawback. In the complex molecular ensemble of a living cell, there is hardly any protein domain that is specialized for a single function or interaction partner. Therefore, most nature-derived sensory domains are prone to numerous modifications and/or interactions, which may impair the desirable single-parameter readout of a sensor. In addition, the expression of a

natural protein domain within a sensor construct may affect the protein interaction network of the living cell and thus create artifacts (290). This problem may become particularly serious due to the need to express a GES at a high level for reliable detection of the fluorescent signal.

To minimize the disturbance of the protein interaction network, it is generally desirable to use sensory domains that are already naturally abundant in a cell. Another way to solve this problem is to modify the sensory domain of a GES to make it unrecognizable by the potential cellular partners. For example, computational redesign of calmodulin and calmodulin-binding peptide M13 made it possible to generate functional calcium-sensitive FRET constructs characterized by low affinity to free cellular calmodulin (327). Yet another way to minimize GES/cellular machinery interactions is to use sensory domains of heterologous origin. For example, the hydrogen peroxide sensor HyPer (see below) incorporates a prokaryotic H<sub>2</sub>O<sub>2</sub>-sensitive domain that has no natural ligands within eukaryotic cells and thus minimally interferes with the cellular environment (39).

GES can be classified into four groups according to the basic principles of their design: 1) single FP-based sensors with no additional protein domains, designed to detect certain ions; 2) single FP-based sensors incorporating (or fused to) a conformationally sensitive detector domain(s); 3) FRET-based sensors based on two FPs; and 4) translocation sensors/assays.

## B. Sensors Based on a Single FP With No Additional Protein Domains

The natural properties of the chromophore and its environment within FPs make it possible to develop mutant variants sensitive to particular analytes. GES based on a single FP were developed to detect changes in pH value (147, 193, 216, 280, 286, 362), concentrations of chloride (190, 464) and metal ions (31, 246), and redox potential (94, 146).

Among these, pH sensors are the most elaborate and are in high demand in various studies. In particular, the acidic pH inside secretory vesicles can be exploited to monitor exocytosis and recycling using pH-sensitive FPs (21, 286). Some sensitivity to pH is the natural property of most FPs carrying either GFP-like or DsRed-like chromophores; thus virtually any FP can be used to monitor pH changes in living cells (23, 147, 193, 216, 252, 280, 286, 310, 362). In FPs with GFP-like chromophores, the proportion of charged ground-state chromophores (corresponding to the excitation peak at ~480 nm) grows upon an increase in pH up to 9.0, while the proportion of those in the protonated form (excitation peak at ~400 nm) diminishes. Therefore, 480–500 nm excited fluorescence of a green or yellow FP usually increases with increased

pH. This fluorescence intensity change in response to pH is reversible and very fast, occurring in <1 ms (216).

Sensitivity of an FP to pH can be described by the apparent  $pK_a$  of the charged chromophore, which is the pH value at which the intensity of green fluorescence excited at 480 nm declines by 50% of the maximal brightness, and the Hill coefficient derived from the slope of fluorescence versus pH curve at the  $pK_a$  point. Common green FPs with a  $pK_a$  at ~6.0 (table in Fig. 10) are suitable to measure pH changes in acidic compartments, while some of the less acid-tolerant yellow FPs can be used to measure pH changes in the cytosol (21).

FP variants with different  $pK_a$  were generated by rational and random mutagenesis. For example, pH-sensitive mutants were designed specifically for monitoring synaptic vesicle cycling at nerve terminals. Fluorescence of the best variants increases >50-fold (our *in vitro* data for the Superecliptic pHluorin, Ref. 372) in response to a pH change from 5.5 to 7.5, which corresponds to the changes that occur upon synaptic vesicle release.

Various GES for monitoring pH were generated, responding either with changes in fluorescent brightness of a single fluorescence peak or with ratiometric changes of two excitation peaks. The latter type of pH sensors imply ratiometric measurement of fluorescence brightness excited at two different wavelengths and hence are free from artifacts due to variable protein concentration, cell thickness, cell movement, excitation intensity, etc. Ratiometric pH sensors commonly respond with a change in the ratio of excitation efficiency at 400 versus 480 nm due to a shift in the protonated/deprotonated chromophore ratio (such as ratiometric pHluorin, Ref. 286). An internal control of overall signal stability can be the intensity of fluorescence excited at the isosbestic point between the two excitation peaks, at ~430 nm. Another type of ratiometric GES utilizes the pH-sensitive efficiency of excited state proton transfer (ESPT) from the protonated GFP chromophore excited at 400 nm. These sensors are excited at 400 nm and respond with a change of fluorescence ratio between 450 and 510 nm (147). Ratiometric pH sensors can also be developed by fusing pH-stable and pH-sensitive variants of different colors. In this case, changes in the fluorescence brightness ratio of the two fused FPs can be measured along with FRET efficiency between the two FPs (23). Recently, a pH-sensitive red FP was reported (193) that can be expected to become a popular pH-GES in molecular neurobiology and other fields requiring multi-parameter imaging.

### C. Sensors Built on a Single FP Fused to the Conformationally Sensitive Detector Domain(s)

Conformational changes or interactions between domains fused to an FP, occurring in response to a specific

protein activity or change in concentration of an analyte of interest, can cause changes in the structure of the FP and thus influence its spectral properties. Occasionally, a working GES can be created by simple end-fusion of a sensor domain to an unmodified FP. However, due to the stability of the  $\beta$ -barrel structure of FPs and spatial and structural isolation of the  $\text{NH}_2$  and  $\text{COOH}$  termini from the chromophore, the influence of end-fused domains on protein fluorescence is usually negligible. Therefore, it is much more effective to place the sensitive domains in close proximity to the FP chromophore. This can be achieved by inserting sensitive domains into the structure of an FP or by end-fusing them to a circularly permuted FP (cpFP).

Circular permutation (254) implies that protein  $\text{NH}_2$  and  $\text{COOH}$  termini are joined together by flexible linkers several amino acids long, and new  $\text{NH}_2$  and  $\text{COOH}$  termini are formed in another part of the protein. Permutation of FPs is usually successful and has become a routine approach to fuse sensitive domains very close to the chromophore, which allows to influence its spectral properties directly (27, 307, 512). This GES design strategy resulted in a number of calcium sensors (306, 309, 322, 407, 424, 428) and was also applied to create sensors of hydrogen peroxide (39), phosphorylation (205), and membrane potential (119, 217), although the latter two directions have not yet produced effective GES.

Within cpFP-based sensitive constructs, conformational changes of sensory domains can cause dramatic structural changes in the chromophore environment and thus strongly influence spectral properties of the cpFP. In principle, this influence can be mediated by a number of factors, including protonation/deprotonation of a GFP-like chromophore as well as changes in its fluorescence quantum yield and molar extinction coefficient. Most if not all currently existing cpFP-based sensors employ changes in the protonation status of a GFP-like chromophore. Due to the openness of the chromophore to the environment (characteristic of the most common permuted variants with a permutation point in the vicinity of amino acid positions 146–147, according to GFP sequence), cpFP-based sensors are usually pH sensitive, with a  $pK_a$  (pH value at which fluorescence brightness is half of a maximal) >7.0. Thus, unfortunately, fluorescent properties of cpFP-based sensors are affected by pH within the physiological range.

However, this dependence is not an inherent property of all FPs capable of protonation/deprotonation of the GFP-like chromophore. Indeed, high-contrast photoactivatable fluorescent proteins PA-GFP (334) and PS-CFP (74) employ deprotonation of the chromophore upon activation but remain pH stable in both the initial and photoactivated states (see sect. viii). Therefore, there is no theoretical barrier to solving the problem of low pH stability of the cpFP-based sensors. This will require the

appropriate design of the chromophore surrounding that would protect the chromophore from the environment and thus make its protonation/deprotonation dependent only on positioning of proximate amino acid residues. These residues, in turn, would be controlled by the fused conformationally sensitive domains. We expect that progress in this direction will be made in the near future with the help of either powerful computational design and/or extensive *in vitro* evolution.

In general, cpFP-based GES are quite promising due to the potentially high dynamic range of achievable changes of fluorescence. Parallels with photoactivatable proteins suggest that chromophore protonation/deprotonation can result in 100-fold fluorescence changes (74, 334). Therefore, although the most elaborated current theme of cpFP-based GES is calcium sensing, we expect that high dynamic range GES of other specificities will be reported.

A remarkable example is the first specific sensor for the hydrogen peroxide, named HyPer (39, 265). HyPer is based on a permuted yellow FP that is inserted into the prokaryotic regulatory domain OxyR, which is sensitive to H<sub>2</sub>O<sub>2</sub>. In the presence of submicromolar concentrations of H<sub>2</sub>O<sub>2</sub>, two cysteine residues of OxyR are oxidized, resulting in dramatic conformational changes of the domain. These changes influence the chromophore environment and ratiometrically change the fluorescence excitation spectrum: fluorescence excited at 420 nm decreases and fluorescence excited at 500 nm grows. Hydrogen peroxide is an important signaling molecule, and HyPer provides a unique possibility to study its functional role in living cells and organisms. As the first independent application of HyPer, it was recently demonstrated that a rise in H<sub>2</sub>O<sub>2</sub> concentration can determine rapid wound detection in zebrafish (316).

#### D. FRET-Based Sensors

The readout of FRET-based sensors is the change in the efficiency of resonance energy transfer between two spectrally differing FPs (see sect. vii about FRET). Efficiency of FRET depends on the distance between the two FPs and orientation of their chromophores relative to each other. Therefore, using a combination of detector protein domain(s) and a pair of FPs of different color, it is possible to engineer a GES that will react to certain intracellular events by changing its spectral properties.

The simplest design of FRET-based GES employs the fusion of two FPs via a peptide linker that can be specifically cleaved by a cellular protease of interest, such as caspase-1 (261), caspase-3 (6, 148, 200, 259, 261, 305, 390, 423, 441, 489, 490, 492), caspase-6 (489), or caspase-8 (490). GES of this type usually demonstrate high dynamic range due to the complete spatial separation of donor and

acceptor FPs after cleavage, but are limited to the monitoring of protease activities.

An inverse approach is to monitor FRET between donor and acceptor FPs fused to the separate interacting domains, which is rather similar to the general approach of FRET-based protein interaction studies (see sect. vii). The difference is that with GES scientists know in advance that the two domains should interact in response to the particular event and use this interaction as the event's reporter. However, the domain fused to the donor FP may interact not only with the domain fused to the acceptor FP, but also with endogenous proteins, which renders the donor molecules nonresponsive and decreases the signal. This effect can essentially preclude the detectable response *in vivo* from a sensor that behaves perfectly well *in vitro*.

In the most universally applicable and therefore widely used FRET-GES design, both donor and acceptor FPs are fused to the single structurally active protein construct, whose conformational changes affect the distance between and the mutual orientation of two FPs. This responding protein construct may consist of one domain or several domains that either interact with each other or undergo structural changes in response to a specific cellular event, such as an increase in ion concentration, modification by the enzyme of interest, change in membrane potential, etc. (Fig. 23). Such a design of FRET sensors implies that donor and acceptor FPs are present in equimolar quantities, and the interacting domains preferentially exhibit intramolecular binding. Therefore, all sensor molecules contribute to FRET changes in a living cell, and thus the FRET signal increases. The intrinsic limitation of this design, however, is that spatial proximity of the donor and acceptor within a single construct before event of interest can lead to a high background FRET signal (290).

The universality and relative simplicity of such a design have led to the development of numerous FRET-based sensors of this type, including GES for monitoring changes in the concentration of Ca<sup>2+</sup> (130, 153, 262, 263, 291, 292, 295, 304, 307, 327, 434), cyclic nucleotides (174, 317, 318, 375, 445, 506), glutamate (323), tryptophan (199), specific saccharides (198), GTPase activities (186, 296), kinase activities (128, 149, 234, 235, 237, 308, 374, 429, 458, 514), mechanical stress (284), and others (Table 2).

One of the notable and rapidly developing GES-related directions is the design of GES for the detection of changes in membrane potential, where FPs are fused to a voltage-sensitive membrane domain. The specific feature of these voltage sensors is that cellular membrane acts as an additional element that influences structural rearrangements. Several variants of FP-based voltage sensors have been proposed, employing a membrane protein domain that undergoes conformational changes in a voltage-dependent manner that lead to changes of a fused FP

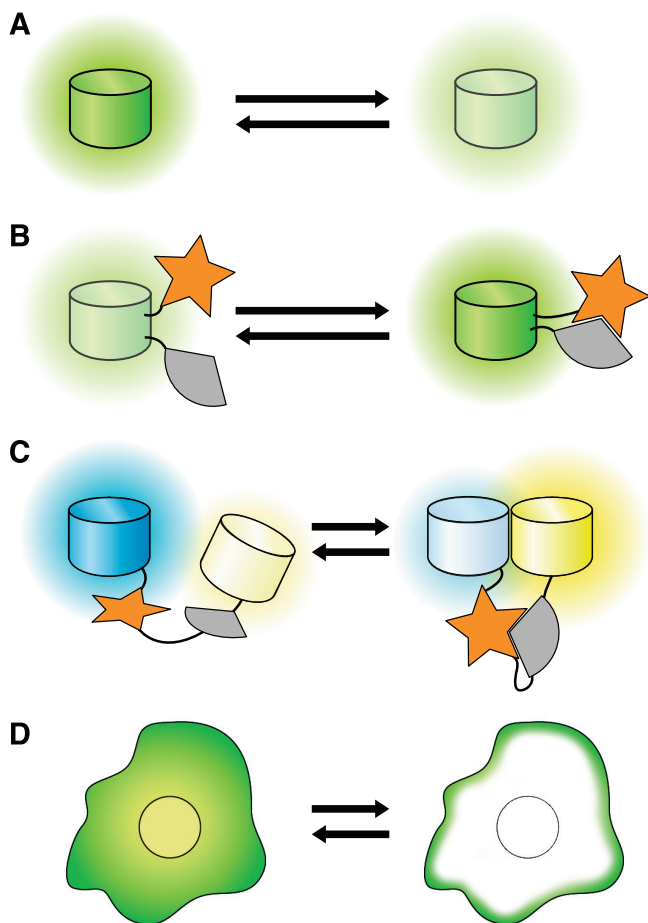


**FIG. 23.** Main types of FP-based fluorescent sensors. FPs are shown as colored barrels; specific sensitive domains are represented by orange stars and gray sectors. *A*: intrinsically sensitive FP changes spectral properties (brightness or excitation-emission wavelengths) depending on the environment, e.g., pH. *B*: FP or circularly permuted FP is fused to specific sensitive domain(s); those conformational changes affect spectral properties of this FP. *C*: two FPs of different colors are fused to sensitive domain(s); those conformational changes influence the efficiency of FRET between these FPs. *D*: translocation sensors: FP fused to specific protein domains demonstrates environmentally dependent changes in intracellular localization.

brightness (339) or FRET efficiency between the two fused FPs (28, 350, 455).

The first designs to appear utilized the fusion of an FP to the terminus of the *Drosophila Shaker K<sup>+</sup>* channel (FlaSh) (401), insertion of FP into skeletal muscle Na<sup>+</sup> channel (22), or fusion of an FP FRET pair to a voltage-sensing K<sup>+</sup> channel Kv2.1 (369). However, these GES are limited in their applicability by their low dynamic range, low sensitivity, slow kinetics, and/or poor function in mammalian cells (28). The most recent design of voltage sensors, named VSFP2s, is based on the voltage-sensing domain from *Ciona intestinalis* phosphatase (Ci-VSP, Ref. 302) and a FRET pair of FPs. In contrast to homologous Kv2.1, Ci-VSP functions as a monomer (222), which significantly improves the performance of Ci-VSP-based

sensors (92, 257, 303). VSFP2 sensors are more effectively targeted to the plasma membrane, providing better readout from the responsive fraction. Some of the recently developed VSFP2 variants are the remarkably high dynamic range green-orange Mermaid (436), and a yellow-far-red VSFP2.4, which is characterized by a fast initial “on” response and prominent decrease of donor fluorescence upon activation (303) (Table 2).

Intrinsically, the performance of FRET-based sensors is limited by FRET efficiency and by all of the FRET-related issues detailed in section vii. The low dynamic range of most FRET-based sensors hampers reliable signal readout and their application for high-throughput screening assays (449). Nevertheless, these sensors have become very popular tools for cell studies in single- and multi-parameter imaging (342), and we believe that their rapid evolution will eventually provide a powerful toolkit for high-throughput drug screening platforms.

#### E. Translocation Sensors/Assays

Cell-based protein translocation assays represent a separate field of FP application that traces the redistribution of an FP or FP-labeled protein between various cell compartments (cytosol, nucleus, membrane, endosomes, etc.) as the primary readout (167, 215). Translocation of proteins between cellular compartments in response to various external stimuli is a widespread phenomenon that ensures the accurate compartmentalization of activities in living cells. Therefore, FP-based sensors of this type in effect monitor the activity of various signaling pathways and other intracellular events. Upon fusion with an FP, many proteins, such as kinases, phosphatases, receptors, and transcription factors, become ready-to-use translocation GES for particular pathways. For example, a fusion construct can accumulate outside or inside the nucleus, in the cytosol or on the cellular membrane, in the cytosol or in endosomes, evenly distributed in the cytosol, or accumulated in specific foci. The translocation can occur very rapidly and can be tracked in real time, often returning finally to the preactivated state after the stimulus. The rational design of more sophisticated GES capable of signal-specific translocation is possible by combining an FP with protein domains bearing opposing localization signals, which determine the protein’s localization in a “tug-of-war” competition (215).

Modern microscopy platforms enable high content screening using translocating FPs. In such assays, screened compounds are tested for their ability to promote protein translocation or, vice versa, to inhibit protein translocation that should occur in response to a particular agonist or external influence. Advanced image recognition software can perform quantitative analysis of translocation events and obtain reliable information con-

TABLE 2. Selected examples of genetically encoded sensors

| Cellular Signals or Protein Activity Measured | Sensor Name         | Sensor Type, Components, and Principle of Work  | Reference Nos. |
|---|---------------------|---|----------------|
| pH  | SynaptopHluorin     | pH-sensitive green FP, pHluorin, fused to VAMP-2 at its luminally exposed COOH terminus                 | 286            |
| pH  | mNect.hCNT3         | pH-sensitive red FP, mNectarine, fused to the intracellularly exposed NH <sub>2</sub> terminus of hCNT3 | 193            |
| cGMP  | GES-DE5             | FRET-based, YFP-GKI-B-CFP, structural rearrangement of domain   | 317            |
| Ca <sup>2+</sup>                              | GCaMP3              | Single cpFP fused to interacting domains, M13-cpGFP-calmodulin  | 424, 428       |
| Ca <sup>2+</sup>                              | Case12              | Single cpFP fused to interacting domains, M13-cpGFP-calmodulin  | 407            |
| Ca <sup>2+</sup>                              | Camgaroo-2          | Insertion of structurally rearranging calmodulin domain into YFP  | 130            |
| Ca <sup>2+</sup>                              | TN-XXL              | FRET-based, CFP-2x(COOH-terminal lobe of troponin C)-cpYFP, structural rearrangement of domain          | 263            |
| Ca <sup>2+</sup>                              | Yellow Cameleon 3.6 | FRET-based, ECFP-calmodulin-M13-cpVenus, interaction of domains   | 307            |
| Ca <sup>2+</sup>                              | Cameleon D3         | FRET-based, ECFP-calmodulin-M13-cpVenus (redesigned calmodulin and M13), interaction of domains         | 327, 466       |
| H <sub>2</sub> O <sub>2</sub>                 | HyPer               | Single cpFP inserted into structurally rearranging domain OxyR  | 39             |
| Redox potential                               | roGFP1              | Single GFP carrying surface-exposed cysteines in positions appropriate to form disulfide bonds          | 94, 146        |
| Caspase-3 activity                            | CaspeR3             | FRET-based, TagGFP-DEVD-TagRFP, cleavage of the linker  | 390            |
| PKA activity                                  | AKAR1               | FRET-based, ECFP-14-3-3-substrate-YFP, interaction of domains   | 514            |
| Membrane potential                            | Mermaid             | FRET-based, Ci-VSP-mUKG-mKO, structural rearrangements near membrane                                    | 436            |
| Membrane potential                            | VSFP2.4             | FRET-based, Ci-VSP-YFP-mKate2, structural rearrangements near membrane                                  | 303            |

cerning the efficiency of the stimulus influence. Typically, the need for standardization of translocation assays for high content microscopy screening requires cell lines stably transfected with GES to achieve optimal responses and to minimize the cell-to-cell heterogeneity of the assay. In general, the rapidly developing field of translocation sensors looks very promising both for the basic science and drug development.

## X. FLUORESCENT PROTEINS AS PHOTOSENSITIZERS

Photosensitizers are dyes capable of efficient light-induced generation of ROS. There are two main types of photosensitizer reactions involving either electron or energy transfer as a primary process (54, 226). The first step of type I reactions is abstraction of an electron from a substrate (X) by an excited photosensitizer (Sens\*) with the formation of radicals X<sup>+</sup> and Sens<sup>-</sup>. Afterward, molecular oxygen oxidizes the photoreduced photosensitizer with the formation of superoxide anion radical (O<sub>2</sub><sup>-</sup>) and the photosensitizer in the ground state. As a result, two radical molecules, X<sup>+</sup> and O<sub>2</sub><sup>-</sup>, are formed. Type II reactions are based on direct energy transfer from an ex-

cited photosensitizer to molecular oxygen with the appearance of singlet oxygen (<sup>1</sup>O<sub>2</sub>). Different photosensitizers use predominately either the type I or the type II mechanism of action. However, in complex biological systems, both reactions usually occur simultaneously, and their relative contribution greatly depends on oxygen concentration, chemical nature and concentration of substrate molecules, and other factors (226).

Photodynamic action results in the oxidation of organic molecules and inflicts considerable damage on cells. In nature, photodynamic reactions are responsible for some diseases in humans and animals (43), as well as dysfunction of photosynthesis (20). Photosensitizers are also used in biological and chemical research as well as in the clinic. In particular, photodynamic therapy (PDT) is based on the selective accumulation of a photosensitizer in tumors followed by local irradiation with light resulting in the targeted death of cancer cells (58, 180, 454). Another important area of application of photosensitizers is chromophore-assisted light inactivation (CALI) of target molecules, mainly proteins (102, 151, 189, 368). Here, photosensitizer molecules are targeted to a protein of interest by a conjugated antibody or by labeling of modified proteins carrying a specific tag such as a tetracyc-

teine motif (432). Then, light illumination results in the spatially and temporally controlled inactivation of the target protein while more distant molecules remain intact due to ROS propagation within the limited volume. CALI has been successfully applied to study the biological function of various proteins (151, 368, 487).

All known efficient photosensitizers are chemical dyes, while a fully genetically encoded photosensitizer (GEPS) would be very desirable for many applications. GFP-like proteins, which are the only known chromophore-producing proteins encoded by a single gene, could become a basis for the development of such photosensitizers.

Although some successful applications of FPs for CALI were documented (355), it is clear that they are inefficient photosensitizers compared with chemical dyes. The main structural reason for this property (undoubtedly beneficial for all other FP applications) is thought to be a protein shell that blocks access of oxygen and external organic molecules to the excited FP chromophore. Moreover, recent studies demonstrated that even a naked synthetic GFP chromophore produces barely detectable amounts of  $^1\text{O}_2$  upon illumination (192), providing an additional explanation of the observed low phototoxicity of FPs. It is reasonable to speculate that this low phototoxicity of wild-type FPs is a feature brought about by natural selection; otherwise, an FP would kill host cells, especially under strong sunlight in the tropics. Thus efficient GEPS likely will not be found among natural GFP-like proteins.

Currently, the rational development of phototoxic FPs is not possible due to the incomplete understanding of the biochemistry of FPs' chromophores, along with the inability to perform effective computational design of FPs. Directed evolution using random mutagenesis or hypermutation technology (468, 469) also seems rather problematic for GEPS design, since the selection will have to be for mutants that severely damage host cells, so the most highly phototoxic clones could not be propagated after testing for phototoxicity.

Owing to these reasons, thus far not a single phototoxic FP was created intentionally. However, manual screening for phototoxicity in bacteria, performed among various randomly chosen mutant FPs, did reveal one protein named KillerRed that demonstrates phototoxic properties (50, 52). KillerRed is a dimeric red FP with fluorescence excitation and emission maxima at 585 and 610 nm, developed on the basis of nonfluorescent, nonphototoxic purple chromoprotein anm2CP cloned from an unidentified anthomedusa (383). *Escherichia coli* cells expressing KillerRed can be killed by white or green light irradiation at least 1,000-fold more effectively than those expressing other green and red FPs tested.

Although KillerRed apparently yields to chemically synthesized photosensitizers in efficiency, it does kill

eukaryotic cells under irradiation, by driving them to either apoptosis or necrosis (50). However, expression of KillerRed in the cytosol provides only a weak phototoxic effect in eukaryotes. Targeting KillerRed to mitochondria or to the plasma membrane results in a much more pronounced phototoxicity. KillerRed in mitochondria can trigger apoptotic pathways (50), while KillerRed on the membrane probably leads to the direct oxidation of lipids, followed by fast necrotic cell death (52). Other intracellular compartments such as lysosomes, endoplasmic reticulum, nucleus, and chromatin could be further tested to reveal the most efficient localization of KillerRed. Notably, specific targeting to tumor cells can be achieved by fusing KillerRed to appropriate antibodies, potentially providing an instrument for the selective photodestruction of tumors (382).

Successful performance of KillerRed for inactivation of proteins was demonstrated both in vitro and in living mammalian cells (50, 52). However, application of KillerRed for CALI techniques is limited by its dimeric nature, preventing functional fusion with many cellular proteins (see sect. iv). Interestingly, phototoxicity for monomeric mCherry (384) in *E. coli* has been mentioned in one recent publication (supplementary data of Ref. 415), although mCherry was not yet compared with KillerRed in a parallel experiment.

Another limitation of KillerRed is its apparently low quantum yield of ROS production, which is not always sufficient for effective inactivation of a fusion protein. The dependence of the phototoxic effect on presence of oxygen indicates that KillerRed acts as a photosensitizer. However, the nature of KillerRed phototoxicity remains unclear. The low quantum yield of ROS production by this protein in response to irradiation generally precludes direct measurements and identification of the ROS species generated. Indirect methods, such as inhibitory analysis, have led to conflicting results, indicating that ROS species produced are either singlet oxygen or superoxide (50). Notably, phototoxicity of KillerRed in deuterium oxide ( $\text{D}_2\text{O}$ ) was considerably lower than that in  $\text{H}_2\text{O}$  (382). Since  $\text{D}_2\text{O}$  is known to extend the lifetime of  $^1\text{O}_2$  and thus increase the efficiency of singlet oxygen-generating photosensitizers (226), these results suggest that  $^1\text{O}_2$  is not the ROS that mediates KillerRed phototoxicity.

A recent crystallographic study of KillerRed revealed an unusual water-filled channel from the cap of the  $\beta$ -barrel to the chromophore area that could be the key structural determinant of its accessibility to external agents, an important prerequisite for manifestation of phototoxicity (345). Also, we found exceptional sensitivity of KillerRed to  $\beta$ -mercaptoethanol, a widely used reducing agent. In the presence of  $\beta$ -mercaptoethanol, KillerRed showed conversion of an absorption peak at 585 nm (mature red chromophore) to a peak at 410 nm (probably, protonated GFP-like chromophore). Notably, these spectral changes

are similar to those observed during KillerRed photo-bleaching. These data suggest that KillerRed probably is a type I photosensitizer.

The dimeric state of KillerRed and its relatively low efficiency in ROS production call for further improvements to create monomeric and more efficient variants of GEPS. Also, the absorption spectrum of GEPS ideally should be as red-shifted as possible to reduce the non-specific phototoxicity, as well as to ensure deeper penetration of the excitation light within living tissues. Such an optimized phototoxic FP would be a useful tool in different areas of experimental biology and possibly in medicine. For example, GEPS can be used in functional studies of proteins using CALI, providing nearly 100% selectivity of fused target protein inactivation. An interesting exception from this “absolute” selectivity is possible inactivation of not only the covalently attached target but also interacting proteins within a complex. This approach can be potentially used to study protein-protein interactions and composition of large protein complexes, as ROS are known to travel 10–50 nm. In addition, GEPS provide a unique opportunity to introduce the same photosensitizer into various cell compartments to investigate ROS-mediated signal transduction, including apoptotic pathways. Also, GEPS-mediated light-induced cell killing can be used for spatially and temporally controlled elimination of specific cell types in developing embryos. Eventually, GEPS could be used for the photodynamic therapy if appropriate methods of delivery of genetic material into solid tumors are developed (504, 505). This would allow the combination of targeted gene delivery with local light irradiation, enabling ultra-high selectivity during tumor cell destruction.

## XI. CONCLUSIONS AND PERSPECTIVES

The study and applications of fluorescent proteins have come a long way from a subject of highly specialized research to indispensable tools for *in vivo* labeling and from a single known member, GFP from jellyfish *Aequorea victoria*, to hundreds of FPs of different colors. Good and sometimes near-perfect FP markers have become available across the entire visible spectrum from blue to far-red, and extensive efforts of many research groups can be expected to further perfect their brightness, photostability, maturation rate, pH stability, and performance in fusions.

The booming growth of FP-based arsenal of instruments for *in vivo* imaging continuously pushes the envelope of experimental biology. Present-day FPs enable multicolor labeling of proteins and nucleic acids, tracking of protein movements, interactions, activities, degradation, organelle motility and fusion-fission events, and monitoring promoter activation, as well as multiparam-

eter imaging of various cellular processes, including changes in concentration of signal molecules, changes of membrane potential, cell state, etc. On the scale of whole organisms, FPs make it possible to visualize cells, tissues, and organs; to monitor division and migration of cells in development, transplantology, inflammation, and carcinogenesis; and to decipher neural circuits.

The development of FP-based techniques is currently proceeding in multiple directions. Some of the most eagerly anticipated fluorescent tools to be developed in the near future include the following: perfected monomeric FPs in the red part of the spectrum that does not yield to *Aequorea victoria* GFP in performance in capricious fusions (see sect. v); reversibly photoactivatable red FPs of high dynamic range that would expand the possibilities of two color PALM (see sect. viii) and introduce effective solutions for the photochromic FRET (see sect. vii); genetically encoded sensors of high dynamic range employing more effective red-shifted FRET pairs or enhanced designs based on permuted FPs (see sect. ix); enhanced split FPs and palettes of split variants providing for combinatorial multicolor labeling to distinguish alternative interactions of multiple proteins of interest (see sect. vii); fully reversible split FPs for dynamic visualization of proteins’ interaction (see sect. vii); enhanced phototoxic FPs and techniques for their effective delivery and application in photodynamic therapies for cancer (see sect. x); monomeric phototoxic FPs for efficient application in CALI techniques (see sect. x); and FPs of enhanced characteristics in red, far-red, and even infra-red that would improve whole body imaging and would be also useful in multicolor labeling and FRET techniques (see sect. vi).

Rapid progress in FP technologies, along with the progress in microscopy, spectroscopy, drug screening platforms, and whole body imaging systems, brings FPs closer and closer to clinical applications each year. We believe that in the next decade, in addition to the growing intensity and diversity of application in basic biomedical research, FPs will become valuable tools in preclinical studies and medicine itself, for example, as targetable labels for the monitoring and excision of tumors (504), photodynamic therapies for cancer (382), and contrasting agents in opto-acoustic sonography (356) and surgery.

FPs are also making considerable headway into the entertainment industry. Within only a few years, the first red FP cloned, DsRed, has traveled a remarkable circle from the *Discosoma* mushroom anemone brought from the Indo-Pacific area to an aquarium in Moscow, to the gene cloned in our lab, which was further commercialized by Clontech in the United States, to the transgenic red fluorescent zebrafish that have become available in pet stores in Moscow. As of today, various transgenic fluorescent animals expressing FPs are known, including chickens, dogs (175), pigs (240), cats (501), and marmosets (373), as well as decorative transgenic plants ([www](http://www).

ekac.org). These examples demonstrate that FPs can rapidly become a part of the entertainment industry and also suggest that future analysis of FP diversity and evolution may be complicated by intense artificial horizontal transfer of FP genes among species.

In addition to their enormous value as practical tools, FPs themselves represent broad opportunities for basic research, many of which remain unexplored. Deciphering the maturation mechanisms of chromophores revealed novel posttranslational reactions never expected in proteins before. However, it remains unclear which features of the protein determine which chromophore will be produced. Such knowledge is the key to the rational design of FPs, which can become the “next-generation” FP tools precisely tailored for the needs of particular applications. The ease of expression and phenotypic characterization of FPs makes them excellent models for experimental studies in the evolution of functional diversity in protein families, using statistical phylogenetics and ancestral reconstruction approaches (108, 442). This kind of research, however, is held back by arguably the biggest secret that the FPs still keep after so many years, which is their biological function. Getting to the bottom of their origin, evolution, biochemistry, and function will provide invaluable insights into the basic protein chemistry, evolution of proteins, and ecology of marine organisms.

#### ACKNOWLEDGMENTS

Present address of M. V. Matz: University of Texas at Austin, 1 University Station C0930, Austin, TX 78712.

Address for reprint requests and other correspondence: K. A. Lukyanov, Institute of Bioorganic Chemistry, Russian Academy of Sciences, Miklukho-Maklaya 16/10, 117997 Moscow, Russia (e-mail: kluk@ibch.ru).

#### GRANTS

This work was supported by Molecular Cell Biology program of Russian Academy of Sciences, Howard Hughes Medical Institute (55005618), Rosnauka (02.512.12.2053), Rosobrazovanie (P-256), the program “State Support of the Leading Scientific Schools” (NS-2395.2008.4), Russian Foundation for Basic Research Grants 08-04-01702-a, 09-04-92603-KO\_a, 09-04-12235-ofi\_m and 09-04-00356-a, and National Institutes of Health Grants R01-GM-78247 and R01-GM-87198.

#### REFERENCES

1. Abbe E. Beitrage zur Theorie des Mikroskops und der mikroskopischen Wahrnehmung. *Arc F Mikr Anat* 9: 413–420, 1873.
2. Adam V, Lelimonous M, Boehme S, Desfonds G, Nienhaus K, Field MJ, Wiedenmann J, McSweeney S, Nienhaus GU, Bourgeois D. Structural characterization of IrisFP, an optical highlighter undergoing multiple photo-induced transformations. *Proc Natl Acad Sci USA* 105: 18343–18348, 2008.
3. Adam V, Nienhaus K, Bourgeois D, Nienhaus GU. Structural basis of enhanced photoconversion yield in green fluorescent protein-like protein Dendra2. *Biochemistry* 48: 4905–4915, 2009.
4. Agmon N. Kinetics of switchable proton escape from a proton-wire within green fluorescence protein. *J Phys Chem B* 111: 7870–7878, 2007.
5. Agmon N. Proton pathways in green fluorescence protein. *Biophys J* 88: 2452–2461, 2005.
6. Ai HW, Hazelwood KL, Davidson MW, Campbell RE. Fluorescent protein FRET pairs for ratiometric imaging of dual biosensors. *Nat Methods* 5: 401–403, 2008.
7. Ai HW, Henderson JN, Remington SJ, Campbell RE. Directed evolution of a monomeric, bright and photostable version of Clavularia cyan fluorescent protein: structural characterization and applications in fluorescence imaging. *Biochem J* 400: 531–540, 2006.
8. Ai HW, Olenych SG, Wong P, Davidson MW, Campbell RE. Hue-shifted monomeric variants of Clavularia cyan fluorescent protein: identification of the molecular determinants of color and applications in fluorescence imaging. *BMC Biol* 6: 13, 2008.
9. Ai HW, Shaner NC, Cheng Z, Tsien RY, Campbell RE. Exploration of new chromophore structures leads to the identification of improved blue fluorescent proteins. *Biochemistry* 46: 5904–5910, 2007.
10. Akemann W, Raj CD, Knopfel T. Functional characterization of permuted enhanced green fluorescent proteins comprising varying linker peptides. *Photochem Photobiol* 74: 356–363, 2001.
11. Albertazzi L, Arosio D, Marchetti L, Ricci F, Beltram F. Quantitative FRET analysis with the EGFP-mCherry fluorescent protein pair. *Photochem Photobiol* 85: 287–297, 2009.
12. Alieva NO, Konzen KA, Field SF, Meleshkevitch EA, Hunt ME, Beltran-Ramirez V, Miller DJ, Wiedenmann J, Salih A, Matz MV. Diversity and evolution of coral fluorescent proteins. *PLoS ONE* 3: e2680, 2008.
13. Allen MD, DiPilato LM, Rahdar M, Ren YR, Chong C, Liu JO, Zhang J. Reading dynamic kinase activity in living cells for high-throughput screening. *ACS Chem Biol* 1: 371–376, 2006.
14. Ando R, Flors C, Mizuno H, Hofkens J, Miyawaki A. Highlighted generation of fluorescence signals using simultaneous two-color irradiation on Dronpa mutants. *Biophys J* 92: L97–99, 2007.
15. Ando R, Hama H, Yamamoto-Hino M, Mizuno H, Miyawaki A. An optical marker based on the UV-induced green-to-red photoconversion of a fluorescent protein. *Proc Natl Acad Sci USA* 99: 12651–12656, 2002.
16. Ando R, Mizuno H, Miyawaki A. Regulated fast nucleocytoplasmic shuttling observed by reversible protein highlighting. *Science* 306: 1370–1373, 2004.
17. Andresen M, Stiel AC, Folling J, Wenzel D, Schonle A, Egner A, Eggeling C, Hell SW, Jakobs S. Photoswitchable fluorescent proteins enable monochromatic multilabel imaging and dual color fluorescence nanoscopy. *Nat Biotechnol* 26: 1035–1040, 2008.
18. Andresen M, Stiel AC, Trowitzsch S, Weber G, Eggeling C, Wahl MC, Hell SW, Jakobs S. Structural basis for reversible photoswitching in Dronpa. *Proc Natl Acad Sci USA* 104: 13005–13009, 2007.
19. Andresen M, Wahl MC, Stiel AC, Grater F, Schafer LV, Trowitzsch S, Weber G, Eggeling C, Grubmuller H, Hell SW, Jakobs S. Structure and mechanism of the reversible photoswitch of a fluorescent protein. *Proc Natl Acad Sci USA* 102: 13070–13074, 2005.
20. Asada K. The water-water cycle in chloroplasts: scavenging of active oxygens and dissipation of excess photons. *Annu Rev Plant Physiol Plant Mol Biol* 50: 601–639, 1999.
21. Ashby MC, Ibaraki K, Henley JM. It's green outside: tracking cell surface proteins with pH-sensitive GFP. *Trends Neurosci* 27: 257–261, 2004.
22. Ataka K, Pieribone VA. A genetically targetable fluorescent probe of channel gating with rapid kinetics. *Biophys J* 82: 509–516, 2002.
23. Awaji T, Hirasawa A, Shirakawa H, Tsujimoto G, Miyazaki S. Novel green fluorescent protein-based ratiometric indicators for monitoring pH in defined intracellular microdomains. *Biochem Biophys Res Commun* 289: 457–462, 2001.
24. Bacia K, Kim SA, Schwille P. Fluorescence cross-correlation spectroscopy in living cells. *Nat Methods* 3: 83–89, 2006.
25. Baehler PJ, Biondi RM, van Bemmelen M, Veron M, Reymond CD. Random insertion of green fluorescent protein into the regulatory subunit of cyclic adenosine monophosphate-dependent protein kinase. *Methods Mol Biol* 183: 57–68, 2002.

26. Baird GS, Zacharias DA, Tsien RY. Biochemistry, mutagenesis, and oligomerization of DsRed, a red fluorescent protein from coral. *Proc Natl Acad Sci USA* 97: 11984–11989, 2000.
27. Baird GS, Zacharias DA, Tsien RY. Circular permutation and receptor insertion within green fluorescent proteins. *Proc Natl Acad Sci USA* 96: 11241–11246, 1999.
28. Baker BJ, Mutoh H, Dimitrov D, Akemann W, Perron A, Iwamoto Y, Jin L, Cohen LB, Isacoff EY, Pieribone VA, Hughes T, Knopfel T. Genetically encoded fluorescent sensors of membrane potential. *Brain Cell Biol* 36: 53–67, 2008.
29. Baltrusch S, Lenzen S. Monitoring of glucose-regulated single insulin secretory granule movement by selective photoactivation. *Diabetologia* 51: 989–996, 2008.
30. Barondeau DP, Kassmann CJ, Tainer JA, Getzoff ED. The case of the missing ring: radical cleavage of a carbon-carbon bond and implications for GFP chromophore biosynthesis. *J Am Chem Soc* 129: 3118–3126, 2007.
31. Barondeau DP, Kassmann CJ, Tainer JA, Getzoff ED. Structural chemistry of a green fluorescent protein Zn biosensor. *J Am Chem Soc* 124: 3522–3524, 2002.
32. Barondeau DP, Kassmann CJ, Tainer JA, Getzoff ED. Understanding GFP chromophore biosynthesis: controlling backbone cyclization and modifying post-translational chemistry. *Biochemistry* 44: 1960–1970, 2005.
33. Barondeau DP, Kassmann CJ, Tainer JA, Getzoff ED. Understanding GFP posttranslational chemistry: structures of designed variants that achieve backbone fragmentation, hydrolysis, and de-carboxylation. *J Am Chem Soc* 128: 4685–4693, 2006.
34. Barondeau DP, Putnam CD, Kassmann CJ, Tainer JA, Getzoff ED. Mechanism and energetics of green fluorescent protein chromophore synthesis revealed by trapped intermediate structures. *Proc Natl Acad Sci USA* 100: 12111–12116, 2003.
35. Bastiaens PI, Squire A. Fluorescence lifetime imaging microscopy: spatial resolution of biochemical processes in the cell. *Trends Cell Biol* 9: 48–52, 1999.
36. Baudendistel N, Muller G, Waldeck W, Angel P, Langowski J. Two-hybrid fluorescence cross-correlation spectroscopy detects protein-protein interactions in vivo. *Chemphyschem* 6: 984–990, 2005.
37. Baumann D, Cook M, Ma L, Mushegian A, Sanders E, Schwartz J, Yu CR. A family of GFP-like proteins with different spectral properties in lancelet *Branchiostoma floridae*. *Biol Direct* 3: 28, 2008.
38. Beach DL, Salmon ED, Bloom K. Localization and anchoring of mRNA in budding yeast. *Curr Biol* 9: 569–578, 1999.
39. Belousov VV, Fradkov AF, Lukyanov KA, Staroverov DB, Shakhbazov KS, Terskikh AV, Lukyanov S. Genetically encoded fluorescent indicator for intracellular hydrogen peroxide. *Nat Methods* 3: 281–286, 2006.
40. Bertrand E, Chartrand P, Schaefer M, Shenoy SM, Singer RH, Long RM. Localization of ASH1 mRNA particles in living yeast. *Mol Cell* 2: 437–445, 1998.
41. Betzig E, Patterson GH, Sougrat R, Lindwasser OW, Olenych S, Bonifacino JS, Davidson MW, Lippincott-Schwartz J, Hess HF. Imaging intracellular fluorescent proteins at nanometer resolution. *Science* 313: 1642–1645, 2006.
42. Bevis BJ, Glick BS. Rapidly maturing variants of the Discosoma red fluorescent protein (DsRed). *Nat Biotechnol* 20: 83–87, 2002.
43. Blum HF. *Photodynamic Action and Diseases Caused by Light*. New York: Hafner, 1964.
44. Bogdanov AM, Bogdanova EA, Chudakov DM, Gorodnicheva TV, Lukyanov S, Lukyanov KA. Cell culture medium affects GFP photostability: a solution. *Nat Methods* 6: 859–860, 2009.
45. Bogdanov AM, Mishin AS, Yampolsky IV, Belousov VV, Chudakov DM, Subach FV, Verkhusha VV, Lukyanov S, Lukyanov KA. Green fluorescent proteins are light-induced electron donors. *Nat Chem Biol* 5: 459–461, 2009.
46. Bokman SH, Ward WW. Renaturation of *Aequorea* green-fluorescent protein. *Biochem Biophys Res Commun* 101: 1372–1380, 1981.
47. Bomati EK, Manning G, Deheyn DD. Amphioxus encodes the largest known family of green fluorescent proteins, which have diversified into distinct functional classes. *BMC Evol Biol* 9: 77, 2009.
48. Bou-Abdallah F, Chasteen ND, Lesser MP. Quenching of super-oxide radicals by green fluorescent protein. *Biochim Biophys Acta* 1760: 1690–1695, 2006.
49. Brejc K, Sixma TK, Kitts PA, Kain SR, Tsien RY, Ormo M, Remington SJ. Structural basis for dual excitation and photoisomerization of the *Aequorea victoria* green fluorescent protein. *Proc Natl Acad Sci USA* 94: 2306–2311, 1997.
50. Bulina ME, Chudakov DM, Britanova OV, Yanushevich YG, Staroverov DB, Chepurnykh TV, Merzlyak EM, Shkrob MA, Lukyanov S, Lukyanov KA. A genetically encoded photosensitizer. *Nat Biotechnol* 24: 95–99, 2006.
51. Bulina ME, Chudakov DM, Mudrik NN, Lukyanov KA. Interconversion of Anthozoa GFP-like fluorescent and non-fluorescent proteins by mutagenesis. *BMC Biochem* 3: 7, 2002.
52. Bulina ME, Lukyanov KA, Britanova OV, Onichtchouk D, Lukyanov S, Chudakov DM. Chromophore-assisted light inactivation (CALI) using the phototoxic fluorescent protein KillerRed. *Nat Protoc* 1: 947–953, 2006.
53. Bulina ME, Verkhusha VV, Staroverov DB, Chudakov DM, Lukyanov KA. Hetero-oligomeric tagging diminishes non-specific aggregation of target proteins fused with Anthozoa fluorescent proteins. *Biochem J* 371: 109–114, 2003.
54. Buytaert E, Dewaele M, Agostinis P. Molecular effectors of multiple cell death pathways initiated by photodynamic therapy. *Biochim Biophys Acta* 1776: 86–107, 2007.
55. Cabantous S, Pedelacq JD, Mark BL, Naranjo C, Terwilliger TC, Waldo GS. Recent advances in GFP folding reporter and split-GFP solubility reporter technologies. Application to improving the folding and solubility of recalcitrant proteins from *Mycobacterium tuberculosis*. *J Struct Funct Genomics* 6: 113–119, 2005.
56. Cabantous S, Terwilliger TC, Waldo GS. Protein tagging and detection with engineered self-assembling fragments of green fluorescent protein. *Nat Biotechnol* 23: 102–107, 2005.
57. Cabantous S, Waldo GS. In vivo and in vitro protein solubility assays using split GFP. *Nat Methods* 3: 845–854, 2006.
58. Calzavara-Pinton PG, Venturini M, Sala R. Photodynamic therapy: update 2006. Part 2: clinical results. *J Eur Acad Dermatol Venereol* 21: 439–451, 2007.
59. Campbell RE, Tour O, Palmer AE, Steinbach PA, Baird GS, Zacharias DA, Tsien RY. A monomeric red fluorescent protein. *Proc Natl Acad Sci USA* 99: 7877–7882, 2002.
60. Carlson HJ, Campbell RE. Genetically encoded FRET-based biosensors for multiparameter fluorescence imaging. *Curr Opin Biotechnol* 20: 19–27, 2009.
61. Carroll L. *Alice's Adventures in Wonderland*. London: Macmillan, 1865.
62. Cavanagh HD, Petroll WM, Jester JV. The application of confocal microscopy to the study of living systems. *Neurosci Biobehav Rev* 17: 483–498, 1993.
63. Chalfie M, Tu Y, Euskirchen G, Ward WW, Prasher DC. Green fluorescent protein as a marker for gene expression. *Science* 263: 802–805, 1994.
64. Chapman S, Faulkner C, Kaiserli E, Garcia-Mata C, Savenkov EI, Roberts AG, Opalka KJ, Christie JM. The photoreversible fluorescent protein iLOV outperforms GFP as a reporter of plant virus infection. *Proc Natl Acad Sci USA* 105: 20038–20043, 2008.
65. Chatteraj M, King BA, Bublitz GU, Boxer SG. Ultra-fast excited state dynamics in green fluorescent protein: multiple states and proton transfer. *Proc Natl Acad Sci USA* 93: 8362–8367, 1996.
66. Chen Y, MacDonald PJ, Skinner JP, Patterson GH, Muller JD. Probing nucleocytoplasmic transport by two-photon activation of PA-GFP. *Microsc Res Tech* 69: 220–226, 2006.
67. Chu J, Zhang Z, Zheng Y, Yang J, Qin L, Lu J, Huang ZL, Zeng S, Luo Q. A novel far-red bimolecular fluorescence complementation system that allows for efficient visualization of protein interactions under physiological conditions. *Biosens Bioelectron* 25: 234–239, 2009.
68. Chudakov DM, Belousov VV, Zaraisky AG, Novoselov VV, Staroverov DB, Zorov DB, Lukyanov S, Lukyanov KA. Kindling fluorescent proteins for precise in vivo photolabeling. *Nat Biotechnol* 21: 191–194, 2003.

69. Chudakov DM, Chepurnykh TV, Belousov VV, Lukyanov S, Lukyanov KA. Fast and precise protein tracking using repeated reversible photoactivation. *Traffic* 7: 1304–1310, 2006.
70. Chudakov DM, Feofanov AV, Mudrik NN, Lukyanov S, Lukyanov KA. Chromophore environment provides clue to “kindling fluorescent protein” riddle. *J Biol Chem* 278: 7215–7219, 2003.
71. Chudakov DM, Lukyanov S, Lukyanov KA. Fluorescent proteins as a toolkit for in vivo imaging. *Trends Biotechnol* 23: 605–613, 2005.
72. Chudakov DM, Lukyanov S, Lukyanov KA. Tracking intracellular protein movements using photoswitchable fluorescent proteins PS-CFP2 and Dendra2. *Nat Protoc* 2: 2024–2032, 2007.
73. Chudakov DM, Lukyanov S, Lukyanov KA. Using photoactivatable fluorescent protein Dendra2 to track protein movement. *Bio-techniques* 42: 553–557, 2007.
74. Chudakov DM, Verkusha VV, Staroverov DB, Souslova EA, Lukyanov S, Lukyanov KA. Photoswitchable cyan fluorescent protein for protein tracking. *Nat Biotechnol* 22: 1435–1439, 2004.
75. Cody CW, Prasher DC, Westler WM, Prendergast FG, Ward WW. Chemical structure of the hexapeptide chromophore of the *Aequorea* green-fluorescent protein. *Biochemistry* 32: 1212–1218, 1993.
76. Corish P, Tyler-Smith C. Attenuation of green fluorescent protein half-life in mammalian cells. *Protein Eng* 12: 1035–1040, 1999.
77. Cormack BP, Valdivia RH, Falkow S. FACS-optimized mutants of the green fluorescent protein (GFP). *Gene* 173: 33–38, 1996.
78. Cubitt AB, Heim R, Adams SR, Boyd AE, Gross LA, Tsien RY. Understanding, improving and using green fluorescent proteins. *Trends Biochem Sci* 20: 448–455, 1995.
79. Cubitt AB, Woollenweber LA, Heim R. Understanding structure-function relationships in the *Aequorea victoria* green fluorescent protein. *Methods Cell Biol* 58: 19–30, 1999.
80. Culter MW, Ward WW. In: *Bioluminescence and Chemiluminescence: Molecular Reporting with Photons*, edited by Hastings JW, Kriska LJ, Stanley PE. New York: Wiley, 1997, p. 403–406.
81. Cvackova Z, Masata M, Stanek D, Fidlerova H, Raska I. Chromatin position in human HepG2 cells: although being non-random, significantly changed in daughter cells. *J Struct Biol* 165: 107–117, 2009.
82. Czirok A, Zach J, Kozel BA, Mecham RP, Davis EC, Rongish BJ. Elastic fiber macro-assembly is a hierarchical, cell motion-mediated process. *J Cell Physiol* 207: 97–106, 2006.
83. D'Angelo C, Denzel A, Vogt A, Matz MV, Oswald F, Salih A, Nienhaus GU, Wiedenmann J. Blue light regulation of GFP-like protein expression in reef-building corals. *Mar Ecol Prog Ser* 364: 97–106, 2008.
84. Daigle N, Ellenberg J. LambdaN-GFP: an RNA reporter system for live-cell imaging. *Nat Methods* 4: 633–636, 2007.
85. Dedecker P, Hotta J, Ando R, Miyawaki A, Engelborghs Y, Hofkens J. Fast and reversible photoswitching of the fluorescent protein dronpa as evidenced by fluorescence correlation spectroscopy. *Biophys J* 91: L45–47, 2006.
86. Deheyn DD, Kubokawa K, McCarthy JK, Murakami A, Porrachia M, Rouse GW, Holland ND. Endogenous green fluorescent protein (GFP) in amphioxus. *Biol Bull* 213: 95–100, 2007.
87. Deliolanis NC, Kasmieh R, Wurdinger T, Tannous BA, Shah K, Ntziachristos V. Performance of the red-shifted fluorescent proteins in deep-tissue molecular imaging applications. *J Biomed Opt* 13: 044008, 2008.
88. Demarco IA, Periasamy A, Booker CF, Day RN. Monitoring dynamic protein interactions with photoquenching FRET. *Nat Methods* 3: 519–524, 2006.
89. Demidov VV, Dokholyan NV, Witte-Hoffmann C, Chalasani P, Yiu HW, Ding F, Yu Y, Cantor CR, Broude NE. Fast complementation of split fluorescent protein triggered by DNA hybridization. *Proc Natl Acad Sci USA* 103: 2052–2056, 2006.
90. Denk W, Strickler JH, Webb WW. Two-photon laser scanning fluorescence microscopy. *Science* 248: 73–76, 1990.
91. Diaspro A, Testa I, Faretta M, Magrassi R, Barozzi S, Parazzoli D, Vicidomini G. 3D localized photoactivation of pa-GFP in living cells using two-photon interactions. *Conf Proc IEEE Eng Med Biol Soc* 1: 389–391, 2006.
92. Dimitrov D, He Y, Mutoh H, Baker BJ, Cohen L, Akemann W, Knopfel T. Engineering and characterization of an enhanced fluorescent protein voltage sensor. *PLoS ONE* 2: e440, 2007.
93. DiPilato LM, Cheng X, Zhang J. Fluorescent indicators of cAMP and Epac activation reveal differential dynamics of cAMP signaling within discrete subcellular compartments. *Proc Natl Acad Sci USA* 101: 16513–16518, 2004.
94. Dooley CT, Dore TM, Hanson GT, Jackson WC, Remington SJ, Tsien RY. Imaging dynamic redox changes in mammalian cells with green fluorescent protein indicators. *J Biol Chem* 279: 22284–22293, 2004.
95. Dove SG, Hoegh-Guldberg O, Ranganathan S. Major colour patterns of reef-building corals are due to a family of GFP-like proteins. *Coral Reefs* 19: 197–204, 2001.
96. Drobizhev M, Tillo S, Makarov NS, Hughes TE, Rebane A. Absolute two-photon absorption spectra and two-photon brightness of orange and red fluorescent proteins. *J Phys Chem B* 113: 855–859, 2009.
97. Dufour P, Dufour S, Castonguay A, McCarthy N, De Koninck Y. Two-photon laser scanning fluorescence microscopy for functional cellular imaging: advantages and challenges or One photon is good...but two is better! *Med Sci* 22: 837–844, 2006.
98. Duncan RR, Greaves J, Wiegand UK, Matskevich I, Bodammer G, Apps DK, Shipston MJ, Chow RH. Functional and spatial segregation of secretory vesicle pools according to vesicle age. *Nature* 422: 176–180, 2003.
99. Dunn CW, Hejnol A, Matus DQ, Pang K, Browne WE, Smith SA, Seaver E, Rouse GW, Obst M, Edgecombe GD, Sorensen MV, Haddock SH, Schmidt-Rhaesa A, Okusu A, Kristensen RM, Wheeler WC, Martindale MQ, Giribet G. Broad phylogenomic sampling improves resolution of the animal tree of life. *Nature* 452: 745–749, 2008.
100. Egner A, Geisler C, von Middendorff C, Bock H, Wenzel D, Medda R, Andresen M, Stiel AC, Jakobs S, Eggeling C, Schonle A, Hell SW. Fluorescence nanoscopy in whole cells by asynchronous localization of photoswitching emitters. *Biophys J* 93: 3285–3290, 2007.
101. Ehrig T, O'Kane DJ, Prendergast FG. Green-fluorescent protein mutants with altered fluorescence excitation spectra. *FEBS Lett* 367: 163–166, 1995.
102. Eustace BK, Buchstaller A, Jay DG. Adapting chromophore-assisted laser inactivation for high throughput functional proteomics. *Brief Funct Genomic Proteomic* 1: 257–265, 2002.
103. Evdokimov AG, Pokross ME, Egorov NS, Zaraisky AG, Yampolsky IV, Merzlyak EM, Shkoporov AN, Sander I, Lukyanov KA, Chudakov DM. Structural basis for the fast maturation of Arthropoda green fluorescent protein. *EMBO Rep* 7: 1006–1012, 2006.
104. Falk MM, Baker SM, Gumpert AM, Segretain D, Buckheit RW 3rd. Gap junction turnover is achieved by the internalization of small endocytic double-membrane vesicles. *Mol Biol Cell* 20: 3342–3352, 2009.
105. Fan JY, Cui ZQ, Wei HP, Zhang ZP, Zhou YF, Wang YP, Zhang XE. Split mCherry as a new red bimolecular fluorescence complementation system for visualizing protein-protein interactions in living cells. *Biochem Biophys Res Commun* 367: 47–53, 2008.
106. Felsenstein J. Cases in which parsimony or compatibility methods will be positively misleading. *Syst Zool* 27: 401–410, 1978.
107. Fernandez-Suarez M, Ting AY. Fluorescent probes for super-resolution imaging in living cells. *Nat Rev Mol Cell Biol* 9: 929–943, 2008.
108. Field SF, Bulina MY, Kelmanson IV, Bielawski JP, Matz MV. Adaptive evolution of multicolored fluorescent proteins in reef-building corals. *J Mol Evol* 62: 332–339, 2006.
109. Field SF, Matz MV. Retracing evolution of red fluorescence in GFP-like proteins from Faviina corals. *Mol Biol Evol* 27: 225–233.
110. Förster T. Zwischenmolekulare Energiewanderung und Fluoreszenz. *Ann Physik* 55: 437, 1948.
111. Forward RB. Diel vertical migration: zooplankton photobiology and behaviour. *Oceanogr Mar Biol Annu Rev* 26: 361–393, 1988.
112. Fradkov AF, Verkusha VV, Staroverov DB, Bulina ME, Yanushevich YG, Martynov VI, Lukyanov S, Lukyanov KA. Far-

- red fluorescent tag for protein labelling. *Biochem J* 368: 17–21, 2002.
113. Fraser ST, Hadjantonakis AK, Sahr KE, Willey S, Kelly OG, Jones EA, Dickinson ME, Baron MH. Using a histone yellow fluorescent protein fusion for tagging and tracking endothelial cells in ES cells and mice. *Genesis* 42: 162–171, 2005.
  114. Fusco D, Accornero N, Lavoie B, Shenoy SM, Blanchard JM, Singer RH, Bertrand E. Single mRNA molecules demonstrate probabilistic movement in living mammalian cells. *Curr Biol* 13: 161–167, 2003.
  115. Gallegos LL, Kunkel MT, Newton AC. Targeting protein kinase C activity reporter to discrete intracellular regions reveals spatio-temporal differences in agonist-dependent signaling. *J Biol Chem* 281: 30947–30956, 2006.
  116. Galperin E, Verkhusha VV, Sorkin A. Three-chromophore FRET microscopy to analyze multiprotein interactions in living cells. *Nat Methods* 1: 209–217, 2004.
  117. Gandia J, Galino J, Amaral OB, Soriano A, Lluis C, Franco R, Ciruela F. Detection of higher-order G protein-coupled receptor oligomers by a combined BRET-BiFC technique. *FEBS Lett* 582: 2979–2984, 2008.
  118. Gasser SM. Visualizing chromatin dynamics in interphase nuclei. *Science* 296: 1412–1416, 2002.
  119. Gautam SG, Perron A, Mutoh H, Knopfel T. Exploration of fluorescent protein voltage probes based on circularly permuted fluorescent proteins. *Front Neuroengineering* 2: 14, 2009.
  120. Giordano L, Jovin TM, Irie M, Jares-Erijman EA. Diheteroarylethenes as thermally stable photoswitchable acceptors in photochromic fluorescence resonance energy transfer (pcFRET). *J Am Chem Soc* 124: 7481–7489, 2002.
  121. Gleeson PA, Teasdale RD, Burke J. Targeting of proteins to the Golgi apparatus. *Glycoconj J* 11: 381–394, 1994.
  122. Goedhart J, van Weeren L, Hink MA, Vischer NO, Jalink K, Gadella TW Jr. Bright cyan fluorescent protein variants identified by fluorescence lifetime screening. *Nat Methods* 7: 137–139, 2010.
  123. Goedhart J, Vermeier JE, Adjobo-Hermann MJ, van Weeren L, Gadella TW Jr. Sensitive detection of p65 homodimers using red-shifted and fluorescent protein-based FRET couples. *PLoS ONE* 2: e1011, 2007.
  124. Gorokhovatsky AY, Rudenko NV, Marchenkov VV, Skosyrev VS, Arzhanov MA, Burkhardt N, Zakharov MV, Semisotnov GV, Vinokurov LM, Alakhov YB. Homogeneous assay for biotin based on *Aequorea victoria* bioluminescence resonance energy transfer system. *Anal Biochem* 313: 68–75, 2003.
  125. Gould SJ, Keller GA, Hosken N, Wilkinson J, Subramani S. A conserved tripeptide sorts proteins to peroxisomes. *J Cell Biol* 108: 1657–1664, 1989.
  126. Gould TJ, Gunewardene MS, Gudheti MV, Verkhusha VV, Yin SR, Goss JA, Hess ST. Nanoscale imaging of molecular positions and anisotropies. *Nat Methods* 5: 1027–1030, 2008.
  127. Grant DM, Zhang W, McGhee EJ, Bunney TD, Talbot CB, Kumar S, Munro I, Dunsby C, Neil MA, Katan M, French PM. Multiplexed FRET to image multiple signaling events in live cells. *Biophys J* 95: L69–L71, 2008.
  128. Green HM, Alberola-Illa J. Development of ERK activity sensor, an in vitro, FRET-based sensor of extracellular regulated kinase activity. *BMC Chem Biol* 5: 1, 2005.
  129. Griesbeck O. Fluorescent proteins as sensors for cellular functions. *Curr Opin Neurobiol* 14: 636–641, 2004.
  130. Griesbeck O, Baird GS, Campbell RE, Zacharias DA, Tsien RY. Reducing the environmental sensitivity of yellow fluorescent protein. Mechanism and applications. *J Biol Chem* 276: 29188–29194, 2001.
  131. Grinberg AV, Hu CD, Kerppola TK. Visualization of Myc/Max/Mad family dimers and the competition for dimerization in living cells. *Mol Cell Biol* 24: 4294–4308, 2004.
  132. Gross LA, Baird GS, Hoffman RC, Baldridge KK, Tsien RY. The structure of the chromophore within DsRed, a red fluorescent protein from coral. *Proc Natl Acad Sci USA* 97: 11990–11995, 2000.
  133. Guo Y, Rebecchi M, Scarlata S. Phospholipase C $\beta$ 2 binds to and inhibits phospholipase C $\delta$ 1. *J Biol Chem* 280: 1438–1447, 2005.
  134. Gurskaya NG, Fradkov AF, Pounkova NI, Staroverov DB, Bulina ME, Yanushevich YG, Labas YA, Lukyanov S, Lukyanov KA. A colourless green fluorescent protein homologue from the non-fluorescent hydromedusa *Aequorea coerulescens* and its fluorescent mutants. *Biochem J* 373: 403–408, 2003.
  135. Gurskaya NG, Savitsky AP, Yanushevich YG, Lukyanov SA, Lukyanov KA. Color transitions in coral's fluorescent proteins by site-directed mutagenesis. *BMC Biochem* 2: 6, 2001.
  136. Gurskaya NG, Verkhusha VV, Shcheglov AS, Staroverov DB, Chepurnykh TV, Fradkov AF, Lukyanov S, Lukyanov KA. Engineering of a monomeric green-to-red photoactivatable fluorescent protein induced by blue light. *Nat Biotechnol* 24: 461–465, 2006.
  137. Gusev VE, Karabutov AA. *Laser Optoacoustics*. New York: American Institute of Physics, 1993.
  138. Gustafsson MG, Agard DA, Sedat JW. i5M: 3D widefield light microscopy with better than 100 nm axial resolution. *J Microsc* 195: 10–16, 1999.
  139. Habuchi S, Ando R, Dedecker P, Verheijen W, Mizuno H, Miyawaki A, Hofkens J. Reversible single-molecule photoswitching in the GFP-like fluorescent protein Dronpa. *Proc Natl Acad Sci USA* 102: 9511–9516, 2005.
  140. Habuchi S, Dedecker P, Hotta J, Flors C, Ando R, Mizuno H, Miyawaki A, Hofkens J. Photo-induced protonation/deprotonation in the GFP-like fluorescent protein Dronpa: mechanism responsible for the reversible photoswitching. *Photochem Photobiol Sci* 5: 567–576, 2006.
  141. Habuchi S, Tsutsui H, Kochaniak AB, Miyawaki A, van Oijen AM. mKikGR, a monomeric photoswitchable fluorescent protein. *PLoS ONE* 3: e3944, 2008.
  142. Haddock SHD. Comparative feeding behavior of planktonic ctenophores. *Integr Comp Biol* 1–7, 2007.
  143. Haddock SHD, Case JF. Bioluminescent spectra of shallow and deep-sea gelatinous zooplankton: ctenophores, medusae and siphonophores. *Marine Biol* 133: 571–582, 1999.
  - 143a. (a) Haddock SH, Mastoian N, Christianson LM. A photoactivatable green-fluorescent protein from the phylum Ctenophora. *Proc Biol Sci* 277: 1155–1160, 2010.
  144. Haigh SE, Twig G, Molina AA, Wikstrom JD, Deutsch M, Shirihai OS. PA-GFP: a window into the subcellular adventures of the individual mitochondrion. *Novartis Found Symp* 287: 21–46, 2007.
  145. Halin C, Rodrigo Mora J, Sumen C, von Andrian UH. In vivo imaging of lymphocyte trafficking. *Annu Rev Cell Dev Biol* 21: 581–603, 2002.
  146. Hanson GT, Aggeler R, Oglesbee D, Cannon M, Capaldi RA, Tsien RY, Remington SJ. Investigating mitochondrial redox potential with redox-sensitive green fluorescent protein indicators. *J Biol Chem* 279: 13044–13053, 2004.
  147. Hanson GT, McAnaney TB, Park ES, Rendell ME, Yarbrough DK, Chu S, Xi L, Boxer SG, Montrose MH, Remington SJ. Green fluorescent protein variants as ratiometric dual emission pH sensors. 1. Structural characterization and preliminary application. *Biochemistry* 41: 15477–15488, 2002.
  148. Harpur AG, Wouters FS, Bastiaens PI. Imaging FRET between spectrally similar GFP molecules in single cells. *Nat Biotechnol* 19: 167–169, 2001.
  149. Harvey CD, Ehrhardt AG, Cellurale C, Zhong H, Yasuda R, Davis RJ, Svoboda K. A genetically encoded fluorescent sensor of ERK activity. *Proc Natl Acad Sci USA* 105: 19264–19269, 2008.
  150. Hastings JW. Bioluminescence. In: *Cell Physiology Source Book*, edited by Sperelakis N. San Diego, CA: Academic, 1995.
  151. Haupschein RS, Sloan KE, Torella C, Moezzifard R, Giel-Moloney M, Zehetmeier C, Unger C, Ilag LL, Jay DG. Functional proteomic screen identifies a modulating role for CD44 in death receptor-mediated apoptosis. *Cancer Res* 65: 1887–1896, 2005.
  152. Hazelwood KL, Ramko EB, Ozarowska AP, Olenych SG, Worthy PN, Guan A, Murphy CS. Searching the fluorescent protein color palette for new FRET pairs. *Proc SPIE* 6868: 68612, 2008.
  153. Heim N, Griesbeck O. Genetically encoded indicators of cellular calcium dynamics based on troponin C and green fluorescent protein. *J Biol Chem* 279: 14280–14286, 2004.

154. **Heim R, Cubitt AB, Tsien RY.** Improved green fluorescence. *Nature* 373: 663–664, 1995.
155. **Heim R, Prasher DC, Tsien RY.** Wavelength mutations and post-translational autoxidation of green fluorescent protein. *Proc Natl Acad Sci USA* 91: 12501–12504, 1994.
156. **Heim R, Tsien RY.** Engineering green fluorescent protein for improved brightness, longer wavelengths and fluorescence resonance energy transfer. *Curr Biol* 6: 178–182, 1996.
157. **Hell SW.** Far-field optical nanoscopy. *Science* 316: 1153–1158, 2007.
158. **Hell SW, Dyba M, Jakobs S.** Concepts for nanoscale resolution in fluorescence microscopy. *Curr Opin Neurobiol* 14: 599–609, 2004.
159. **Hell SW, Stelzer EHK.** Fundamental improvement of resolution with a 4Pi-confocal fluorescence microscope using two-photon excitation. *Opt Comm* 93: 277–282, 1992.
160. **Henderson JN, Ai HW, Campbell RE, Remington SJ.** Structural basis for reversible photobleaching of a green fluorescent protein homologue. *Proc Natl Acad Sci USA* 104: 6672–6677, 2007.
161. **Henderson JN, Gepshtain R, Heenan JR, Kallio K, Huppert D, Remington SJ.** Structure and mechanism of the photoactivatable green fluorescent protein. *J Am Chem Soc* 131: 4176–4177, 2009.
162. **Henderson JN, Remington SJ.** Crystal structures and mutational analysis of amFP486, a cyan fluorescent protein from *Anemonia majano*. *Proc Natl Acad Sci USA* 102: 12712–12717, 2005.
163. **Henikoff S, Ahmad K, Platero JS, van Steensel B.** Heterochromatic deposition of centromeric histone H3-like proteins. *Proc Natl Acad Sci USA* 97: 716–721, 2000.
164. **Herring PJ.** Bioluminescence of invertebrates other than insects. In: *Bioluminescence in Action*, edited by Herring PJ. London: Academic, 1978.
165. **Hess ST, Girirajan TP, Mason MD.** Ultra-high resolution imaging by fluorescence photoactivation localization microscopy. *Biophys J* 91: 4258–4272, 2006.
166. **Hess ST, Gould TJ, Gudheti MV, Maas SA, Mills KD, Zimmerberg J.** Dynamic clustered distribution of hemagglutinin resolved at 40 nm in living cell membranes discriminates between raft theories. *Proc Natl Acad Sci USA* 104: 17370–17375, 2007.
167. **Heydorn A, Lundholt BK, Praestegaard M, Pagliaro L.** Protein translocation assays: key tools for accessing new biological information with high-throughput microscopy. *Methods Enzymol* 414: 513–530, 2006.
168. **Hirrlinger PG, Scheller A, Braun C, Quintela-Schneider M, Fuss B, Hirrlinger J, Kirchhoff F.** Expression of reef coral fluorescent proteins in the central nervous system of transgenic mice. *Mol Cell Neurosci* 30: 291–303, 2005.
169. **Hoffman RM.** A better fluorescent protein for whole-body imaging. *Trends Biotechnol* 26: 1–4, 2008.
170. **Hoffman RM.** Imaging cancer dynamics in vivo at the tumor and cellular level with fluorescent proteins. *Clin Exp Metastasis* 26: 345–355, 2009.
171. **Hoffman RM.** The multiple uses of fluorescent proteins to visualize cancer in vivo. *Nat Rev Cancer* 5: 796–806, 2005.
172. **Hofmann M, Eggeling C, Jakobs S, Hell SW.** Breaking the diffraction barrier in fluorescence microscopy at low light intensities by using reversibly photoswitchable proteins. *Proc Natl Acad Sci USA* 102: 17565–17569, 2005.
173. **Hollingsworth LL, Kinzie RA, Lewis TD, Krupp DA, Leong JAC.** Phototaxis of motile zooxanthellae to green light may facilitate symbiont capture by coral larvae. *Coral Reefs* 24: 523, 2005.
174. **Honda A, Adams SR, Sawyer CL, Lev-Ram V, Tsien RY, Dostmann WR.** Spatiotemporal dynamics of guanosine 3',5'-cyclic monophosphate revealed by a genetically encoded, fluorescent indicator. *Proc Natl Acad Sci USA* 98: 2437–2442, 2001.
175. **Hong SG, Kim MK, Jang G, Oh HJ, Park JE, Kang JT, Koo OJ, Kim T, Kwon MS, Koo BC, Ra JC, Kim DY, Ko C, Lee BC.** Generation of red fluorescent protein transgenic dogs. *Genesis* 47: 314–322, 2009.
176. **Hopf M, Gohring W, Mann K, Timpl R.** Mapping of binding sites for nidogens, fibulin-2, fibronectin and heparin to different Ig modules of perlecan. *J Mol Biol* 311: 529–541, 2001.
177. **Hopf M, Gohring W, Ries A, Timpl R, Hohenester E.** Crystal structure and mutational analysis of a perlecan-binding fragment of nidogen-1. *Nat Struct Biol* 8: 634–640, 2001.
178. **Hu CD, Chinenov Y, Kerppola TK.** Visualization of interactions among bZIP and Rel family proteins in living cells using bimolecular fluorescence complementation. *Mol Cell* 9: 789–798, 2002.
179. **Hu CD, Kerppola TK.** Simultaneous visualization of multiple protein interactions in living cells using multicolor fluorescence complementation analysis. *Nat Biotechnol* 21: 539–545, 2003.
180. **Huang Z.** A review of progress in clinical photodynamic therapy. *Technol Cancer Res Treat* 4: 283–293, 2005.
181. **Huelsenbeck JP, Ronquist F.** MRBAYES: Bayesian inference of phylogenetic trees. *Bioinformatics* 17: 754–755, 2001.
182. **Huisken J, Swoger J, Del Bene F, Wittbrodt J, Stelzer EH.** Optical sectioning deep inside live embryos by selective plane illumination microscopy. *Science* 305: 1007–1009, 2004.
183. **Ianushevich Iu G, Gurskaia NG, Staroverov DB, Luk'ianov SA, Luk'ianov KA.** [A natural fluorescent protein that changes its fluorescence during maturation]. *Bioorg Khim* 29: 356–360, 2003.
184. **Ip DT, Chan SH, Allen MD, Bycroft M, Wan DC, Wong KB.** Crystallization and preliminary crystallographic analysis of a novel orange fluorescent protein from the Cnidaria tube anemone *Cerianthus sp.* *Acta Cryst D Biol Crystallogr* 60: 340–341, 2004.
185. **Ip DT, Wong KB, Wan DC.** Characterization of novel orange fluorescent protein cloned from cnidarian tube anemone *Cerianthus sp.* *Mar Biotechnol* 9: 469–478, 2007.
186. **Itoh RE, Kurokawa K, Ohba Y, Yoshizaki H, Mochizuki N, Matsuda M.** Activation of rac and cdc42 video imaged by fluorescent resonance energy transfer-based single-molecule probes in the membrane of living cells. *Mol Cell Biol* 22: 6582–6591, 2002.
187. **Jach G, Pesch M, Richter K, Frings S, Uhrig JF.** An improved mRFP1 adds red to bimolecular fluorescence complementation. *Nat Methods* 3: 597–600, 2006.
188. **Jares-Erijman EA, Jovin TM.** Imaging molecular interactions in living cells by FRET microscopy. *Curr Opin Chem Biol* 10: 409–416, 2006.
189. **Jay DG.** Selective destruction of protein function by chromophore-assisted laser inactivation. *Proc Natl Acad Sci USA* 85: 5454–5458, 1988.
190. **Jayaraman S, Haggie P, Wachter RM, Remington SJ, Verkman AS.** Mechanism and cellular applications of a green fluorescent protein-based halide sensor. *J Biol Chem* 275: 6047–6050, 2000.
191. **Jerlov NG.** *Marine Optics*. Amsterdam: Elsevier, 1976.
192. **Jimenez-Banzo A, Nonell S, Hofkens J, Flors C.** Singlet oxygen photosensitization by EGFP and its chromophore HBDI. *Biophys J* 94: 168–172, 2008.
193. **Johnson DE, Ai HW, Wong P, Young JD, Campbell RE, Casey J.** Red fluorescent protein pH biosensor to detect concentrative nucleoside transport. *J Biol Chem* 284: 20499–20511, 2009.
194. **Johnson FH, Shimomura O, Saiga Y, Gershman LC, Reynolds GT, Waters JR.** Quantum efficiency of *Cypridina* luminescence, with a note on that of *Aequorea*. *J Cell Comp Physiol* 60: 85–103, 1962.
195. **Jones JT, Myers JW, Ferrell JE, Meyer T.** Probing the precision of the mitotic clock with a live-cell fluorescent biosensor. *Nat Biotechnol* 22: 306–312, 2004.
196. **Kalderon D, Roberts BL, Richardson WD, Smith AE.** A short amino acid sequence able to specify nuclear location. *Cell* 39: 499–509, 1984.
197. **Kanda T, Sullivan KF, Wahl GM.** Histone-GFP fusion protein enables sensitive analysis of chromosome dynamics in living mammalian cells. *Curr Biol* 8: 377–385, 1998.
198. **Kaper T, Lager I, Looger LL, Chermak D, Frommer WB.** Fluorescence resonance energy transfer sensors for quantitative monitoring of pentose and disaccharide accumulation in bacteria. *Biootechnol Biofuels* 1: 11, 2008.
199. **Kaper T, Looger LL, Takanaga H, Platten M, Steinman L, Frommer WB.** Nanosensor detection of an immunoregulatory tryptophan influx/kynurenone efflux cycle. *PLoS Biol* 5: e257, 2007.
200. **Karasawa S, Araki T, Nagai T, Mizuno H, Miyawaki A.** Cyan-emitting and orange-emitting fluorescent proteins as a donor/acceptor pair for fluorescence resonance energy transfer. *Biochem J* 381: 307–312, 2004.
201. **Karasawa S, Araki T, Yamamoto-Hino M, Miyawaki A.** A green-emitting fluorescent protein from *Galaxeidae* coral and its mono-

- meric version for use in fluorescent labeling. *J Biol Chem* 278: 34167–34171, 2003.
202. Katayama H, Yamamoto A, Mizushima N, Yoshimori T, Miyawaki A. GFP-like proteins stably accumulate in lysosomes. *Cell Struct Funct* 33: 1–12, 2008.
  203. Kato N, Lam E. Detection of chromosomes tagged with green fluorescent protein in live *Arabidopsis thaliana* plants. *Genome Biol* 2: 45, 2001.
  204. Kawaguti S. On the physiology of reef corals. VI. Study of the pigments. *Palao Trop Biol Stn Stud* 2: 617–674, 1944.
  205. Kawai Y, Sato M, Umezawa Y. Single color fluorescent indicators of protein phosphorylation for multicolor imaging of intracellular signal flow dynamics. *Anal Chem* 76: 6144–6149, 2004.
  206. Kelmanson I, Matz M. Molecular basis and evolutionary origins of color diversity in great star coral *Montastraea cavernosa* (Scleractinia: Faviidae). *Mol Biol Evol* 20: 1125–1133, 2003.
  207. Kerppola TK. Bimolecular fluorescence complementation: visualization of molecular interactions in living cells. *Methods Cell Biol* 85: 431–470, 2008.
  208. Kerppola TK. Visualization of molecular interactions by fluorescence complementation. *Nat Rev Mol Cell Biol* 7: 449–456, 2006.
  209. Kettling U, Koltermann A, Schwille P, Eigen M. Real-time enzyme kinetics monitored by dual-color fluorescence cross-correlation spectroscopy. *Proc Natl Acad Sci USA* 95: 1416–1420, 1998.
  210. Kikuchi A, Fukumura E, Karasawa S, Mizuno H, Miyawaki A, Shiro Y. Structural characterization of a thiazoline-containing chromophore in an orange fluorescent protein, monomeric Kusabira Orange. *Biochemistry* 47: 11573–11580, 2008.
  211. Kim SA, Heinze KG, Bacia K, Waxham MN, Schwille P. Two-photon cross-correlation analysis of intracellular reactions with variable stoichiometry. *Biophys J* 88: 4319–4336, 2005.
  212. Kim SA, Heinze KG, Waxham MN, Schwille P. Intracellular calmodulin availability accessed with two-photon cross-correlation. *Proc Natl Acad Sci USA* 101: 105–110, 2004.
  213. Kim SA, Schwille P. Intracellular applications of fluorescence correlation spectroscopy: prospects for neuroscience. *Curr Opin Neurobiol* 13: 583–590, 2003.
  214. Kirber MT, Chen K, Keaney JF Jr. YFP photoconversion revisited: confirmation of the CFP-like species. *Nat Methods* 4: 767–768, 2007.
  215. Knauer SK, Moodt S, Berg T, Liebel U, Pepperkok R, Stauber RH. Translocation biosensors to study signal-specific nucleo-cytoplasmic transport, protease activity and protein-protein interactions. *Traffic* 6: 594–606, 2005.
  216. Kneen M, Farinas J, Li Y, Verkman AS. Green fluorescent protein as a noninvasive intracellular pH indicator. *Biophys J* 74: 1591–1599, 1998.
  217. Knopfel T, Tomita K, Shimazaki R, Sakai R. Optical recordings of membrane potential using genetically targeted voltage-sensitive fluorescent proteins. *Methods* 30: 42–48, 2003.
  218. Kodama Y, Wada M. Simultaneous visualization of two protein complexes in a single plant cell using multicolor fluorescence complementation analysis. *Plant Mol Biol* 70: 211–217, 2009.
  219. Kogure T, Karasawa S, Araki T, Saito K, Kinjo M, Miyawaki A. A fluorescent variant of a protein from the stony coral *Montipora* facilitates dual-color single-laser fluorescence cross-correlation spectroscopy. *Nat Biotechnol* 24: 577–581, 2006.
  220. Kogure T, Kawano H, Abe Y, Miyawaki A. Fluorescence imaging using a fluorescent protein with a large Stokes shift. *Methods* 45: 223–226, 2008.
  221. Kohl T, Heinze KG, Kuhleman R, Koltermann A, Schwille P. A protease assay for two-photon crosscorrelation and FRET analysis based solely on fluorescent proteins. *Proc Natl Acad Sci USA* 99: 12161–12166, 2002.
  222. Kohout SC, Ulbrich MH, Bell SC, Isacoff EY. Subunit organization and functional transitions in Ci-VSP. *Nat Struct Mol Biol* 15: 106–108, 2008.
  223. Konig K. Multiphoton microscopy in life sciences. *J Microsc* 200: 83–104, 2000.
  224. Koster AJ, Klumperman J. Electron microscopy in cell biology: integrating structure and function. *Nat Rev Mol Cell Biol Suppl*: SS6–10, 2003.
  225. Kozel BA, Rongish BJ, Czirok A, Zach J, Little CD, Davis EC, Knutsen RH, Wagenseil JE, Levy MA, Mecham RP. Elastic fiber formation: a dynamic view of extracellular matrix assembly using timer reporters. *J Cell Physiol* 207: 87–96, 2006.
  226. Krasnovsky AA Jr. Primary mechanisms of photoactivation of molecular oxygen. History of development and the modern status of research. *Biochemistry* 72: 1065–1080, 2007.
  227. Kredel S, Nienhaus K, Oswald F, Wolff M, Ivanchenko S, Cymer F, Jeromin A, Michel FJ, Spindler KD, Heilker R, Nienhaus GU, Wiedenmann J. Optimized and far-red-emitting variants of fluorescent protein eqFP611. *Chem Biol* 15: 224–233, 2008.
  228. Kredel S, Oswald F, Nienhaus K, Deuschle K, Rocker C, Wolff M, Heilker R, Nienhaus GU, Wiedenmann J. mRuby, a bright monomeric red fluorescent protein for labeling of subcellular structures. *PLoS ONE* 4: e4391, 2009.
  229. Kremers GJ, Goedhart J. Visible fluorescent proteins for FRET in Laboratory Techniques in Biochemistry and Molecular Biology. *FRET and FLIM Techniques* 33: 171–224, 2008.
  230. Kremers GJ, Goedhart J, van den Heuvel DJ, Gerritsen HC, Gadella TW Jr. Improved green and blue fluorescent proteins for expression in bacteria and mammalian cells. *Biochemistry* 46: 3775–3783, 2007.
  231. Kremers GJ, Goedhart J, van Munster EB, Gadella TW Jr. Cyan and yellow super fluorescent proteins with improved brightness, protein folding, and FRET Forster radius. *Biochemistry* 45: 6570–6580, 2006.
  232. Kremers GJ, Hazelwood KL, Murphy CS, Davidson MW, Piston DW. Photoconversion in orange and red fluorescent proteins. *Nat Methods* 6: 355–358, 2009.
  233. Kremers GJ, Piston DW. Turning fluorescent proteins into energy-saving light bulbs. *Nat Methods* 5: 472–473, 2008.
  234. Kunkel MT, Ni Q, Tsien RY, Zhang J, Newton AC. Spatio-temporal dynamics of protein kinase B/Akt signaling revealed by a genetically encoded fluorescent reporter. *J Biol Chem* 280: 5581–5587, 2005.
  235. Kunkel MT, Toker A, Tsien RY, Newton AC. Calcium-dependent regulation of protein kinase D revealed by a genetically encoded kinase activity reporter. *J Biol Chem* 282: 6733–6742, 2007.
  236. Kural C, Nonet ML, Selvin PR. FIONA on *Caenorhabditis elegans*. *Biochemistry* 48: 4663–4665, 2009.
  237. Kurokawa K, Mochizuki N, Ohba Y, Mizuno H, Miyawaki A, Matsuda M. A pair of fluorescent resonance energy transfer-based probes for tyrosine phosphorylation of the CrkII adaptor protein in vivo. *J Biol Chem* 276: 31305–31310, 2001.
  238. Kvansakul M, Hopf M, Ries A, Timpl R, Hohenester E. Structural basis for the high-affinity interaction of nidogen-1 with immunoglobulin-like domain 3 of perlecan. *EMBO J* 20: 5342–5346, 2001.
  239. Labas YA, Gurskaya NG, Yanushevich YG, Fradkov AF, Lukyanov KA, Lukyanov SA, Matz MV. Diversity and evolution of the green fluorescent protein family. *Proc Natl Acad Sci USA* 99: 4256–4261, 2002.
  240. Lai L, Park KW, Cheong HT, Kuhholzer B, Samuel M, Bonk A, Im GS, Rieke A, Day BN, Murphy CN, Carter DB, Prather RS. Transgenic pig expressing the enhanced green fluorescent protein produced by nuclear transfer using colchicine-treated fibroblasts as donor cells. *Mol Reprod Dev* 62: 300–306, 2002.
  241. Lanford RE, Kanda P, Kennedy RC. Induction of nuclear transport with a synthetic peptide homologous to the SV40 T antigen transport signal. *Cell* 46: 575–582, 1986.
  242. Lange S, Katayama Y, Schmid M, Burkacky O, Brauchle C, Lamb DC, Jansen RP. Simultaneous transport of different localized mRNA species revealed by live-cell imaging. *Traffic* 9: 1256–1267, 2008.
  243. Lauf U, Lopez P, Falk MM. Expression of fluorescently tagged connexins: a novel approach to rescue function of oligomeric DsRed-tagged proteins. *FEBS Lett* 498: 11–15, 2001.
  244. Lemay NP, Morgan AL, Archer EJ, Dickson LA, Megley CM, Zimmer M. The role of the tight-turn, broken hydrogen bonding, Glu222 and Arg96 in the post-translational green fluorescent protein chromophore formation. *Chem Phys* 348: 152–160, 2008.

245. Li X, Zhao X, Fang Y, Jiang X, Duong T, Fan C, Huang CC, Kain SR. Generation of destabilized green fluorescent protein as a transcription reporter. *J Biol Chem* 273: 34970–34975, 1998.
246. Li Y, Agrawal A, Sakon J, Beitle RR. Characterization of metal affinity of green fluorescent protein and its purification through salt promoted, immobilized metal affinity chromatography. *J Chromatogr A* 909: 183–190, 2001.
247. Lidsky PV, Hato S, Bardina MV, Aminev AG, Palmenberg AC, Sheval EV, Polyakov VY, van Kuppeveld FJ, Agol VI. Nucleocytoplasmic traffic disorder induced by cardioviruses. *J Virol* 80: 2705–2717, 2006.
248. Lin MZ, McKeown MR, Ng HL, Aguilera TA, Shaner NC, Campbell RE, Adams SR, Gross LA, Ma W, Alber T, Tsien RY. Autofluorescent proteins with excitation in the optical window for intravital imaging in mammals. *Chem Biol* 16: 1169–1179, 2009.
249. Lindhout BI, Fransz P, Tessadori F, Meckel T, Hooykaas PJ, van der Zaal BJ. Live cell imaging of repetitive DNA sequences via GFP-tagged polydactyl zinc finger proteins. *Nucleic Acids Res* 35: e107, 2007.
250. Lippincott-Schwartz J, Altan-Bonnet N, Patterson GH. Photobleaching and photoactivation: following protein dynamics in living cells. *Nat Cell Biol Suppl*: S7–S14, 2003.
251. Livet J, Weissman TA, Kang H, Draft RW, Lu J, Bennis RA, Sanes JR, Lichtman JW. Transgenic strategies for combinatorial expression of fluorescent proteins in the nervous system. *Nature* 450: 56–62, 2007.
252. Llopis J, McCaffery JM, Miyawaki A, Farquhar MG, Tsien RY. Measurement of cytosolic, mitochondrial, and Golgi pH in single living cells with green fluorescent proteins. *Proc Natl Acad Sci USA* 95: 6803–6808, 1998.
253. Loening AM, Fenn TD, Gambhir SS. Crystal structures of the luciferase and green fluorescent protein from *Renilla reniformis*. *J Mol Biol* 374: 1017–1028, 2007.
254. Luger K, Hommel U, Herold M, Hofsteenge J, Kirschner K. Correct folding of circularly permuted variants of a beta alpha barrel enzyme in vivo. *Science* 243: 206–210, 1989.
255. Lukyanov KA, Chudakov DM, Lukyanov S, Verkhuska VV. Innovation: photoactivatable fluorescent proteins. *Nat Rev Mol Cell Biol* 6: 885–891, 2005.
256. Lukyanov KA, Fradkov AF, Gurskaya NG, Matz MV, Labas YA, Savitsky AP, Markelov ML, Zaraisky AG, Zhao X, Fang Y, Tan W, Lukyanov SA. Natural animal coloration can be determined by a nonfluorescent green fluorescent protein homolog. *J Biol Chem* 275: 25879–25882, 2000.
257. Lundby A, Mutoh H, Dimitrov D, Akemann W, Knopfel T. Engineering of a genetically encodable fluorescent voltage sensor exploiting fast Ci-VSP voltage-sensing movements. *PLoS ONE* 3: e2514, 2008.
258. Luo H, Nakatsu F, Furuno A, Kato H, Yamamoto A, Ohno H. Visualization of the post-Golgi trafficking of multiphoton photoactivated transferrin receptors. *Cell Struct Funct* 31: 63–75, 2006.
259. Luo KQ, Yu VC, Pu Y, Chang DC. Application of the fluorescence resonance energy transfer method for studying the dynamics of caspase-3 activation during UV-induced apoptosis in living HeLa cells. *Biochem Biophys Res Commun* 283: 1054–1060, 2001.
260. Magliery TJ, Wilson CG, Pan W, Mishler D, Ghosh I, Hamilton AD, Regan L. Detecting protein-protein interactions with a green fluorescent protein fragment reassembly trap: scope and mechanism. *J Am Chem Soc* 127: 146–157, 2005.
261. Mahajan NP, Harrison-Shostak DC, Michaux J, Herman B. Novel mutant green fluorescent protein protease substrates reveal the activation of specific caspases during apoptosis. *Chem Biol* 6: 401–409, 1999.
262. Mank M, Reiff DF, Heim N, Friedrich MW, Borst A, Griesbeck O. A FRET-based calcium biosensor with fast signal kinetics and high fluorescence change. *Biophys J* 90: 1790–1796, 2006.
263. Mank M, Santos AF, Direnberger S, Mrsic-Flogel TD, Hofer SB, Stein V, Hendel T, Reiff DF, Levelt C, Borst A, Bonhoeffer T, Hubener M, Griesbeck O. A genetically encoded calcium indicator for chronic in vivo two-photon imaging. *Nat Methods* 5: 805–811, 2008.
264. Marchant JS, Stutzmann GE, Leissring MA, LaFerla FM, Parker I. Multiphoton-evoked color change of DsRed as an optical highlighter for cellular and subcellular labeling. *Nat Biotechnol* 19: 645–649, 2001.
265. Markvicheva KN, Bogdanova EA, Staroverov DB, Lukyanov S, Belousov VV. Imaging of intracellular hydrogen peroxide production with HyPer upon stimulation of HeLa cells with epidermal growth factor. *Methods Mol Biol* 476: 76–83, 2009.
266. Marriott G, Mao S, Sakata T, Ran J, Jackson DK, Petchprapoon C, Gomez TJ, Warp E, Tulyathan O, Aaron HL, Isacoff EY, Yan Y. Optical lock-in detection imaging microscopy for contrast-enhanced imaging in living cells. *Proc Natl Acad Sci USA* 105: 17789–17794, 2008.
267. Marshall AT, Wright OP. Confocal laser scanning light microscopy of the extra-thecal epithelia of undecalcified scleractinian corals. *Cell Tissue Res* 272: 533–543, 1993.
268. Marshall NJ, Cronin TW, Frank TM. Visual adaptations in crustaceans: chromatic, developmental, and temporal aspects. In: *Sensory Processing in Aquatic Environments*, edited by Collin SP, Marshall NJ. New York: Springer, 2003, p. 343–372.
269. Martini J, Schmied K, Palmisano R, Toensing K, Anselmetti D, Merkle T. Multifocal two-photon laser scanning microscopy combined with photo-activatable GFP for in vivo monitoring of intracellular protein dynamics in real time. *J Struct Biol* 158: 401–409, 2007.
270. Martynov VI, Maksimov BI, Martynova NY, Pakhomov AA, Gurskaya NG, Lukyanov SA. A purple-blue chromoprotein from *Goniopora tenuidens* belongs to the DsRed subfamily of GFP-like proteins. *J Biol Chem* 278: 46288–46292, 2003.
271. Martynov VI, Savitsky AP, Martynova NY, Savitsky PA, Lukyanov KA, Lukyanov SA. Alternative cyclization in GFP-like proteins family. The formation and structure of the chromophore of a purple chromoprotein from *Anemonia sulcata*. *J Biol Chem* 276: 21012–21016, 2001.
272. Massol RH, Larsen JE, Kirchhausen T. Possible role of deep tubular invaginations of the plasma membrane in MHC-I trafficking. *Exp Cell Res* 306: 142–149, 2005.
273. Masuda H, Takenaka Y, Yamaguchi A, Nishikawa S, Mizuno H. A novel yellowish-green fluorescent protein from the marine copepod, *Chiridius poppei*, its use as a reporter protein in HeLa cells. *Gene* 372: 18–25, 2006.
274. Matsuda T, Miyawaki A, Nagai T. Direct measurement of protein dynamics inside cells using a rationally designed photoconvertible protein. *Nat Methods* 5: 339–345, 2008.
275. Matz MV, Fradkov AF, Labas YA, Savitsky AP, Zaraisky AG, Markelov ML, Lukyanov SA. Fluorescent proteins from nonbioluminescent Anthozoa species. *Nat Biotechnol* 17: 969–973, 1999.
276. Matz MV, Labas YA, Ugalde J. Evolution of functions and color in GFP-like proteins. In: *Green Fluorescent Protein: Properties, Applications and Protocols* (2nd ed.), edited by Chalfie M, Kain SR. New York: Wiley, 2006.
277. Matz MV, Marshall NJ, Vorobyev M. Are corals colorful? *Photochem Photobiol* 82: 345–350, 2006.
278. Matzke AJ, Huettel B, van der Winden J, Matzke M. Use of two-color fluorescence-tagged transgenes to study interphase chromosomes in living plants. *Plant Physiol* 139: 1586–1596, 2005.
279. Mazel CH, Lesser MP, Gorbunov MY, Barry TM, Farrell JH, Wyman KD, Falkowski PG. Green-fluorescent proteins in Caribbean corals. *Limnol Oceanogr* 48: 402–411, 2003.
280. McAnaney TB, Park ES, Hanson GT, Remington SJ, Boxer SG. Green fluorescent protein variants as ratiometric dual emission pH sensors. 2. Excited-state dynamics. *Biochemistry* 41: 15489–15494, 2002.
281. McKinney SA, Murphy CS, Hazelwood KL, Davidson MW, Looger LL. A bright and photostable photoconvertible fluorescent protein. *Nat Methods* 6: 131–133, 2009.
282. Mempel TR, Scimone ML, Mora JR, von Andrian UH. In vivo imaging of leukocyte trafficking in blood vessels and tissues. *Curr Opin Immunol* 16: 406–417, 2004.
283. Mena MA, Treynor TP, Mayo SL, Daugherty PS. Blue fluorescent proteins with enhanced brightness and photostability from a structurally targeted library. *Nat Biotechnol* 24: 1569–1571, 2006.
284. Meng F, Suchyna TM, Sachs F. A fluorescence energy transfer-based mechanical stress sensor for specific proteins in situ. *FEBS J* 275: 3072–3087, 2008.

285. Merzlyak EM, Goedhart J, Shcherbo D, Bulina ME, Shcheglov AS, Fradkov AF, Gaintzeva A, Lukyanov KA, Lukyanov S, Gadella TW, Chudakov DM. Bright monomeric red fluorescent protein with an extended fluorescence lifetime. *Nat Methods* 4: 555–557, 2007.
286. Miesenbock G, De Angelis DA, Rothman JE. Visualizing secretion and synaptic transmission with pH-sensitive green fluorescent proteins. *Nature* 394: 192–195, 1998.
287. Mirabella R, Franken C, van der Krogt GN, Bisseling T, Geurts R. Use of the fluorescent timer DsRED-E5 as reporter to monitor dynamics of gene activity in plants. *Plant Physiol* 135: 1879–1887, 2004.
288. Mishin AS, Subach FV, Yampolsky IV, King W, Lukyanov KA, Verkushava VV. The first mutant of the *Aequorea victoria* green fluorescent protein that forms a red chromophore. *Biochemistry* 47: 4666–4673, 2008.
289. Miyatsuka T, Li Z, German MS. The chronology of islet differentiation revealed by temporal cell labeling. *Diabetes* 58: 1863–1868, 2009.
290. Miyawaki A. Visualization of the spatial and temporal dynamics of intracellular signaling. *Dev Cell* 4: 295–305, 2003.
291. Miyawaki A, Griesbeck O, Heim R, Tsien RY. Dynamic and quantitative  $\text{Ca}^{2+}$  measurements using improved cameleons. *Proc Natl Acad Sci USA* 96: 2135–2140, 1999.
292. Miyawaki A, Llopis J, Heim R, McCaffery JM, Adams JA, Ikura M, Tsien RY. Fluorescent indicators for  $\text{Ca}^{2+}$  based on green fluorescent proteins and calmodulin. *Nature* 388: 882–887, 1997.
293. Miyawaki A, Tsien RY. Monitoring protein conformations and interactions by fluorescence resonance energy transfer between mutants of green fluorescent protein. *Methods Enzymol* 327: 472–500, 2000.
294. Mizuno H, Mal TK, Tong KI, Ando R, Furuta T, Ikura M, Miyawaki A. Photo-induced peptide cleavage in the green-to-red conversion of a fluorescent protein. *Mol Cell* 12: 1051–1058, 2003.
295. Mizuno H, Sawano A, Eli P, Hama H, Miyawaki A. Red fluorescent protein from Discosoma as a fusion tag and a partner for fluorescence resonance energy transfer. *Biochemistry* 40: 2502–2510, 2001.
296. Mochizuki N, Yamashita S, Kurokawa K, Ohba Y, Nagai T, Miyawaki A, Matsuda M. Spatio-temporal images of growth-factor-induced activation of Ras and Rap1. *Nature* 411: 1065–1068, 2001.
297. Molina AJ, Shirihai OS. Monitoring mitochondrial dynamics with photoactivatable green fluorescent protein. *Methods Enzymol* 457: 289–304, 2009.
298. Moradpour D, Evans MJ, Gosert R, Yuan Z, Blum HE, Goff SP, Lindenbach BD, Rice CM. Insertion of green fluorescent protein into nonstructural protein 5A allows direct visualization of functional hepatitis C virus replication complexes. *J Virol* 78: 7400–7409, 2004.
299. Morin JG. Coastal bioluminescence: patterns and functions. *Bull Mar Sci* 33: 787–817, 1983.
300. Morin JG, Hastings JW. Energy transfer in a bioluminescent system. *J Cell Physiol* 77: 313–318, 1971.
301. Morise H, Shimomur O, Johnson FH, Winant J. Intermolecular energy-transfer in bioluminescent system of *Aequorea*. *Biochemistry* 13: 2656–2662, 1974.
302. Murata Y, Iwasaki H, Sasaki M, Inaba K, Okamura Y. Phosphoinositide phosphatase activity coupled to an intrinsic voltage sensor. *Nature* 435: 1239–1243, 2005.
303. Mutoh H, Perron A, Dimitrov D, Iwamoto Y, Akemann W, Chudakov DM, Knopfel T. Spectrally-resolved response properties of the three most advanced FRET based fluorescent protein voltage probes. *PLoS ONE* 4: e4555, 2009.
304. Nagai T, Ibata K, Park ES, Kubota M, Mikoshiba K, Miyawaki A. A variant of yellow fluorescent protein with fast and efficient maturation for cell-biological applications. *Nat Biotechnol* 20: 87–90, 2002.
305. Nagai T, Miyawaki A. A high-throughput method for development of FRET-based indicators for proteolysis. *Biochem Biophys Res Commun* 319: 72–77, 2004.
306. Nagai T, Sawano A, Park ES, Miyawaki A. Circularly permuted green fluorescent proteins engineered to sense  $\text{Ca}^{2+}$ . *Proc Natl Acad Sci USA* 98: 3197–3202, 2001.
307. Nagai T, Yamada S, Tominaga T, Ichikawa M, Miyawaki A. Expanded dynamic range of fluorescent indicators for  $\text{Ca}^{2+}$  by circularly permuted yellow fluorescent proteins. *Proc Natl Acad Sci USA* 101: 10554–10559, 2004.
308. Nagai Y, Miyazaki M, Aoki R, Zama T, Inouye S, Hirose K, Iino M, Hagiwara M. A fluorescent indicator for visualizing cAMP-induced phosphorylation in vivo. *Nat Biotechnol* 18: 313–316, 2000.
309. Nakai J, Ohkura M, Imoto K. A high signal-to-noise  $\text{Ca}^{2+}$  probe composed of a single green fluorescent protein. *Nat Biotechnol* 19: 137–141, 2001.
310. Nakanishi T, Ikawa M, Yamada S, Toshimori K, Okabe M. Alkalization of acrosome measured by GFP as a pH indicator and its relation to sperm capacitation. *Dev Biol* 237: 222–231, 2001.
311. Nguyen AW, Daugherty PS. Evolutionary optimization of fluorescent proteins for intracellular FRET. *Nat Biotechnol* 23: 355–360, 2005.
312. Nienhaus GU, Nienhaus K, Holzle A, Ivanchenko S, Renzi F, Oswald F, Wolff M, Schmitt F, Rocker C, Vallone B, Weidemann W, Heilker R, Nar H, Wiedenmann J. Photoconvertible fluorescent protein EosFP: biophysical properties and cell biology applications. *Photochem Photobiol* 82: 351–358, 2006.
313. Nienhaus K, Nar H, Heilker R, Wiedenmann J, Nienhaus GU. *Trans-cis* isomerization is responsible for the red-shifted fluorescence in variants of the red fluorescent protein eqFP611. *J Am Chem Soc* 130: 12578–12579, 2008.
314. Nienhaus K, Nienhaus GU, Wiedenmann J, Nar H. Structural basis for photo-induced protein cleavage and green-to-red conversion of fluorescent protein EosFP. *Proc Natl Acad Sci USA* 102: 9156–9159, 2005.
315. Nienhaus K, Vallone B, Renzi F, Wiedenmann J, Nienhaus GU. Crystallization and preliminary X-ray diffraction analysis of the red fluorescent protein eqFP611. *Acta Crystallogr D Biol Crystallogr* 59: 1253–1255, 2003.
316. Niethammer P, Grabher C, Look AT, Mitchison TJ. A tissue-scale gradient of hydrogen peroxide mediates rapid wound detection in zebrafish. *Nature* 459: 996–999, 2009.
317. Nikolaev VO, Gambaryan S, Lohse MJ. Fluorescent sensors for rapid monitoring of intracellular cGMP. *Nat Methods* 3: 23–25, 2006.
318. Nikolaev VO, Lohse MJ. Monitoring of cAMP synthesis and degradation in living cells. *Physiology* 21: 86–92, 2006.
319. Nyqvist D, Mattsson G, Kohler M, Lev-Ram V, Andersson A, Carlsson PO, Nordin A, Berggren PO, Jansson L. Pancreatic islet function in a transgenic mouse expressing fluorescent protein. *J Endocrinol* 186: 333–341, 2005.
320. O'Connell KM, Tamkun MM. Targeting of voltage-gated potassium channel isoforms to distinct cell surface microdomains. *J Cell Sci* 118: 2155–2166, 2005.
321. Ohashi T, Galiaicy SD, Briscoe G, Erickson HP. An experimental study of GFP-based FRET, with application to intrinsically unstructured proteins. *Protein Sci* 16: 1429–1438, 2007.
322. Ohkura M, Matsuzaki M, Kasai H, Imoto K, Nakai J. Genetically encoded bright  $\text{Ca}^{2+}$  probe applicable for dynamic  $\text{Ca}^{2+}$  imaging of dendritic spines. *Anal Chem* 77: 5861–5869, 2005.
323. Okumoto S, Looger LL, Micheva KD, Reimer RJ, Smith SJ, Frommer WB. Detection of glutamate release from neurons by genetically encoded surface-displayed FRET nanosensors. *Proc Natl Acad Sci USA* 102: 8740–8745, 2005.
324. Ormo M, Cubitt AB, Kallio K, Gross LA, Tsien RY, Remington SJ. Crystal structure of the *Aequorea victoria* green fluorescent protein. *Science* 273: 1392–1395, 1996.
325. Ozawa T, Natori Y, Sato M, Umezawa Y. Imaging dynamics of endogenous mitochondrial RNA in single living cells. *Nat Methods* 4: 413–419, 2007.
326. Pakhomov AA, Pletneva NV, Balashova TA, Martynov VI. Structure and reactivity of the chromophore of a GFP-like chromoprotein from *Condylactis gigantea*. *Biochemistry* 45: 7256–7264, 2006.
- 326a. Pakhomov AA, Martynov VI. Chromophore aspartate oxidation-decarboxylation in the green-to-red conversion of a fluorescent protein from Zoanthus sp. 2. *Biochemistry* 46: 11528–11535, 2007.

327. Palmer AE, Giacomello M, Kortemme T, Hires SA, Lev-Ram V, Baker D, Tsien RY. Ca<sup>2+</sup> indicators based on computationally redesigned calmodulin-peptide pairs. *Chem Biol* 13: 521–530, 2006.
328. Palmer AE, Jin C, Reed JC, Tsien RY. Bcl-2-mediated alterations in endoplasmic reticulum Ca<sup>2+</sup> analyzed with an improved genetically encoded fluorescent sensor. *Proc Natl Acad Sci USA* 101: 17404–17409, 2004.
329. Palmer CV, Mydlarz LD, Willis BL. Evidence of an inflammatory-like response in non-normally pigmented tissues of two scleractinian corals. *Proceedings* 275: 2687–2693, 2008.
330. Palmer CV, Roth MS, Gates RD. Red fluorescent protein responsible for pigmentation in trematode-infected *Porites compressa* tissues. *Biol Bull* 216: 68–74, 2009.
331. Partridge JC. The colour sensitivity and vision of fishes. In: *Light and Life in the Sea*, edited by Herring PJ, Campbell AK, Whitfield M, Maddock L. Cambridge, UK: Cambridge Univ. Press, 1990, p. 167–184.
332. Partridge JC, Cummings ME. Adaptation of visual pigments to the aquatic environment. In: *Adaptive Mechanisms in the Ecology of Vision*, edited by Archer SN, Djambaz MBA, Loew ER, Partridge JC, Vallerga S. Dordrecht: Kluwer Academic, 1999, p. 251–283.
333. Passamaneck YJ, Di Gregorio A, Papaioannou VE, Hadjantonakis AK. Live imaging of fluorescent proteins in chordate embryos: from ascidians to mice. *Microsc Res Tech* 69: 160–167, 2006.
334. Patterson GH, Lippincott-Schwartz J. A photoactivatable GFP for selective photolabeling of proteins and cells. *Science* 297: 1873–1877, 2002.
335. Patterson GH, Lippincott-Schwartz J. Selective photolabeling of proteins using photoactivatable GFP. *Methods* 32: 445–450, 2004.
336. Patterson GH, Pistor DW, Barisic BG. Förster distances between green fluorescent protein pairs. *Anal Biochem* 284: 438–440, 2000.
337. Pedelacq JD, Cabantous S, Tran T, Terwilliger TC, Waldo GS. Engineering and characterization of a superfolder green fluorescent protein. *Nat Biotechnol* 24: 79–88, 2006.
338. Peelle B, Gururaja TL, Payan DG, Anderson DC. Characterization and use of green fluorescent proteins from *Renilla mulleri* and *Ptilosarcus guernei* for the human cell display of functional peptides. *J Protein Chem* 20: 507–519, 2001.
339. Perron A, Mutoh H, Launey T, Knopfel T. Red-shifted voltage-sensitive fluorescent proteins. *Chem Biol* 16: 1268–1277, 2009.
340. Petersen J, Wilmann PG, Beddoe T, Oakley AJ, Devenish RJ, Prescott M, Rossjohn J. The 2.0-A crystal structure of eqFP611, a far red fluorescent protein from the sea anemone *Entacmaea quadricolor*. *J Biol Chem* 278: 44626–44631, 2003.
341. Phair RD, Misteli T. High mobility of proteins in the mammalian cell nucleus. *Nature* 404: 604–609, 2000.
342. Piljic A, Schultz C. Simultaneous recording of multiple cellular events by FRET. *ACS Chem Biol* 3: 156–160, 2008.
343. Pistor DW, Kremers GJ. Fluorescent protein FRET: the good, the bad and the ugly. *Trends Biochem Sci* 32: 407–414, 2007.
344. Plautz JD, Day RN, Dailey GM, Welsh SB, Hall JC, Halpoin S, Kay SA. Green fluorescent protein and its derivatives as versatile markers for gene expression in living *Drosophila melanogaster*, plant and mammalian cells. *Gene* 173: 83–87, 1996.
345. Pletnev S, Gurskaya N, Pletneva NV, Lukyanov KA, Chudakov DM, Martynov VI, Popov VO, Kovalchuk MV, Wlodawer A, Dauter Z, Pletnev V. Structural basis for phototoxicity of the genetically encoded photosensitizer KillerRed. *J Biol Chem* 284: 32028–32039, 2009.
346. Pletnev S, Shcherbo D, Chudakov DM, Pletneva N, Merzlyak EM, Wlodawer A, Dauter Z, Pletnev V. A crystallographic study of bright far-red fluorescent protein mKate reveals pH-induced *cis-trans* isomerization of the chromophore. *J Biol Chem* 283: 28980–28987, 2008.
347. Pletneva NV, Pletnev SV, Chudakov DM, Tikhonova TV, Popov VO, Martynov VI, Wlodawer A, Dauter Z, Pletnev VZ. Three-dimensional structure of yellow fluorescent protein zYFP538 from Zoanthus sp. at the resolution 1.8 angstrom. *Bioorg Khim* 33: 421–430, 2007.
348. Prasher DC, Eckenrode VK, Ward WW, Prendergast FG, Cormier MJ. Primary structure of the *Aequorea victoria* green-fluorescent protein. *Gene* 111: 229–233, 1992.
349. Prescott M, Ling M, Beddoe T, Oakley AJ, Dove S, Hoegh-Guldberg O, Devenish RJ, Rossjohn J. The 2.2 Å crystal structure of a pectenoporin pigment reveals a nonplanar chromophore conformation. *Structure* 11: 275–284, 2003.
350. Qiu DL, Akemann W, Chu CP, Araki R, Knopfel T. Targeted optical probing of neuronal circuit dynamics using fluorescent protein sensors. *Neurosignals* 16: 289–299, 2008.
351. Querido E, Chartrand P. Using fluorescent proteins to study mRNA trafficking in living cells. *Methods Cell Biol* 85: 273–292, 2008.
352. Quillin ML, Anstrom DM, Shu X, O'Leary S, Kallio K, Chudakov DM, Remington SJ. Kindling fluorescent protein from *Anemonia sulcata*: dark-state structure at 1.38 Å resolution. *Biochemistry* 44: 5774–5787, 2005.
353. Raarup MK, Fjorback AW, Jensen SM, Muller HK, Kjaergaard MM, Poulsen H, Wiborg O, Nyengaard JR. Enhanced yellow fluorescent protein photoconversion to a cyan fluorescent protein-like species is sensitive to thermal and diffusion conditions. *J Biomed Opt* 14: 034039, 2009.
354. Rackham O, Brown CM. Visualization of RNA-protein interactions in living cells: FMRP and IMP1 interact on mRNAs. *EMBO J* 23: 3346–3355, 2004.
355. Rajfur Z, Roy P, Otey C, Romer L, Jacobson K. Dissecting the link between stress fibres and focal adhesions by CALI with EGFP fusion proteins. *Nat Cell Biol* 4: 286–293, 2002.
356. Razansky D, Distel M, Vinegoni C, Ma R, Perrimon N, Koester RW, Ntziachristos V. Multispectral opto-acoustic tomography of deep-seated fluorescent proteins in vivo. *Nat Photonics* 3: 412–417, 2009.
357. Reid BG, Flynn GC. Chromophore formation in green fluorescent protein. *Biochemistry* 36: 6786–6791, 1997.
358. Remington SJ. Fluorescent proteins: maturation, photochemistry and photophysics. *Curr Opin Struct Biol* 16: 714–721, 2006.
359. Remington SJ, Wachter RM, Yarbrough DK, Branchaud B, Anderson DC, Kallio K, Lukyanov KA. zFP538, a yellow-fluorescent protein from Zoanthus, contains a novel three-ring chromophore. *Biochemistry* 44: 202–212, 2005.
360. Rizzo MA, Springer GH, Granada B, Pistor DW. An improved cyan fluorescent protein variant useful for FRET. *Nat Biotechnol* 22: 445–449, 2004.
361. Rizzuto R, Brini M, De Giorgi F, Rossi R, Heim R, Tsien RY, Pozzan T. Double labelling of subcellular structures with organelle-targeted GFP mutants in vivo. *Curr Biol* 6: 183–188, 1996.
362. Robey RB, Ruiz O, Santos AV, Ma J, Kear F, Wang LJ, Li CJ, Bernardo AA, Arruda JA. pH-dependent fluorescence of a heterologously expressed *Aequorea* green fluorescent protein mutant: in situ spectral characteristics and applicability to intracellular pH estimation. *Biochemistry* 37: 9894–9901, 1998.
363. Robinett CC, Straight A, Li G, Willhelm C, Sudlow G, Murray A, Belmont AS. In vivo localization of DNA sequences and visualization of large-scale chromatin organization using lac operator/repressor recognition. *J Cell Biol* 135: 1685–1700, 1996.
364. Rocheleau JV, Edidin M, Pistor DW. Intrasequence GFP in class I MHC molecules, a rigid probe for fluorescence anisotropy measurements of the membrane environment. *Biophys J* 84: 4078–4086, 2003.
365. Rodriguez AJ, Condeelis J, Singer RH, Dictenberg JB. Imaging mRNA movement from transcription sites to translation sites. *Semin Cell Dev Biol* 18: 202–208, 2007.
366. Rosenow MA, Huffman HA, Phail ME, Wachter RM. The crystal structure of the Y66L variant of green fluorescent protein supports a cyclization-oxidation-dehydration mechanism for chromophore maturation. *Biochemistry* 43: 4464–4472, 2004.
367. Rosenow MA, Patel HN, Wachter RM. Oxidative chemistry in the GFP active site leads to covalent cross-linking of a modified leucine side chain with a histidine imidazole: implications for the mechanism of chromophore formation. *Biochemistry* 44: 8303–8311, 2005.

368. Rubenwolf S, Niewohner J, Meyer E, Petit-Frere C, Rudert F, Hoffmann PR, Ilag LL. Functional proteomics using chromophore-assisted laser inactivation. *Proteomics* 2: 241–246, 2002.
369. Sakai R, Repunte-Canonigo V, Raj CD, Knopfel T. Design and characterization of a DNA-encoded, voltage-sensitive fluorescent protein. *Eur J Neurosci* 13: 2314–2318, 2001.
370. Sakaue-Sawano A, Kurokawa H, Morimura T, Hanyu A, Hama H, Osawa H, Kashiwagi S, Fukami K, Miyata T, Miyoshi H, Imamura T, Ogawa M, Masai H, Miyawaki A. Visualizing spatiotemporal dynamics of multicellular cell-cycle progression. *Cell* 132: 487–498, 2008.
371. Salih A, Larkum A, Cox G, Kuhl M. Fluorescent pigments in corals are photoprotective. *Nature* 408: 850–853, 2000.
372. Sankaranarayanan S, De Angelis D, Rothman JE, Ryan TA. The use of pHluorins for optical measurements of presynaptic activity. *Biophys J* 79: 2199–2208, 2000.
373. Sasaki E, Suemizu H, Shimada A, Hanazawa K, Oiwa R, Kamioka M, Tomioka I, Sotomaru Y, Hirakawa R, Eto T, Shiozawa S, Maeda T, Ito M, Ito R, Kito C, Yagihashi C, Kawai K, Miyoshi H, Tanioka Y, Tamaoki N, Habu S, Okano H, Nomura T. Generation of transgenic non-human primates with germline transmission. *Nature* 459: 523–527, 2009.
374. Sasaki K, Sato M, Umezawa Y. Fluorescent indicators for Akt/protein kinase B and dynamics of Akt activity visualized in living cells. *J Biol Chem* 278: 30945–30951, 2003.
375. Sato M, Hida N, Ozawa T, Umezawa Y. Fluorescent indicators for cyclic GMP based on cyclic GMP-dependent protein kinase Ialpha and green fluorescent proteins. *Anal Chem* 72: 5918–5924, 2000.
376. Sato T, Takahoko M, Okamoto H. HuC:Kaede, a useful tool to label neural morphologies in networks in vivo. *Genesis* 44: 136–142, 2006.
377. Schneider M, Barozzi S, Testa I, Fareta M, Diaspro A. Two-photon activation and excitation properties of PA-GFP in the 720–920-nm region. *Biophys J* 89: 1346–1352, 2005.
378. Schnitzler CE, Keenan RJ, McCord R, Matysik A, Christianson LM, Haddock SH. Spectral diversity of fluorescent proteins from the anthozoan *Corynactis californica*. *Mar Biotechnol* 10: 328–342, 2008.
379. Schultz C, Schleifenbaum A, Goedhart J, Gadella TW Jr. Multiparameter imaging for the analysis of intracellular signaling. *ChemBioChem* 6: 1323–1330, 2005.
380. Schwentker MA, Bock H, Hofmann M, Jakobs S, Bewersdorf J, Eggeling C, Hell SW. Wide-field subdiffraction RESOLFT microscopy using fluorescent protein photoswitching. *Microsc Res Tech* 70: 269–280, 2007.
381. Schwille P, Meyer-Almes FJ, Rigler R. Dual-color fluorescence cross-correlation spectroscopy for multicomponent diffusional analysis in solution. *Biophys J* 72: 1878–1886, 1997.
382. Serebrovskaya EO, Edelweiss EF, Stremovskiy OA, Lukyanov KA, Chudakov DM, Deyev SM. Targeting cancer cells by using an antireceptor antibody-photosensitizer fusion protein. *Proc Natl Acad Sci USA* 106: 9221–9225, 2009.
383. Shagin DA, Barsova EV, Yanushevich YG, Fradkov AF, Lukyanov KA, Labas YA, Semenova TN, Ugalde JA, Meyers A, Nunez JM, Widder EA, Lukyanov SA, Matz MV. GFP-like proteins as ubiquitous metazoan superfamily: evolution of functional features and structural complexity. *Mol Biol Evol* 21: 841–850, 2004.
384. Shaner NC, Campbell RE, Steinbach PA, Giepmans BN, Palmer AE, Tsien RY. Improved monomeric red, orange and yellow fluorescent proteins derived from *Discosoma* sp. red fluorescent protein. *Nat Biotechnol* 22: 1567–1572, 2004.
385. Shaner NC, Lin MZ, McKeown MR, Steinbach PA, Hazelwood KL, Davidson MW, Tsien RY. Improving the photostability of bright monomeric orange and red fluorescent proteins. *Nat Methods* 5: 545–551, 2008.
386. Shaner NC, Patterson GH, Davidson MW. Advances in fluorescent protein technology. *J Cell Sci* 120: 4247–4260, 2007.
387. Shaner NC, Steinbach PA, Tsien RY. A guide to choosing fluorescent proteins. *Nat Methods* 2: 905–909, 2005.
388. Shcherbo D, Merzlyak EM, Chepurnykh TV, Fradkov AF, Ermakova GV, Solovieva EA, Lukyanov KA, Bogdanova EA, Zaraisky AG, Lukyanov S, Chudakov DM. Bright far-red fluorescent protein for whole-body imaging. *Nat Methods* 4: 741–746, 2007.
389. Shcherbo D, Murphy CS, Ermakova GV, Solovieva EA, Chepurnykh TV, Shcheglov AS, Verkhusha VV, Pletnev VZ, Hazelwood KL, Roche PM, Lukyanov S, Zaraisky AG, Davidson MW, Chudakov DM. Far-red fluorescent tags for protein imaging in living tissues. *Biochem J* 418: 567–574, 2009.
390. Shcherbo D, Souslova EA, Goedhart J, Chepurnykh TV, Gaintzeva A, Shemyakina II, Gadella TW, Lukyanov S, Chudakov DM. Practical and reliable FRET/FLIM pair of fluorescent proteins. *BMC Biotechnol* 9: 24, 2009.
391. Shimomura O. Structure of the chromophore of *Aequorea* green fluorescent protein. *FEBS Lett* 104: 220–222, 1979.
392. Shimomura O, Johnson FH, Saiga Y. Extraction, purification and properties of aequorin, a bioluminescent protein from the luminous hydromedusan, *Aequorea*. *J Cell Comp Physiol* 59: 223–239, 1962.
393. Shkrob MA, Mishin AS, Chudakov DM, Labas Iu A, Luk'ianov KA. Chromoproteins of the green fluorescent protein family: properties and applications. *Bioorg Khim* 34: 581–590, 2008.
394. Shkrob MA, Yanushevich YG, Chudakov DM, Gurskaya NG, Labas YA, Poponov SY, Mudrik NN, Lukyanov S, Lukyanov KA. Far-red fluorescent proteins evolved from a blue chromoprotein from *Actinia equina*. *Biochem J* 392: 649–654, 2005.
395. Shroff H, Galbraith CG, Galbraith JA, White H, Gillette J, Olenych S, Davidson MW, Betzig E. Dual-color superresolution imaging of genetically expressed probes within individual adhesion complexes. *Proc Natl Acad Sci USA* 104: 20308–20313, 2007.
396. Shu X, Royant A, Lin MZ, Aguilera TA, Lev-Ram V, Steinbach PA, Tsien RY. Mammalian expression of infrared fluorescent proteins engineered from a bacterial phytochrome. *Science* 324: 804–807, 2009.
397. Shu X, Shaner NC, Yarbrough CA, Tsien RY, Remington SJ. Novel chromophores and buried charges control color in mFruits. *Biochemistry* 45: 9639–9647, 2006.
398. Shyu YJ, Liu H, Deng X, Hu CD. Identification of new fluorescent protein fragments for bimolecular fluorescence complementation analysis under physiological conditions. *Biotechniques* 40: 61–66, 2006.
399. Shyu YJ, Suarez CD, Hu CD. Visualization of AP-1 NF-kappaB ternary complexes in living cells by using a BiFC-based FRET. *Proc Natl Acad Sci USA* 105: 151–156, 2008.
400. Shyu YJ, Suarez CD, Hu CD. Visualization of ternary complexes in living cells by using a BiFC-based FRET assay. *Nat Protoc* 3: 1693–1702, 2008.
401. Siegel MS, Isacoff EY. A genetically encoded optical probe of membrane voltage. *Neuron* 19: 735–741, 1997.
402. Siegel RM, Chan FK, Zacharias DA, Swofford R, Holmes KL, Tsien RY, Lenardo MJ. Measurement of molecular interactions in living cells by fluorescence resonance energy transfer between variants of the green fluorescent protein. *Sci STKE* 2000: PL1, 2000.
403. Sinnecker D, Voigt P, Hellwig N, Schaefer M. Reversible photobleaching of enhanced green fluorescent proteins. *Biochemistry* 44: 7085–7094, 2005.
404. Sniegowski JA, Lappe JW, Patel HN, Huffman HA, Wachter RM. Base catalysis of chromophore formation in Arg96 and Glu222 variants of green fluorescent protein. *J Biol Chem* 280: 26248–26255, 2005.
405. Sniegowski JA, Phail ME, Wachter RM. Maturation efficiency, trypsin sensitivity, and optical properties of Arg96, Glu222, and Gly67 variants of green fluorescent protein. *Biochem Biophys Res Commun* 332: 657–663, 2005.
406. Solimena M, Gerdes HH. Secretary granules: and the last shall be first. *Trends Cell Biol* 13: 399–402, 2003.
407. Souslova EA, Belousov VV, Lock JG, Stromblad S, Kasparov S, Bolshakov AP, Pinelis VG, Labas YA, Lukyanov S, Mayr LM, Chudakov DM. Single fluorescent protein-based  $\text{Ca}^{2+}$  sensors with increased dynamic range. *BMC Biotechnol* 7: 37, 2007.
408. Souslova EA, Chudakov DM. Genetically encoded intracellular sensors based on fluorescent proteins. *Biochemistry* 72: 683–697, 2007.
409. Souslova EA, Chudakov DM. Photoswitchable cyan fluorescent protein as a FRET donor. *Microsc Res Tech* 69: 207–209, 2006.

410. Srivastava J, Barber DL, Jacobson MP. Intracellular pH sensors: design principles and functional significance. *Physiology* 22: 30–39, 2007.
411. Stark DA, Kulesa PM. An in vivo comparison of photoactivatable fluorescent proteins in an avian embryo model. *Dev Dyn* 236: 1583–1594, 2007.
412. Stephens DJ, Allan VJ. Light microscopy techniques for live cell imaging. *Science* 300: 82–86, 2003.
413. Stiel AC, Andreesen M, Bock H, Hilbert M, Schilde J, Schonle A, Eggeling C, Egner A, Hell SW, Jakobs S. Generation of monomeric reversibly switchable red fluorescent proteins for fast-field fluorescence nanoscopy. *Biophys J* 95: 2989–2997, 2008.
414. Stiel AC, Trowitzsch S, Weber G, Andreesen M, Eggeling C, Hell SW, Jakobs S, Wahl MC. 1.8 Å bright-state structure of the reversibly switchable fluorescent protein Dronpa guides the generation of fast switching variants. *Biochem J* 402: 35–42, 2007.
415. Strack RL, Strongin DE, Bhattacharyya D, Tao W, Berman A, Broxmeyer HE, Keenan RJ, Glick BS. A noncytotoxic DsRed variant for whole-cell labeling. *Nat Methods* 5: 955–957, 2008.
- 415a. Strack RL, Strongin DE, Mets L, Glick BS, Keenan RJ. Chromophore formation in DsRed occurs by a branched pathway. *J Am Chem Soc* 2010, published online May 28, doi: 10.1021/ja1030084.
416. Strongin DE, Bevis B, Khuong N, Downing ME, Strack RL, Sundaram K, Glick BS, Keenan RJ. Structural rearrangements near the chromophore influence the maturation speed and brightness of DsRed variants. *Protein Eng Des Sel* 20: 525–534, 2007.
417. Subach FV, Patterson GH, Manley S, Gillette JM, Lippincott-Schwartz J, Verkushava VV. Photoactivatable mCherry for high-resolution two-color fluorescence microscopy. *Nat Methods* 6: 153–159, 2009.
418. Subach FV, Subach OM, Gundorov IS, Morozova KS, Piatkevich KD, Cuervo AM, Verkushava VV. Monomeric fluorescent timers that change color from blue to red report on cellular trafficking. *Nat Chem Biol* 5: 118–126, 2009.
419. Subach OM, Gundorov IS, Yoshimura M, Subach FV, Zhang J, Gruenwald D, Souslova EA, Chudakov DM, Verkushava VV. Conversion of red fluorescent protein into a bright blue probe. *Chem Biol* 15: 1116–1124, 2008.
- 419a. Subach OM, Malashkevich VN, Zencheck WD, Morozova KS, Piatkevich KD, Almo SC, Verkushava VV. Structural characterization of acylimine-containing blue and red chromophores in mTagBFP and TagRFP fluorescent proteins. *Chem Biol* 17: 333–341, 2010.
420. Sugita M, Shiba Y. Genetic tracing shows segregation of taste neuronal circuitries for bitter and sweet. *Science* 309: 781–785, 2005.
421. Sugiyama M, Sakaue-Sawano A, Iimura T, Fukami K, Kitaguchi T, Kawakami K, Okamoto H, Higashijima SI, Miyawaki A. Illuminating cell-cycle progression in the developing zebrafish embryo. *Proc Natl Acad Sci USA* 106: 20812–20817, 2009.
422. Tachibana K, Hara M, Hattori Y, Kishimoto T. Cyclin B-cdk1 controls pronuclear union in interphase. *Curr Biol* 18: 1308–1313, 2008.
423. Takemoto K, Nagai T, Miyawaki A, Miura M. Spatio-temporal activation of caspase revealed by indicator that is insensitive to environmental effects. *J Cell Biol* 160: 235–243, 2003.
424. Tallini YN, Ohkura M, Choi BR, Ji G, Imoto K, Doran R, Lee J, Plan P, Wilson J, Xin HB, Sanbe A, Gulick J, Mathai J, Robbins J, Salama G, Nakai J, Kotlikoff MI. Imaging cellular signals in the heart in vivo: cardiac expression of the high-signal  $\text{Ca}^{2+}$  indicator GCaMP2. *Proc Natl Acad Sci USA* 103: 4753–4758, 2006.
425. Terskikh A, Fradkov A, Ermakova G, Zaraisky A, Tan P, Kajava AV, Zhao X, Lukyanov S, Matz M, Kim S, Weissman I, Siebert P. “Fluorescent timer”: protein that changes color with time. *Science* 290: 1585–1588, 2000.
426. Testa I, Garre M, Parazzoli D, Barozzi S, Ponzanelli I, Mazza D, Fareta M, Diaspro A. Photoactivation of pa-GFP in 3D: optical tools for spatial confinement. *Eur Biophys J* 37: 1219–1227, 2008.
427. Testa I, Parazzoli D, Barozzi S, Garre M, Fareta M, Diaspro A. Spatial control of pa-GFP photoactivation in living cells. *J Microsc* 230: 48–60, 2008.
428. Tian L, Hires SA, Mao T, Huber D, Chiappe ME, Chalasani SH, Petreanu L, Akerboom J, McKinney SA, Schreiter ER, Bargmann CI, Jayaraman V, Svoboda K, Looger LL. Imaging neural activity in worms, flies and mice with improved GCaMP calcium indicators. *Nat Methods* 6: 875–881, 2009.
429. Ting AY, Kain KH, Klemke RL, Tsien RY. Genetically encoded fluorescent reporters of protein tyrosine kinase activities in living cells. *Proc Natl Acad Sci USA* 98: 15003–15008, 2001.
430. Tomosugi W, Matsuda T, Tani T, Nemoto T, Kotera I, Saito K, Horikawa K, Nagai T. An ultramarine fluorescent protein with increased photostability and pH insensitivity. *Nat Methods* 6: 351–353, 2009.
431. Tomura M, Yoshida N, Tanaka J, Karasawa S, Miwa Y, Miyawaki A, Kanagawa O. Monitoring cellular movement in vivo with photoconvertible fluorescence protein “Kaede” transgenic mice. *Proc Natl Acad Sci USA* 105: 10871–10876, 2008.
432. Tour O, Meijer RM, Zacharias DA, Adams SR, Tsien RY. Genetically targeted chromophore-assisted light inactivation. *Nat Biotechnol* 21: 1505–1508, 2003.
433. Tretyakova YA, Pakhomov AA, Martynov VI. Chromophore structure of the kindling fluorescent protein asFP595 from *Anemonia sulcata*. *J Am Chem Soc* 129: 7748–7749, 2007.
434. Truong K, Sawano A, Mizuno H, Hama H, Tong KI, Mal TK, Miyawaki A, Ikura M. FRET-based in vivo  $\text{Ca}^{2+}$  imaging by a new calmodulin-GFP fusion molecule. *Nat Struct Biol* 8: 1069–1073, 2001.
435. Tsien RY. The green fluorescent protein. *Annu Rev Biochem* 67: 509–544, 1998.
436. Tsutsui H, Karasawa S, Okamura Y, Miyawaki A. Improving membrane voltage measurements using FRET with new fluorescent proteins. *Nat Methods* 5: 683–685, 2008.
437. Tsutsui H, Karasawa S, Shimizu H, Nukina N, Miyawaki A. Semi-rational engineering of a coral fluorescent protein into an efficient highlighter. *EMBO Rep* 6: 233–238, 2005.
438. Tunggal J, Wartenberg M, Paulsson M, Smyth N. Expression of the nidogen-binding site of the laminin gamma 1 chain disturbs basement membrane formation and maintenance in F9 embryoid bodies. *J Cell Sci* 116: 803–812, 2003.
439. Turchin IV, Kamensky VA, Plehanov VI, Orlova AG, Kleshnin MS, Fiks II, Shirmanova MV, Meerovich IG, Arslanbaeva LR, Jerdeva VV, Savitsky AP. Fluorescence diffuse tomography for detection of red fluorescent protein expressed tumors in small animals. *J Biomed Opt* 13: 041310, 2008.
440. Tyagi S. Imaging intracellular RNA distribution and dynamics in living cells. *Nat Methods* 6: 331–338, 2009.
441. Tyas L, Brophy VA, Pope A, Rivett AJ, Tavare JM. Rapid caspase-3 activation during apoptosis revealed using fluorescence-resonance energy transfer. *EMBO Rep* 1: 266–270, 2000.
442. Ugalde JA, Chang BSW, Matz MV. Evolution of coral pigments recreated. *Science* 305: 1433, 2004.
443. Valencia-Burton M, McCullough RM, Cantor CR, Broude NE. RNA visualization in live bacterial cells using fluorescent protein complementation. *Nat Methods* 4: 421–427, 2007.
444. Valentin G, Verheggen C, Piolot T, Neel H, Coppey-Moisan M, Bertrand E. Photoconversion of YFP into a CFP-like species during acceptor photobleaching FRET experiments. *Nat Methods* 2: 801, 2005.
445. Van der Krog GN, Ogink J, Ponsioen B, Jalink K. A comparison of donor-acceptor pairs for genetically encoded FRET sensors: application to the Epac cAMP sensor as an example. *PLoS ONE* 3: e1916, 2008.
446. Van Munster EB, Gadella TW. Fluorescence lifetime imaging microscopy (FLIM). *Adv Biochem Eng Biotechnol* 95: 143–175, 2005.
447. Van Rheenen J, Langeslag M, Jalink K. Correcting confocal acquisition to optimize imaging of fluorescence resonance energy transfer by sensitized emission. *Biophys J* 86: 2517–2529, 2004.
448. Van Thor JJ, Gensch T, Hellingwerf KJ, Johnson LN. Photo-transformation of green fluorescent protein with UV and visible light leads to decarboxylation of glutamate 222. *Nat Struct Biol* 9: 37–41, 2002.
449. VanEngelenburg SB, Palmer AE. Fluorescent biosensors of protein function. *Curr Opin Chem Biol* 12: 60–65, 2008.

450. Verkhusha VV, Chudakov DM, Gurskaya NG, Lukyanov S, Lukyanov KA. Common pathway for the red chromophore formation in fluorescent proteins and chromoproteins. *Chem Biol* 11: 845–854, 2004.
451. Verkhusha VV, Kuznetsova IM, Stepanenko OV, Zaraisky AG, Shavlovsky MM, Turoverov KK, Uversky VN. High stability of *Discosoma* DsRed as compared to *Aequorea* EGFP. *Biochemistry* 42: 7879–7884, 2003.
452. Verkhusha VV, Lukyanov KA. The molecular properties and applications of Anthozoa fluorescent proteins and chromoproteins. *Nat Biotechnol* 22: 289–296, 2004.
453. Verkhusha VV, Sorkin A. Conversion of the monomeric red fluorescent protein into a photoactivatable probe. *Chem Biol* 12: 279–285, 2005.
454. Verma S, Watt GM, Mai Z, Hasan T. Strategies for enhanced photodynamic therapy effects. *Photochem Photobiol* 83: 996–1005, 2007.
455. Villalba-Galea CA, Sandtner W, Starace DM, Bezanilla F. S4-based voltage sensors have three major conformations. *Proc Natl Acad Sci USA* 105: 17600–17607, 2008.
456. Vincent P, Maskos U, Charvet I, Bourgeais L, Stoppini L, Leresche N, Changeux JP, Lambert R, Meda P, Paupardin-Tritsch D. Live imaging of neural structure and function by fibred fluorescence microscopy. *EMBO Rep* 7: 1154–1161, 2006.
457. Vinkenborg JL, Evers TH, Reulen SW, Meijer EW, Merkx M. Enhanced sensitivity of FRET-based protease sensors by redesign of the GFP dimerization interface. *Chembiochem* 8: 1119–1121, 2007.
458. Violin JD, Zhang J, Tsien RY, Newton AC. A genetically encoded fluorescent reporter reveals oscillatory phosphorylation by protein kinase C. *J Cell Biol* 161: 899–909, 2003.
459. Violot S, Carpentier P, Blanchoin L, Bourgeois D. Reverse pH-dependence of chromophore protonation explains the large Stokes shift of the red fluorescent protein mKeima. *J Am Chem Soc* 131: 10356–10357, 2009.
460. Vogel SS, Thaler C, Koushik SV. Fanciful FRET. *Sci STKE* 2006: re2, 2006.
461. Vorvis C, Markus SM, Lee WL. Photoactivatable GFP tagging cassettes for protein-tracking studies in the budding yeast *Saccharomyces cerevisiae*. *Yeast* 25: 651–659, 2008.
462. Waadt R, Schmidt LK, Lohse M, Hashimoto K, Bock R, Kudla J. Multicolor bimolecular fluorescence complementation reveals simultaneous formation of alternative CBL/CIPK complexes in planta. *Plant J* 56: 505–516, 2008.
463. Wachter RM, Elsliger MA, Kallio K, Hanson GT, Remington SJ. Structural basis of spectral shifts in the yellow-emission variants of green fluorescent protein. *Structure* 6: 1267–1277, 1998.
464. Wachter RM, Remington SJ. Sensitivity of the yellow variant of green fluorescent protein to halides and nitrate. *Curr Biol* 9: R628–629, 1999.
465. Wall MA, Socolich M, Ranganathan R. The structural basis for red fluorescence in the tetrameric GFP homolog DsRed. *Nat Struct Biol* 7: 1133–1138, 2000.
466. Wallace DJ, Meyer zum Alten Borgloh S, Astori S, Yang Y, Bausen M, Kugler S, Palmer AE, Tsien RY, Sprengel R, Kerr JN, Denk W, Hasan MT. Single-spike detection in vitro and in vivo with a genetic  $\text{Ca}^{2+}$  sensor. *Nat Methods* 5: 797–804, 2008.
467. Wang F, Dennis JE, Awadallah A, Solchaga LA, Molter J, Kuang Y, Salem N, Lin Y, Tian H, Kolthammer JA, Kim Y, Love ZB, Gerson SL, Lee Z. Transcriptional profiling of human mesenchymal stem cells transduced with reporter genes for imaging. *Physiol Genomics* 37: 23–34, 2009.
468. Wang L, Jackson WC, Steinbach PA, Tsien RY. Evolution of new nonantibody proteins via iterative somatic hypermutation. *Proc Natl Acad Sci USA* 101: 16745–16749, 2004.
469. Wang L, Tsien RY. Evolving proteins in mammalian cells using somatic hypermutation. *Nat Protoc* 1: 1346–1350, 2006.
470. Wang S, Hazelrigg T. Implications for bcd mRNA localization from spatial distribution of exu protein in *Drosophila* oogenesis. *Nature* 369: 400–403, 1994.
471. Wang X, Pang Y, Ku G, Xie X, Stoica G, Wang LV. Noninvasive laser-induced photoacoustic tomography for structural and functional in vivo imaging of the brain. *Nat Biotechnol* 21: 803–806, 2003.
472. Ward WW. *Green Fluorescent Protein: Properties, Applications, and Protocols* (2nd ed.), edited by Chalfie M, Kain SR. New York: Wiley-Interscience, 2006, p. 39–65.
473. Ward WW, Bokman SH. Reversible denaturation of *Aequorea* green-fluorescent protein: physical separation and characterization of the renatured protein. *Biochemistry* 21: 4535–4540, 1982.
474. Ward WW, Cormier MJ. In vitro energy-transfer in *Renilla* bioluminescence. *J Phys Chem* 80: 2289–2291, 1976.
475. Wen W, Meinkoth JL, Tsien RY, Taylor SS. Identification of a signal for rapid export of proteins from the nucleus. *Cell* 82: 463–473, 1995.
476. Wiedenmann J, Elke C, Spindler KD, Funke W. Cracks in the beta-can: fluorescent proteins from *Anemonia sulcata* (Anthozoa, Actinaria). *Proc Natl Acad Sci USA* 97: 14091–14096, 2000.
477. Wiedenmann J, Ivanchenko S, Oswald F, Nienhaus GU. Identification of GFP-like proteins in nonbioluminescent, azooxanthellate anthozoa opens new perspectives for bioprospecting. *Mar Biotechnol* 6: 270–277, 2004.
478. Wiedenmann J, Ivanchenko S, Oswald F, Schmitt F, Rocker C, Salih A, Spindler KD, Nienhaus GU. EosFP, a fluorescent marker protein with UV-inducible green-to-red fluorescence conversion. *Proc Natl Acad Sci USA* 101: 15905–15910, 2004.
479. Wiedenmann J, Nienhaus GU. Live-cell imaging with EosFP and other photoactivatable marker proteins of the GFP family. *Expert Rev Proteomics* 3: 361–374, 2006.
480. Wiedenmann J, Schenk A, Rocker C, Girod A, Spindler KD, Nienhaus GU. A far-red fluorescent protein with fast maturation and reduced oligomerization tendency from *Entacmaea quadricolor* (Anthozoa, Actinaria). *Proc Natl Acad Sci USA* 99: 11646–11651, 2002.
481. Wiedenmann J, Vallone B, Renzi F, Nienhaus K, Ivanchenko S, Rocker C, Nienhaus GU. Red fluorescent protein eqFP611 and its genetically engineered dimeric variants. *J Biomed Opt* 10: 14003, 2005.
482. Willem M, Miosge N, Halfter W, Smyth N, Jannetti I, Burghart E, Timpl R, Mayer U. Specific ablation of the nidogen-binding site in the laminin gamma 1 chain interferes with kidney and lung development. *Development* 129: 2711–2722, 2002.
483. Wilmann PG, Battad J, Petersen J, Wilce MC, Dove S, Devenish RJ, Prescott M, Rossjohn J. The 2.1 Å crystal structure of copGFP, a representative member of the copepod clade within the green fluorescent protein superfamily. *J Mol Biol* 359: 890–900, 2006.
484. Wilmann PG, Petersen J, Devenish RJ, Prescott M, Rossjohn J. Variations on the GFP chromophore: a polypeptide fragmentation within the chromophore revealed in the 2.1-Å crystal structure of a nonfluorescent chromoprotein from *Anemonia sulcata*. *J Biol Chem* 280: 2401–2404, 2005.
485. Wilmann PG, Petersen J, Pettikiriarachchi A, Buckle AM, Smith SC, Olsen S, Perugini MA, Devenish RJ, Prescott M, Rossjohn J. The 2.1 Å crystal structure of the far-red fluorescent protein HcRed: inherent conformational flexibility of the chromophore. *J Mol Biol* 349: 223–237, 2005.
486. Wilmann PG, Turcic K, Battad JM, Wilce MC, Devenish RJ, Prescott M, Rossjohn J. The 1.7 Å crystal structure of Dronpa: a photoswitchable green fluorescent protein. *J Mol Biol* 364: 213–224, 2006.
487. Wong EV, David S, Jacob MH, Jay DG. Inactivation of myelin-associated glycoprotein enhances optic nerve regeneration. *J Neurosci* 23: 3112–3117, 2003.
488. Wu JC, Spin JM, Cao F, Lin S, Xie X, Gheysens O, Chen IY, Sheikh AY, Robbins RC, Tsalenko A, Gambhir SS, Quertermous T. Transcriptional profiling of reporter genes used for molecular imaging of embryonic stem cell transplantation. *Physiol Genomics* 25: 29–38, 2006.
489. Wu X, Simone J, Hewgill D, Siegel R, Lipsky PE, He L. Measurement of two caspase activities simultaneously in living cells by a novel dual FRET fluorescent indicator probe. *Cytometry A* 69: 477–486, 2006.

490. Wu Y, Xing D, Chen WR. Single cell FRET imaging for determination of pathway of tumor cell apoptosis induced by photofrin-PDT. *Cell Cycle* 5: 729–734, 2006.
491. Xia J, Kim SH, Macmillan S, Truant R. Practical three color live cell imaging by widefield microscopy. *Biol Proced Online* 8: 63–68, 2006.
492. Xu X, Gerard AL, Huang BC, Anderson DC, Payan DG, Luo Y. Detection of programmed cell death using fluorescence energy transfer. *Nucleic Acids Res* 26: 2034–2035, 1998.
493. Yampolsky IV, Balashova TA, Lukyanov KA. Synthesis and spectral and chemical properties of the yellow fluorescent protein zFP538 chromophore. *Biochemistry* 48: 8077–8082, 2009.
494. Yampolsky IV, Kislukhin AA, Amatov TT, Shcherbo D, Potapov VK, Lukyanov S, Lukyanov KA. Synthesis and properties of the red chromophore of the green-to-red photoconvertible fluorescent protein Kaede and its analogs. *Bioorg Chem* 36: 96–104, 2008.
495. Yampolsky IV, Remington SJ, Martynov VI, Potapov VK, Lukyanov S, Lukyanov KA. Synthesis and properties of the chromophore of the asFP595 chromoprotein from *Anemonia sulcata*. *Biochemistry* 44: 5788–5793, 2005.
496. Yang M, Baranov E, Jiang P, Sun FX, Li XM, Li L, Hasegawa S, Bouvet M, Al-Tuwaijri M, Chishima T, Shimada H, Moossa AR, Penman S, Hoffman RM. Whole-body optical imaging of green fluorescent protein-expressing tumors and metastases. *Proc Natl Acad Sci USA* 97: 1206–1211, 2000.
497. Yang TT, Cheng L, Kain SR. Optimized codon usage and chromophore mutations provide enhanced sensitivity with the green fluorescent protein. *Nucleic Acids Res* 24: 4592–4593, 1996.
498. Yang TT, Sinai P, Green G, Kitts PA, Chen YT, Lybarger L, Chervenak R, Patterson GH, Piston DW, Kain SR. Improved fluorescence and dual color detection with enhanced blue and green variants of the green fluorescent protein. *J Biol Chem* 273: 8212–8216, 1998.
499. Yanushevich YG, Staroverov DB, Savitsky AP, Fradkov AF, Gurskaya NG, Bulina ME, Lukyanov KA, Lukyanov SA. A strategy for the generation of non-aggregating mutants of Anthozoa fluorescent proteins. *FEBS Lett* 511: 11–14, 2002.
500. Yarbrough D, Wachter RM, Kallio K, Matz MV, Remington SJ. Refined crystal structure of DsRed, a red fluorescent protein from coral, at 2.0-A resolution. *Proc Natl Acad Sci USA* 98: 462–467, 2001.
501. Yin XJ, Lee HS, Yu XF, Choi E, Koo BC, Kwon MS, Lee YS, Cho SJ, Jin GZ, Kim LH, Shin HD, Kim T, Kim NH, Kong IK. Generation of cloned transgenic cats expressing red fluorescence protein. *Biol Reprod* 78: 425–431, 2008.
502. Young P, Feng G. Labeling neurons *in vivo* for morphological and functional studies. *Curr Opin Neurobiol* 14: 642–646, 2004.
503. Yu J, Xiao J, Ren X, Lao K, Xie XS. Probing gene expression in live cells, one protein molecule at a time. *Science* 311: 1600–1603, 2006.
504. Yu YA, Shabahang S, Timiryasova TM, Zhang Q, Beltz R, Gentschev I, Goebel W, Szalay AA. Visualization of tumors and metastases in live animals with bacteria and vaccinia virus encoding light-emitting proteins. *Nat Biotechnol* 22: 313–320, 2004.
505. Yu YA, Timiryasova T, Zhang Q, Beltz R, Szalay AA. Optical imaging: bacteria, viruses, and mammalian cells encoding light-emitting proteins reveal the locations of primary tumors and metastases in animals. *Anal Bioanal Chem* 377: 964–972, 2003.
506. Zaccole M, De Giorgi F, Cho CY, Feng L, Knapp T, Negulescu PA, Taylor SS, Tsien RY, Pozzan T. A genetically encoded, fluorescent indicator for cyclic AMP in living cells. *Nat Cell Biol* 2: 25–29, 2000.
507. Zacharias DA, Violin JD, Newton AC, Tsien RY. Partitioning of lipid-modified monomeric GFPs into membrane microdomains of live cells. *Science* 296: 913–916, 2002.
508. Zagranichny VE, Rudenko NV, Gorokhovatsky AY, Zakharov MV, Balashova TA, Arseniev AS. Traditional GFP-type cyclization and unexpected fragmentation site in a purple chromoprotein from *Anemonia sulcata*, asFP595. *Biochemistry* 43: 13598–13603, 2004.
509. Zagranichny VE, Rudenko NV, Gorokhovatsky AY, Zakharov MV, Shenkarev ZO, Balashova TA, Arseniev AS. zFP538, a yellow fluorescent protein from coral, belongs to the DsRed subfamily of GFP-like proteins but possesses the unexpected site of fragmentation. *Biochemistry* 43: 4764–4772, 2004.
510. Zakharova MY, Kuznetsov NA, Dubiley SA, Kozyr AV, Fedorova OS, Chudakov DM, Knorre DG, Shemyakin IG, Gabibov AG, Kolesnikov AV. Substrate recognition of anthrax lethal factor examined by combinatorial and pre-steady-state kinetic approaches. *J Biol Chem* 284: 17902–17913, 2009.
511. Zamyatnin AA Jr, Solovyev AG, Bozhkov PV, Valkonen JP, Morozov SY, Savenkov EI. Assessment of the integral membrane protein topology in living cells. *Plant J* 46: 145–154, 2006.
512. Zapata-Hommer O, Griesbeck O. Efficiently folding and circularly permuted variants of the Sapphire mutant of GFP. *BMC Biotechnol* 3: 5, 2003.
513. Zhang J, Campbell RE, Ting AY, Tsien RY. Creating new fluorescent probes for cell biology. *Nat Rev Mol Cell Biol* 3: 906–918, 2002.
514. Zhang J, Ma Y, Taylor SS, Tsien RY. Genetically encoded reporters of protein kinase A activity reveal impact of substrate tethering. *Proc Natl Acad Sci USA* 98: 14997–15002, 2001.
515. Zhang L, Gurskaya NG, Merzlyak EM, Staroverov DB, Mudrik NN, Samarkina ON, Vinokurov LM, Lukyanov S, Lukyanov KA. Method for real-time monitoring of protein degradation at the single cell level. *Biotechniques* 42: 446–450, 2007.
516. Zhang S, Ma C, Chalfie M. Combinatorial marking of cells and organelles with reconstituted fluorescent proteins. *Cell* 119: 137–144, 2004.
517. Zimmermann T, Rietdorf J, Girod A, Georget V, Pepperkok R. Spectral imaging and linear un-mixing enables improved FRET efficiency with a novel GFP2-YFP FRET pair. *FEBS Lett* 531: 245–249, 2002.